Axion Cosmology

Juuso Oskari Leskinen

UNIVERSITY OF JYVÄSKYLÄ
DEPARTMENT OF PHYSICS

Master's thesis
Supervisor: Jukka Maalampi
Spring 2016

Abstract

In this master's thesis we study the cosmological consequences of the new scalar field, the axion, that appears in the $\mathrm{U}(1)_{\mathrm{PQ}}$ extension of the standard model of particle physics. We start by presenting some essential fragments of the standard model of Big Bang cosmology, that are needed when we describe the evolution of the axion field in the early Universe. We also review the basics of phase transitions in the early Universe, and go through the creation and evolution of the topological defects that emerge from these symmetry-breaking transitions.

We also study the so-called $\mathrm{U}(1)_{\mathrm{A}}$ problem of the QCD, and the resolution that yields the strong CP problem that are closely related to the axion physics. The minimal Peccei-Quinn extension and the axions are usually taken to be the most elegant solution to this latter problem. The global and chiral $\mathrm{U}(1)_{\mathrm{PQ}}$ required by this extension can be implemented into the theory in multiple ways, and therefore we study the different axion models proposed in the literature. We also go through certain phenomenological aspects of axions, and review the model-parameter constraints coming from astrophysical observations. A discussion of the different direct detection methods and experiments is also given.

The focal point of this thesis is to study the role of axions as a candidate for dark matter. Through the coherent oscillation of the so-called zero-momentum modes of the axion field and the decay of axionic topological defects (cosmic strings, domain walls) the Universe can contain a significant axionic cold dark matter population, that is an essential part of the cosmological concordance model ΛCDM. Following the earlier work presented in the literature, we compute the contribution of the axion dark matter to the overall energy density, and also discuss the finer details of these mechanisms, such as the possible isocurvature fluctuations that the axion field can produce during inflation. We also give a brief review on the proposed idea of the axion Bose-Einstein condensate.

Tiivistelmä

Tässä pro gradu -tutkielmassa tarkastellaan hiukkasfysiikan standardimallin $U(1)_{PQ}$-laajennukseen kuuluvan uuden skalaarikentän, aksionin, roolia kosmologiassa. Aluksi esittelemme valittuja paloja kosmologian standardimallista, joita tarvitsemme tarkasteltaessa aksionikentän evoluutiota varhaisessa maailmankaikkeudessa. Teemme myös katsauksen varhaisen maailmankaikkeuden faasitransitioihin ja niiden mukanaan tuomiin topologisiin defekteihin.

Käymme myös läpi ns. $U(1)_A$-ongelman ja tätä seuranneen vahvan CP-ongelman perusteet. Jälkimmäisen ongelman yhtenä eleganteimmista ratkaisuista pidetään ns. Peccei-Quinn -laajennusta ja aksionikenttää. Tämän minimaalisen laajennuksen globaali kiraalinen $U(1)_{PQ}$-symmetria voidaan liittää hiukkasfysiikan standardimalliin usealla eri tavalla, joten kiinnitämme huomiota kirjallisuudessa ehdotettuihin erilaisiin aksionimalleihin. Tarkastelemme myös yleisesti aksionien hiukkasfenomenologiaa, teemme yleisen katsauksen kirjallisuuteen ja listaamme eri astrofysikaalisista havainnoista saatavia rajoitteita malliparametreille. Esittelemme myös lyhyesti aksionien löytämiseksi kehitettyjä havaintomenetelmiä ja koejärjestelmiä.

Tutkielman pääpainona on tarkastella aksionien roolia pimeän aineen hiukkasena. Aksionit voivat muodostaa kosmologian standardimallin vaatiman kylmän pimeän aineen populaation joko ns. nolla-liikemäärä -moodiratkaisujen koherentilla oskillaatiolla, tai $U(1)_{PQ}$-symmetrian spontaanista symmetriarikosta syntyvien topologisten defektien, kuten säikeiden ja seinämien hajoamisella aksioneiksi. Laskemme näiden mekanismien tuottaman aksionien energiatiheyden, ja keskustelemme aksionituoton yksityskohdista, kuten aksionikentän tuottamista isokurvatuurifluktuaatioista inflaation aikana. Lopuksi teemme myös katsauksen kirjallisuudessa ehdotetun aksionien muodostaman Bose-Einstein kondensaatin keskeisiin väittämiin.

Contents

1 Introduction

The concordance model of cosmology, ΛCDM, assumes that a quarter of the total energy-budget of the Universe is in the form of weakly-interacting matter, that we refer to as cold dark matter (CDM). The presence of this matter is required by the gravitational observational data coming from the galactic rotation curve measurements, weak-lensing surveys and the large-scale structure formation studies. Although there have been propositions that baryonic – or ordinary – matter, such as massive compact halo objects (MACHOs), can constitute as dark matter, it seems that these populations cannot contribute significantly to the observed energy density.

Unfortunately, the standard model of particle physics, which is extremely well-established and consistent with experimental data, does not offer a suitable dark matter candidate. One has then to look for physics beyond the Standard Model (SM). In the literature there are numerous propositions for the possible extensions of the SM, such as the supersymmetric theories, that provide naturally suitable dark matter candidate particles. The most theoretically and experimentally studied dark matter candidates are the so-called weakly-interacting massive particles (WIMPs), which usually have masses in the range of $m_{\mathrm{WIMP}} \sim 10 - 10^4$ GeV. Another well-motivated and studied dark matter candidate is a sterile neutrino ($m_s \sim 1 - 100$ keV), a new neutral fermion additional to the three so-called active neutrinos present in the Standard Model. However, these are just a few examples, as the literature is filled with different extensions with potential hypothetical particle classes. This issue of the nature of the dark matter is usually dubbed as the dark matter problem.

The standard model of particle physics, which is a quantum field theory that describes the elementary particles and forces between them, does have other deficiencies in addition to the lack of a proper dark matter particle. For example, the theory contains naturalness – or fine-tuning – problems, where the values of the theory-parameters have to be extremely fine-tuned for the theory to retain its predictability. One of these fine-tuning problems is the so-called strong CP problem. This problem is related to the non-observation of the neutron electric dipole moment, requiring that one of the parameters of the theory, denoted by $\bar{\theta}$, has to be fine-tuned to an extremely small value.

Perhaps the most elegant solution to the strong CP problem is the Peccei-Quinn mechanism [1, 2], which is an extension of the Standard Model, where an additional global $\mathrm{U}(1)_{\mathrm{PQ}}$ symmetry is included in the theory. Miracu-

lously, the spontaneous and explicit breaking of this added symmetry produces a weakly-interacting and extremely light pseudoscalar particle, referred to as the axion, that is a suitable dark matter candidate. As expected, both the theoretical and experimental studies of axions are highly-motivated due to this simultaneous solution to both of the aforementioned problems. This is also the subject of this thesis, where we study the cosmological consequences of the axion field, with the focal point being the production of axion dark matter.

This thesis is structured as follows. In Chapter 2 we give an overview of the different aspects of cosmology needed in describing the evolution of the axion field in the early Universe. As the topological defects emerging from the phase transitions in the early Universe are closely related to the production of axions, we study these configurations carefully in Chapter 3. In Chapter 4 we consider the aforementioned strong CP problem [3] and the historically preceding $\mathrm{U(1)_A}$ problem [4], which are related to the low-energy phenomena of the QCD theory. In this chapter we also present the Peccei-Quinn mechanism [1, 2], that solves the strong CP problem with the additional the axion field. Chapter 5 is dedicated to the axion and its properties. We describe the different methods proposed to implement the $\mathrm{U(1)_{PQ}}$ symmetry to the Standard Model, and also discuss the phenomenology of the different axion models. In addition to this, we also give a brief overview on the model-parameter constraints coming from astrophysical observations and the different direct detection methods and experiments that search for the axions permeating the investigated solar system and the Milky Way.

The center of our attention, the production of axionic dark matter, is studied in Chapter 6. We first study the thermal production of axions, showing it to yield a negligible population of hot dark matter. Following the literature, we then study and compute the cold axion populations generated by the coherent oscillation of the zero-momentum modes of the axion field and the decay of the axionic topological defects (cosmic string, domain walls). The production of axions through these mechanisms is then compared with the observed cold dark matter energy density, which allows us to constraint the model-parameters. We also discuss the finer details of these mechanisms, such as the possible isocurvature fluctuations that the axion field can cause during the inflation. The final chapter, Chapter 7, is dedicated for a short review on the proposed idea of the axion Bose-Einstein condensate.

2 Overview of cosmology

In this chapter we briefly review some aspects of cosmology needed for describing the evolution of a scalar particle in the Universe. We start by going through standard quantities that are related to the Friedmann-Lemaître-Robertson-Walker metric that describes the expanding Universe, and move on to discuss the main points of cosmological inflation. After this we touch on the subject of thermodynamics in the early Universe, deriving some quantities that are needed in studying interactions between particles in the primordial particle plasma. We conclude this chapter by discussing how the current energy-budget of the Universe is shared between different components.

2.1 The Friedmann-Lemaître-Robertson-Walker metric

The Friedmann-Lemaître-Robertson-Walker (FLRW) metric describes a homogeneous, isotropic universe:

$$\mathrm{d}s^2 = -\mathrm{d}t^2 + R^2(t)\left(\frac{\mathrm{d}r^2}{1-kr^2} + r^2\mathrm{d}\theta^2 + r^2\sin^2(\theta)\mathrm{d}\phi^2\right), \tag{1}$$

where t is the physical time, $R(t)$ is the scale factor that describes the relative expansion of the Universe, and the three-metric part represents the spatial line element in spherical coordinates. The parameter k describes the curvature of the space: positive, negative and zero curvature indicate closed, open and flat universe. Note that throughout this thesis we will use the *natural units*

$$\hbar = c = k_\mathrm{B} = 1, \tag{2}$$

where $\hbar$ is the reduced Planck constant, c is the speed of light and k_B is the Boltzmann constant.

From the FLRW metric (1) and the Einstein equations

$$\mathcal{R}_{\mu\nu} - \frac{1}{2}g_{\mu\nu}\mathcal{R} = 8\pi G_\mathrm{N} T_{\mu\nu} + g_{\mu\nu}\Lambda, \tag{3}$$

we obtain the Friedmann equations

$$H^2 + \frac{k}{R^2} = \frac{8\pi G_\mathrm{N}}{3}\rho_\mathrm{tot}, \tag{4}$$

$$\frac{\ddot{R}}{R} = -\frac{4\pi G_\mathrm{N}}{3}\left(\rho_\mathrm{tot} + 3p_\mathrm{tot}\right), \tag{5}$$

where the Hubble parameter is defined as $H \equiv \dot{R}(t)/R(t)$, $G_{\rm N}$ is the Newtonian gravitational constant, and $\rho_{\rm tot}$ and $p_{\rm tot}$ describe the total energy density and the total pressure of the fluid system, respectively. Note that we have defined the vacuum energy density as $\rho_\Lambda \equiv \Lambda/8\pi G_{\rm N}$ and included it to the total energy density. When we consider processes in the early Universe we assume a negligible vacuum energy, $\Lambda = 0$, and that the Universe is reasonably well described by a flat geometry, i.e. we set $k = 0$.

The two Friedmann equations (4) and (5) can be used to derive the continuity equation

$$\dot{\rho}_{\rm tot} + 3H(t)\left(\rho_{\rm tot} + p_{\rm tot}\right) = 0. \tag{6}$$

In the cosmological models considered there are different types of fluids present. For example, we consider non-relativistic matter fluid with density ρ_m and radiation fluid (photons etc.) with density ρ_r. These different fluids have different equations of state $p = \rho(t)$: non-relativistic matter has a negligible pressure, $p_m = 0$, while radiation has e.o.s. of an ideal relativistic gas, $p_r = \rho_r/3$. In cosmology, one then usually defines the general equation of the state as

$$p_i = w_{{\rm eos},i}\rho_i, \tag{7}$$

where $w_{{\rm eos},m} = 0$, $w_{{\rm eos},r} = 1/3$ and $w_{{\rm eos},\Lambda} = -1$.

We can then check from the equations (6) and (7) how the energy density scales and how the scale factor $R(t)$ and the Hubble parameter $H(t)$ depend on t during radiation and matter dominated epochs, $\rho_{\rm tot} \approx \rho_r$ and $\rho_{\rm tot} \approx \rho_m$:

$$\text{rad. dom. } \rho_r \propto R^{-4}(t),\ R(t) \propto t^{1/2},\ H(t) = \frac{1}{2t} \tag{8}$$

$$\text{mat. dom. } \rho_m \propto R^{-3}(t),\ R(t) \propto t^{2/3},\ H(t) = \frac{2}{3t}. \tag{9}$$

One also defines the dimensionless density parameter

$$\Omega_i = \frac{\rho_i}{\rho_{\rm crit}}, \tag{10}$$

where $\rho_{\rm crit} \equiv \rho_c \equiv 3H^2(t)/8\pi G_{\rm N}$ is the so-called critical energy density, that corresponds to a flat universe. If we denote the present time by t_0 we can

write Eq. (5) in the form

$$H^2(t) = H^2(t_0)\left[\Omega_r\left(\frac{R(t_0)}{R(t)}\right)^4 + \Omega_m\left(\frac{R(t_0)}{R(t)}\right)^3 + \Omega_k\left(\frac{R(t_0)}{R(t)}\right)^2 + \Omega_\Lambda + \Omega_i\left(\frac{R(t_0)}{R(t)}\right)^{3(1+w_{\mathrm{eos},i})}\right], \quad (11)$$

where we defined the curvature density $\Omega_k \equiv -k/R^2H^2$, and Ω_i denotes other additional fluids that might obey different equations of state.

2.2 Cosmic inflation and fluctuations

The standard Hot Big Bang model predicts and explains in great detail the Hubble's law and the expansion of space, the origin of cosmic microwave background (CMB) radiation, the abundance of primordial light elements and the large-scale structure (LSS, galaxies etc.) formation. However, the Big Bang model does have several problems, such as the horizon problem, the flatness problem and the problem of unwanted relics (e.g. magnetic monopoles – see Section 3). Also, it does not explain the origin of the small inhomogeneities necessary for the structure formation as "the seeds of galaxies". The inflationary paradigm, a scenario where the Universe undergoes an epoch of exponential expansion, was introduced to solve the former problems, and alongside it gave a natural explanation for the seeds of structure growth. For more information and reviews on the problems of the Big Bang model and inflation mechanism, see for example Refs. [5, 6, 7]

For the Universe to undergo a period of accelerated expansion, the total energy density has be dominated by vacuum energy – see Eq. (11). The observed present day accelerated expansion is believed to be due to the domination of dark energy, but the origin of the primordial vacuum energy domination is still unclear. In the most inflation models considered one assumes that there is a scalar field, inflaton, that is responsible for the inflationary dynamics. It is then assumed that before inflation the inflaton rests in a high-energy state, and during the inflationary period the inflaton releases its energy slowly while rolling towards to the minimum of its flat potential[1]. The transition period between inflation and the beginning of the standard Hot Big Bang evolution of the Universe is referred to as the *reheating*. Inflation ends when the inflaton reaches minimum of its potential and starts to

[1]This is usually referred to as the slow-roll inflation.

oscillate around it. The inflaton decays through these oscillations into the Standard Model and other possible exotic particles present in the primordial plasma of the Hot Big Bang Model.

In the previous section we described the Universe as a homogeneous and isotropic FLRW-universe. However, the Universe today is inhomogeneous and possesses both large- and small-scale structures. It is now believed that these structures are generated from the evolution of primordial inhomogeneities, that are created from the quantum fluctuations of the fields present during inflation, e.g. inflaton. After inflation these small inhomogeneities then grow and form the observed structure of the Universe. There are two different types of primordial fluctuations: adiabatic and non-adiabatic – or *curvature* and *isocurvature* – fluctuations.

We do not go into details here, but the curvature and isocurvature fluctuations are related to the fluctuations in the energy density and entropy, respectively. We can write the energy density of the non-FLRW-universe as $\rho(t, \vec{x}) = \bar{\rho}(t) + \delta\rho(t, \vec{x})$, where $\bar{\rho}$ is the energy density of the background FLRW-universe and $\delta\rho$ is the perturbation that measures the deviation from the background value. When discussing about the primordial fluctuations one needs to note that in the very early regime all cosmologically interesting modes are outside the horizon, meaning that the causal microphysical processes are disconnected. At later times these scales (fluctuations) are inside the horizon and are again causally connected.

In short, in the early regime we can consider curvature fluctuations to be fluctuations in the energy density, i.e. $\delta\rho \neq 0$. These perturbations are characterized by that the fluctuations in the local number density of the particle species relative to the entropy density vanishes, i.e. $\delta(n_i/s) = 0$. On the other hand, isocurvature fluctuations are perturbations in the entropy, or in the local equation of state, and not in the energy density or local curvature, i.e. for super-horizon sized modes $\delta\rho = 0$. The isocurvature fluctuations are characterized by $\delta(n_i/s) \neq 0$. When the studied modes become sub-horizon sized their fluctuations can be converted into the fluctuations in the energy density. [5] It happens that if the particles of our interest, axions, are present during inflation they can generate isocurvature fluctuations – this will be discussed in Section 6.5.

2.3 Thermodynamics in the early Universe

After inflation the evolution of the Universe is assumed to follow the standard Hot Big Bang cosmological model. In the very early times the Universe is assumed to be filled with the Standard Model particles and possible other particles still unknown, such as dark matter particles. At these high temperatures the Universe is assumed to be in thermal equilibrium, and the particles are assumed to follow the equation of state of a relativistic ideal gas, i.e. the Universe is radiation dominated. In this section we will introduce the basic thermodynamical quantities needed in describing the thermal history of the early Universe.

In kinetic equilibrium particles follow either the Bose-Einstein $(-)$ or the Fermi-Dirac $(+)$ phase space distribution

$$f(\vec{p}) = \frac{1}{\mathrm{e}^{(E-\mu)/T} \pm 1}, \tag{12}$$

where E is the energy of the particle, $E(\vec{p}) = \sqrt{|\vec{p}|^2 + m^2}$, T is the temperature related to the total energy of the system, and μ is the chemical potential that is related to the total particle number. In the following we will assume that the chemical potential is negligible.

The particle number density n, energy density ρ, pressure p and entropy density s are related to the phase space distribution function $f(\vec{p})$ and are given by

$$n(T) = \frac{g}{(2\pi)^3} \int f(\vec{p}) \ \mathrm{d}^3p, \tag{13}$$

$$\rho(T) = \frac{g}{(2\pi)^3} \int E(\vec{p}) f(\vec{p}) \mathrm{d}^3p \tag{14}$$

$$p(T) = \frac{g}{(2\pi)^3} \int \frac{|\vec{p}|^2}{3E} f(\vec{p}) \mathrm{d}^3p, \tag{15}$$

$$s(T) = \frac{g}{(2\pi)^3} \int \frac{4|\vec{p}|^2 + 3m^2}{3ET} f(\vec{p}) \mathrm{d}^3p, \tag{16}$$

where g is the number of the intrinsic degrees of freedom (spin, polarization, etc.), e.g. for photons $g = 2$.

Assuming a negligible chemical potential, the number density and energy

density reduce in the ultrarelativistic limit ($T \gg m$) to

$$n(T) = \begin{cases} (3/4\pi^2)\zeta(3)gT^3 & \text{fermions} \\ (1/\pi^2)\zeta(3)gT^3 & \text{bosons,} \end{cases} \tag{17}$$

$$\rho(T) = \begin{cases} (7/8)(\pi^2/30)gT^4 & \text{fermions} \\ (\pi^2/30)gT^4 & \text{bosons.} \end{cases} \tag{18}$$

Here $\zeta(3) = 1.20206\ldots$ is the Riemann zeta function. As we treat particles as radiation, we have that equation of state is given by $w_{\text{eos},r} = 1/3$.

Since the energy density and pressure of relativistic particles are much greater than those of non-relativistic particles, it is enough to consider only the relativistic particles when considering the radiation-dominated epoch of the early Universe. Total energy density and pressure are then

$$\rho(T) = \sum \rho_i(T) = \frac{\pi^2}{30} g_*(T) T^4 \tag{19}$$

$$p(T) = \frac{1}{3}\rho(T) = \frac{\pi^2}{90} g_*(T) T^4, \tag{20}$$

where $g_*(T)$ is given by

$$g_*(T) \equiv \sum_{i=\text{bosons}} g_i \left(\frac{T_i}{T}\right)^4 + \frac{7}{8} \sum_{j=\text{fermions}} g_j \left(\frac{T_j}{T}\right)^4, \tag{21}$$

where the sums go over relativistic bosons and fermions. In Eq. (21) T_i is the temperature of the relativistic particle at which the particle in question looses contact with the other particle species and decouples from the thermal equilibrium.

Neglecting the curvature and vacuum energy density, the Friedmann Eq. (4) is given by

$$H^2 = \frac{8\pi G_{\text{N}}}{3}\rho(T) = \frac{4\pi^3}{45} g_*(T) \frac{T^4}{m_{\text{Pl}}^2}, \tag{22}$$

where $m_{\text{Pl}} = 1/\sqrt{G_{\text{N}}} \approx 1.22 \times 10^{19}$ GeV is the Planck mass.

As $g_*(T)$ is slowly changing in the early Universe, it is sometimes valid to approximate it as constant, $g_*(T) \simeq g_*$. From the Eq. (22) one then obtains a relation between time t and temperature T:

$$t = \frac{1}{2}H^{-1} = \frac{1}{2}\sqrt{\frac{45}{4\pi^3 g_*}} \frac{m_{\text{Pl}}}{T^2} \approx 0.301 g_*^{-1/2} \frac{m_{\text{Pl}}}{T^2}. \tag{23}$$

Table 1: The values of g_* at different temperature regimes in the early Universe.

Temperature	Significant events	g_*
$T \sim 200$ GeV	all SM particles present	106.75
$T \sim \mathcal{O}(100)$ GeV	electroweak phase transition	106.75
$T < 170$ GeV	top-quark annihilation	96.25
$T < 125$ GeV	Higgs	95.25
$T < 80$ GeV	$W^{\pm}$, Z	86.25
$T < 4$ GeV	bottom-quark	75.75
$T < 1$ GeV	charm-quark, τ	61.75
$T \sim \mathcal{O}(100)$ MeV	QCD phase transition	17.25
$T < 100$ MeV	$\pi^{\pm}$, π^0, μ	10.75
$T < 0.5$ MeV	e^- annihilation	7.25

According to the fundamental equation of thermodynamics the internal energy of system U is given by

$$U = TS - pV + \sum_i \mu_i N_i. \tag{24}$$

When neglecting chemical potential, the following equations follows for the entropy density $s = S/V$:

$$s = \frac{\rho + p}{T}. \tag{25}$$

In the early Universe the equation of state is $p = \rho/3$, and the dominant contribution to the energy density is given by the relativistic particles. Therefore the entropy density s is to a good approximation given by

$$s = \frac{4}{3}\frac{\rho}{T} = \frac{4}{3}\frac{1}{T}\sum \rho_i(T) = \frac{2\pi^2}{45} g_{*\mathrm{s}}(T) T^3, \tag{26}$$

where $g_{*\mathrm{s}}$ is defined as the entropy degrees of freedom

$$g_{*\mathrm{s}}(T) \equiv \sum_{i=\mathrm{bosons}} g_i \left(\frac{T_i}{T}\right)^3 + \frac{7}{8} \sum_{j=\mathrm{fermions}} g_j \left(\frac{T_j}{T}\right)^3. \tag{27}$$

Comparing this with Eq. (21) shows that if all particle species have the same temperature, that is $T_i \simeq T$ for all particles i, in the radiation-dominated epoch, one has

$$g_*(T) \approx g_{*\mathrm{s}}(T). \tag{28}$$

These two quantities start to deviate from each other when the temperature goes below $T \sim 0.5$ MeV.

Using eqs. (22), (23) and (26) we find the following relation between the entropy density and the scale factor:

$$\frac{\dot{s}}{s} = -3\frac{\dot{R}}{R}. \tag{29}$$

Therefore the entropy density scales as $s \sim R^{-3}$. This implies that the total entropy of the universe $S = sV$ stays constant. Conservation of entropy also implies that

$$g_{*\mathrm{s}}(T)T^3R^3 = \text{constant}. \tag{30}$$

2.4 Matter and energy content of the Universe

After inflation, the epoch dominated by vacuum energy, and the reheating the very early Universe was dominated by radiation. The Universe then moved to a matter-dominated epoch. Later on the Universe moved to the its present dark energy dominated phase, which presents itself in the observed accelerated expansion of the Universe. At present, the energy-budget of the Universe is shared between relativistic particles (radiation; photons, neutrinos), non-relativistic matter (baryons, dark matter) and dark energy, the last one constituting about 69 % of the total energy density [8].

From the Big Bang nucleosynthesis and observations from the galactic rotation curve measurements and gravitational lensing surveys it has been for long known that the ordinary baryonic matter can substitute only a small fraction of the total non-relativistic matter content of the Universe: the recent Planck observations favour the baryonic energy density value $\Omega_b \approx 0.048$, while the total matter density is $\Omega_m \approx 0.315$ [8]. This means that about 85 % of the present matter content is in an unknown form, referred to as dark matter, that might be made up of one or several new massive weakly-interacting particle species.

It is now known from CMB and LSS observations that a majority of the dark matter has to be in the form of *cold* dark matter (CDM), which is, along with the dark energy, the main building block of the cosmological concordance model ΛCDM. The cold dark matter relics, created in the early Universe, have a small internal velocity dispersion, meaning that they were non-relativistic already during the formation of galaxies. In the case of CDM, the structure growth proceeds hierarchically: larger structures form through the mergers of smaller objects. The other limiting case would be hot dark

matter (HDM), where the particles are still relativistic during galaxy formation. With HDM the evolution of large-scale structures goes from "top to bottom", where the larger structures fragment and condense into smaller, galaxy-sized objects. The Planck experiment infers from the combination of CMB power spectra and other external data the following value for the present CDM energy density [8]

$$\Omega_c h^2 = 0.1188, \tag{31}$$

where the Hubble parameter h is defined as $h \equiv H(t_0)/(100\text{km s}^{-1}\ \text{Mpc}^{-1})$.

3 Topological defects in cosmology

According to our present understanding the Universe may have undergone series of phase transitions early in its history. In addition to electroweak phase transition, many grand unification theories (GUT), for example, predict several spontaneous symmetry breakings (SSB) to take place at higher temperatures. These phase transitions, where a local or global symmetry is broken, allow the emergence of topological defects. These defects are stable configurations of matter related to the remnants of the false vacuum preceding the SSB, that persist after the phase transition. Depending on the type of the broken symmetry, there are a number of distinct configurations, the most well-known being domain walls, strings and monopoles. Phase transitions and topological defects are often studied in the condensed matter physics, but they might also have a significant role in cosmology through the Kibble mechanism. As topological defects may also have an important role in axion physics, we next briefly describe the basic features of phase transitions and topological defects related to them. This chapter follows mainly Refs. [5, 9].

3.1 Phase transitions in the early Universe

Let use consider the spontaneous symmetry breaking by in a model described by the Lagrangian

$$\mathcal{L} = -\partial_\mu S^* \partial^\mu S - V(S), \tag{32}$$

where S is a complex scalar field and $V(S)$ is the zero-temperature potential given by

$$V(S) = \frac{1}{4}\lambda \left(|S|^2 - v_S^2\right)^2. \tag{33}$$

Here v_S and λ are positive constants. This model is invariant under the global U(1) phase transformation

$$S(x) \to \mathrm{e}^{i\alpha} S(x), \tag{34}$$

where α is independent of the spacetime coordinates x.

This potential has a degenerate minima that corresponds to a circle around the bottom of the mexican hat potential (see Figure 2). The vacuum or the ground state of the theory is defined such a way that

$$\langle 0|S|0\rangle \equiv \langle S\rangle = v_S \mathrm{e}^{i\theta}, \tag{35}$$

where θ is an arbitrary phase, and we refer to v_S as the vacuum expectation value. When the field chooses its ground state (35) it is not anymore invariant under the global transformation (34), which now corresponds to the shift $\theta \to \theta + \alpha$. The symmetry is then spontaneously broken, and we refer to the potential in Eq. (33) as the symmetry breaking potential. The local maximum of the potential, the symmetric state $\langle S \rangle = 0$, is referred to as the false vacuum.

The discussion above is somewhat simplistic as the considered potential is purely classical. In reality the field S interacts with itself and other particles and the potential receives radiative corrections. Without going into details of the calculation here, we just quote the resulting general one-loop effective potential [9]:

$$V_{\text{eff}}(S) = V(S) + \frac{1}{64\pi^2}\left\{ \text{Tr}\left[M^4 \log\left(\frac{M^2}{\sigma^2}\right)\right] \right. \\ \left. +3\text{Tr}\left[M_g^4 \log\left(\frac{M_g^2}{\sigma^2}\right)\right] - 4\text{Tr}\left[M_s^4 \log\left(\frac{M_s^2}{\sigma^2}\right)\right]\right\}, \quad (36)$$

where σ is the renormalization scale and M, M_g and M_s are the scalar, vector (gauge boson) and spinor (fermion) mass matrices, respectively.

Theories such as the Standard Model and GUTs imply that the underlying symmetry is larger than our low energy state possesses. For example, in the standard Hot Big Bang model it is assumed that the Universe has undergone the so-called electroweak phase transition that is associated with the breakdown of $\text{SU}(2)_L \otimes \text{U}(1)_Y \to \text{U}(1)_{\text{EM}}$. In a cosmological setting we then expect the symmetries broken at low temperatures are restored at higher temperatures. We can describe the high-temperature symmetry restoration with the quantitative tools of finite-temperature quantum field theory, where the fields are considered to be coupled in a thermal bath with non-zero temperature T. To lowest order one can consider non-interacting thermal particles and compute the corrections to the zero-temperature potential:

$$V_{\text{eff}}(S,T) = V(S) + \sum_n F_n(S,T), \quad (37)$$

where F_n is the free energy of the system.

Without going into details, the high-temperature effective potential for the model (32), where we only consider self-interactions, can be expressed as [9]

$$V_{\text{eff}}(S,T) = \frac{1}{4}\lambda|S|^4 - \frac{1}{2}\lambda v_S^2|S|^2 + \frac{1}{12}\lambda T^2|S|^2, \quad (38)$$

where we have dropped the S-independent terms. At high-temperatures the potential (38) is effectively quadratic and the field lives in the symmetric state. The phase transition from the symmetric phase to the broken phase occurs when the Universe cools down to the temperatures below the critical temperature T_c, which is given by $T_c = \sqrt{6}v_S$. This process is not instantaneous, as it takes some time for the field to reach its new equilibrium value described by Eq. (35).

3.2 Classification

After the breaking of a discrete symmetry the vacuum manifold $\mathcal{M}$ consists of number of disconnected regions separated by domain walls. An example of this is the standard one-dimensional Goldstone-model, where the real scalar field chooses positive or negative value after moving from the false vacuum. The domain wall is then recognized to be the region between two domains with different field values. The field cannot be transformed continuously in the whole vacuum manifold while maintaining the same value, i.e. we say that there exist non-trivial elements in the homotopy group of the manifold $\mathcal{M}$, which correspond to finite energy configurations. The criterion for the formation of domain walls from the symmetry breaking $\mathcal{G} \to \mathcal{H}$ is $\pi_{\mathrm{D}-1}(\mathcal{M}) \neq \mathcal{I}$, where $\mathcal{G}$ is a symmetry group and $\mathcal{H}$ is its subgroup, $\pi_{\mathrm{D}-1}$ is the homotopy group that counts disconnected components and the vacuum manifold is $\mathcal{M} = \mathcal{G}/\mathcal{H}$. The mentioned one-dimensional Goldstone-model, which is also discussed in Section 3.5.1, corresponds to $\mathcal{G} = \mathcal{Z}_2$, $\mathcal{H} = \mathcal{I}$, $\mathcal{M} = \mathcal{Z}_2/\mathcal{I} = \mathcal{Z}_2$ and $\pi_0(\mathcal{Z}_2) \neq \mathcal{I}$.

The topological defects called strings might emerge in models where the vacuum manifold $\mathcal{M}$ is non-simply connected, meaning that there are holes in $\mathcal{M}$ that prevent contracting loops (on the surface) to a point. In two-dimensional space these holes correspond to finite energy configurations, and in three-dimensional space the configurations stack up to a tube-like structures to minimize the energy. Using the above mathematical notation, the strings arise in theories where a continuous symmetry $\mathcal{G}$ is spontaneously broken to its subgroup $\mathcal{H}$, with the assumption that the vacuum manifold is non-trivial, i.e. $\pi_1(\mathcal{G}/\mathcal{H}) \neq \mathcal{I}$. One example of string formation is the spontaneous breaking of a global U(1) symmetry which will be discussed in Section 3.4. However, the broken symmetry can also be any continuous symmetry, e.g. SU(2), and the details of the string formation and dynamics depend if the broken symmetry is local or global or if the symmetry of the

theory is abelian or non-abelian.

There are also other defects that may form from phase transitions, such as monopoles and textures. Monopoles are point-like defects that emerge from broken spherical symmetries and they are predicted in many GUTs. In cosmology the creation of monopoles is a problem, as these defects can dominate the overall energy density. This is not observed, and as we mentioned, the inflationary paradigm provides a solution to this problem. Textures arise when complicated symmetry groups break. In the condensed matter studies textures appear for example in superfluid ^{3}He.

3.3 The Kibble mechanism

Topological defects may play an important role in the evolution of the Universe. It actually seems that if topological defects are predicted in a certain theory, they are bound to form in a cosmological setting via the Kibble mechanism[2]. The Kibble mechanism is based on the idea that the correlation length $\xi(t)$ of a field in the phase transition is limited by the causal particle horizon d_{H} given by

$$d_{\mathrm{H}} = R(t) \int_0^t \frac{\mathrm{d}t'}{R(t')}. \tag{39}$$

The causality constraint $\xi(t) < d_{\mathrm{H}}$ implies that the correlation length of the field cannot grow endlessly, and there are bound to be separate regions in space where the field in the phase transition is settled on a different value.

For example, in the case of a single real scalar field ϕ discussed in Section 3.5.1, the field chooses one of the two degenerate minima $\pm v_\phi$ that develop below the critical temperature T_c. The choice of minimum depends on the random fluctuations of the field, that have a certain correlation length. If there are then two regions separated by a distance larger than $\xi(t)$ the field can freeze into a different value in these patches which results in a domain wall formation. The same reasoning applies to formation of cosmic strings and other defects, when the theory manifold $\mathcal{M}$ has a non-trivial homotopy group.

In Figure 1 the Kibble mechanism is illustrated in the case of domain wall

[2]Sometimes this is referred to as the Kibble-Zurek mechanism. T. W. B. Kibble studied phase transitions in the early Universe, while W. H. Zurek worked on condensed matter systems.

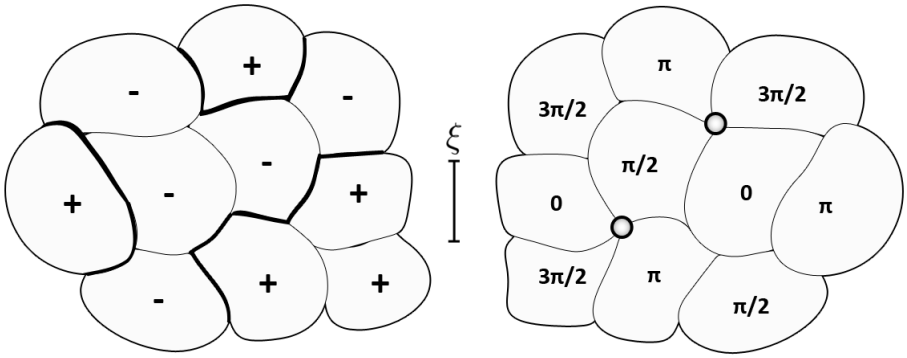

Figure 1: Defect formation via the Kibble mechanism. Left: the domain walls are formed between regions with different discrete field values. Right: the cosmic strings are formed when there is a non-trivial winding around a point.

and string formation. In this case the domain walls form between the regions where the field has chosen either positive or negative value, and the strings form around the region of the false vacuum. We have assumed that the string solution is of the form $v_S e^{i\theta}$, where the phase θ can obtain values between 0 and 2π, as will be discussed in the next section.

3.4 Global cosmic strings

3.4.1 An example: global U(1) strings

A standard text-book example of string formation is the abelian-Higgs model, where the Lagrangian contains a U(1) gauge field and a complex Higgs field. In this model the so-called gauge strings emerge from the spontaneous symmetry breaking of the local U(1) symmetry. However, in this thesis we study axions that are related to a new *global* U(1) symmetry, so there are no gauge fields present in the Lagrangian. The cosmological properties of the global U(1) strings are similar to those of gauge strings, albeit there are some differences – for example, as we are about to see, the energy density of the global strings is logarithmically divergent, while the gauge string energy density is localized[3]. In this section we derive some quantities relevant for global

[3]There is a theorem related to the existence of non-localized stable configurations called Derrick's theorem, see Ref. [9] for details.

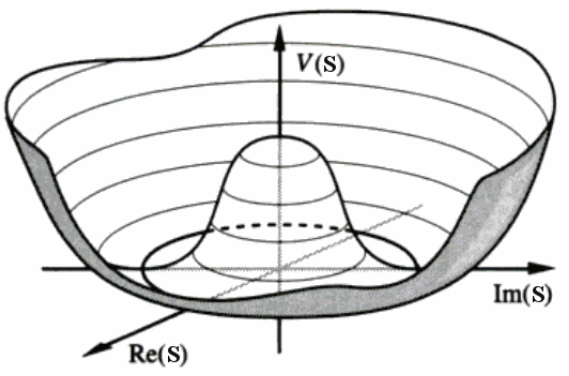

Figure 2: Degenerate circle of minima in the mexican hat potential related to the broken U(1) symmetry. Figure adapted from Ref. [9].

strings and needed in describing axionic strings.

Theory with a complex scalar field S and a global U(1) symmetric Lagrangian density with no gauge fields present is described the model already discussed:

$$\mathcal{L} = -\partial_\mu S^* \partial^\mu S - V(S), \tag{40}$$

where the symmetry breaking potential is

$$V(S) = \frac{1}{4}\lambda \left(|S|^2 - v_S^2\right)^2. \tag{41}$$

Here v_S is the vacuum expectation value of the field S and we have neglected temperature correction terms.

As discussed earlier, during the SSB the field rolls down towards the newly developed minimum. In the case of a complex scalar field, the degenerate minima corresponds to a circle in the bottom of the mexican hat potential – see Figure 2. The phase transition mechanism does not determine the phase of the complex scalar, as the vacuum expectation value depends only upon $|S|$. We are thus left with a phase degree of freedom θ, and the string is formed from this winding around the bottom of the potential. We can then seek a string solution, which we assume for simplicity to be a cylindrically symmetric and static configuration. For a straight static string lying along the z-axis we have the ansatz [9]

$$S(t, \vec{x}) = S(r, \theta) = v_S f(r) \mathrm{e}^{in\theta}, \tag{42}$$

where (r, θ) are given in the standard polar coordinates and n is an integer, called the string winding number, that counts the number of cycles around

the non-trivial region of the false vacuum. The field S approaches v_S far from the false vacuum, which acts as the string core, so the wanted asymptotic behaviour of the unknown real-valued function $f(r)$ is [9]

$$f(r) \to \begin{cases} 1, & r \to \infty \\ 0, & r \to 0. \end{cases} \tag{43}$$

The equation of motion for the complex scalar field S written in the spherical coordinates reduces to the following when considering the ansatz (42) in a flat Minkowski space:

$$\tilde{r}^2 \frac{\partial^2 f(\tilde{r})}{\partial \tilde{r}^2} + \tilde{r} \frac{\partial f(\tilde{r})}{\partial \tilde{r}} - n^2 f(\tilde{r}) - \tilde{r}^2 f(\tilde{r}) \left(f^2(\tilde{r}) - 1 \right) = 0, \tag{44}$$

where $\tilde{r} = \sqrt{\lambda/2} v_S r$. It happens that the winding numbers $n = \pm 1$ correspond to the lowest energy string configurations. We will consider only the case $n = 1$. For a discussion on the higher valued winding numbers, that lead to a more complex inner string structure, see Ref. [9].

We do not know the explicit solution for Eq. (44), but we can use the asymptotic behaviour of the function $f(r)$ to obtain an approximative solution for small r [9]. In this case we can linearize the Eq. (44) in the limit where $\tilde{r} \to 0$ by dropping the $f^3(\tilde{r})$ term. This gives us a familiar Bessel differential equation with an asymptotic form for the solution given by the Bessel function of the first kind $J_1(\tilde{r})$:

$$f(\tilde{r}) \simeq C_1 \times J_1(\tilde{r}) \approx C_1 \times \frac{1}{2} \left(\sqrt{\lambda/2} v_S r \right) \sim \sqrt{\lambda} v_S r, \tag{45}$$

where C_1 is a constant with a value $\mathcal{O}(1)$ [9]. The deviation from the asymptotic limit can be interpret as the width of the string core [9]

$$\delta_s \sim \left(\sqrt{\lambda} v_S \right)^{-1}, \tag{46}$$

which will appear in the string energy density that we will derive next.

Let us compute the energy per unit length of a global string. On length scales larger than the string core width we can neglect the details of the internal structure of the string and the stress-energy tensor can be computed following Ref. [10]. In this case the effective stress-energy tensor for a straight string lying in the z-axis is

$$\tilde{T}^{\mu}_{\nu} \equiv \delta(x)\delta(y) \int T^{\nu}_{\mu} \, \mathrm{d}x \, \mathrm{d}y. \tag{47}$$

By using the invariance under the Lorentz boosts in the z-direction and the conservation of stress-energy tensor[4], $\partial_\nu T^{\mu\nu} = 0$, it can be shown that the only non-zero components of the effective tensor are $\tilde{T}^0_0$ and $\tilde{T}^3_3$. These are then interpreted as the energy density, $\tilde{T}^0_0 = \rho$, and pressure $\tilde{T}^3_3 = -p$, and one can also show that they are equal $\tilde{T}^0_0 = \tilde{T}^3_3$. The pressure is then interpret as the string tension, which is (up to a sign) equal to the energy density of the string. The effective stress-energy tensor can then be written as [10]

$$\tilde{T}^\mu_\nu = \mu_s \delta(x)\delta(y) \times \mathrm{diag}(1, 0, 0, 1), \tag{48}$$

where μ_s is the linear energy density of the string

$$\mu_s = \int T^0_0 \mathrm{d}x\mathrm{d}y = -\int T_{00} \mathrm{d}x\mathrm{d}y. \tag{49}$$

By using the canonical stress-energy tensor

$$T_{\mu\nu}(x) = \sum_i \frac{\partial \mathcal{L}}{\partial\left(\partial^\nu \phi^i\right)}\, \partial_\mu \phi^i - g_{\mu\nu}\mathcal{L}. \tag{50}$$

in the static string case, described by Eq. (44), the linear energy density reduces to

$$\begin{aligned}
\mu_s &= -\int \mathcal{L}\ \mathrm{d}x\mathrm{d}y = \int \mathrm{d}x\mathrm{d}y \left(\partial_\mu S^* \partial^\mu S + V(|S|)\right) \\
&= \int_0^\infty \int_0^{2\pi} \mathrm{d}r\mathrm{d}\theta\ r \left[\frac{\partial S}{\partial r}\frac{\partial S^*}{\partial r} + \frac{1}{r^2}\frac{\partial S}{\partial \theta}\frac{\partial S^*}{\partial \theta} + V(|S|)\right] \\
&= \int_0^\infty \mathrm{d}r 2\pi v_S^2 r \left[\left(\frac{\partial f(r)}{\partial r}\right)^2 + \frac{f^2(r)}{r^2} + \frac{1}{4}\lambda v_S^2 \left(f^2(r) - 1\right)^2\right].
\end{aligned} \tag{51}$$

Assuming that the function $f(r)$ changes all at once from one asymptotic value to another, i.e. from zero to one at $r = \delta_s \simeq \left(\sqrt{\lambda} v_S\right)^{-1}$, the above integral yields

$$\mu_s \approx \frac{\pi}{4} v_S^2 + \left[2\pi v_S^2 \log(r)\right]\Big|_{r=\delta_s}^\infty. \tag{52}$$

As we see, the energy density diverges logarithmically and we must impose a cut-off L at some large radius. This logarithmic divergence arises from the long-range interactions of the Goldstone boson field and it is not present in

[4]Here we assume negligible gravity and cartesian coordinates.

the case of standard gauge strings [9]. In a cosmological setting this imposed cut-off L, that characterizes the length scale of the string, can be thought as the distance between neighbouring strings or as the curvature radius of the strings. We expect that the length scale L is comparable to the horizon scale, i.e. $L \sim H^{-1} \sim t$. In the literature it is usually assumed that in the case of global strings one can neglect the contribution of the string core. Then the linear energy density is given by

$$\mu_s \approx 2\pi v_S^2 \log\left(\frac{L}{\delta_s}\right). \tag{53}$$

3.4.2 Global string evolution

The study of the local and global string evolution has a long history with semianalytical and numerical studies done by several groups. The gauge strings have gotten more attention, but according to field-theoretic simulations these two types of strings have many similarities. Their dynamics do not differ greatly on cosmological scales, and the main difference between them is the enhanced radiative decay of the global strings into the Nambu-Goldstone bosons. Due to the shared similarities, one usually assumes that the global U(1) strings, or in our case axionic strings, behave approximately as local Nambu strings. [9, 11]

The strings that emerge from the phase transition form a complicated string-network that permeates through the entire Universe. After formation the whole network is comprised of two main components: an infinite network of long strings and smaller closed string loops forming a sub-dominant component. How the whole network evolves in the early Universe depends on the details of the model, but the basic picture is quite well understood.

If the strings interact with other particles in the primordial plasma and the symmetry breaking scale is high enough, they go through an epoch, where the strings experience a damping force from the radiation background. During this damped evolution epoch string loops will decay and any possible substructure in the long-string network is smoothened out. At later times the effect of damping forces will be negligible and the long strings can move more freely and develop relativistic velocities. Through the frequent intersection and reconnection of strings the long-string networks fragment into string loops, which can then further fragment into smaller configurations. For global U(1) string loops the main energy-loss mechanism is the radiation to NGBs in just $\mathcal{O}(10)$ oscillations. The emission of the NGBs is also

possible for long strings, as they are perturbed by small-scale "kinks". This mechanism prevents the string-network from dominating the overall energy density of the Universe. However, string domination is possible in certain models where strings are non-intercommuting, meaning that they can just pass through each other [9].

A well established observation in the literature is that the local and global string networks enter the so-called scaling solution, where the large-scale structure scales with the horizon scale [9]. In this regime the energy density of the long-string network is described by

$$\rho_s = \frac{\mu_s}{L^2} = \xi_s \frac{\mu_s}{t^2}, \tag{54}$$

where the scaling parameter ξ_s essentially counts the average number of long strings in a Hubble volume [12].

There are several approaches and different interpretations discussed in the literature when studying the evolution of global strings and the produced number of NGBs. The standard approach used is to start from either the total string network density consisting of the long string and string loop energy densities, or just the long string energy density assuming that it dominates the system, and numerically follow the evolution of these components. The procedure with slightly different methods in axion context is described for example in Refs. [9, 11, 13] and Refs. [12, 14]. Here we will follow one of these, and assume that the long-string energy density dominates and evolves according to [14]

$$\frac{\mathrm{d}\rho_s}{\mathrm{d}t} = -2H\left(1 + \langle v^2 \rangle\right)\rho_s - \Gamma_{\mathrm{loop}}\rho_s - \Gamma_{\mathrm{NG}}\rho_s, \tag{55}$$

where $\langle v^2 \rangle$ is the average of the string velocity squared, Γ_{loop} is the loop production rate and Γ_{NG} is the direct emission rate of NGBs. If we neglect the NGB and loop production terms, the string evolution is governed by

$$\frac{\mathrm{d}\rho_s}{\mathrm{d}t} = -2H\left(1 + \langle v^2 \rangle\right)\rho_s, \tag{56}$$

where the first term on the right-hand side takes into account the dilution ($-3H\rho_s$) and stretching ($H\rho_s$) of the strings. The equation of state parameter for these strings is $w_{\mathrm{eos,string}} = -1/3 + 2/3\langle v^2 \rangle$.

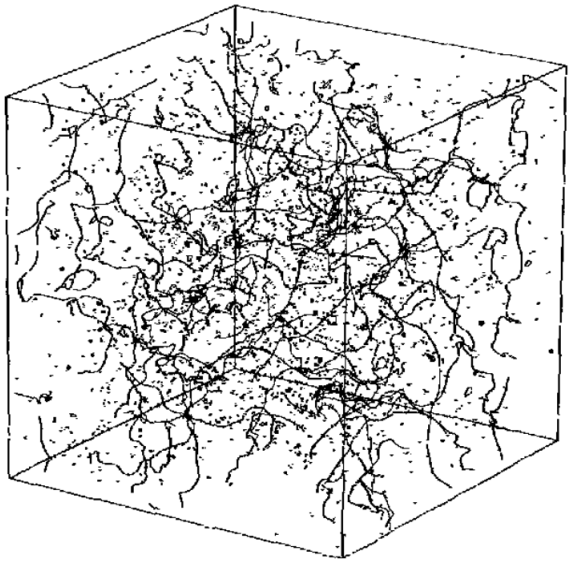

Figure 3: A numerical simulation of a U(1) cosmic string network, that consists of infinite strings and finite string loops. Figure from Ref. [5].

3.5 Domain walls

3.5.1 Examples

The simplest one-dimensional Goldstone model for a real scalar field ϕ is given by the Lagrangian density

$$\mathcal{L} = -\frac{1}{2}\partial_\mu\phi\partial^\mu\phi - V(\phi). \tag{57}$$

The symmetry-breaking potential $V(\phi)$ has the standard double-well form

$$V(\phi) = \frac{1}{4}\lambda\left(\phi^2 - v_\phi^2\right)^2, \tag{58}$$

and it has a *discrete* set of degenerate minima. The potential above breaks the discrete $\mathcal{Z}_2$ reflection symmetry when the field ϕ adopts one of the two possible values, $\langle\phi\rangle = \pm v_\phi$. In a cosmological setting the domain wall forms between the different causal regions, where the field obtains different value in the phase transition. The transition region where the scalar field smoothly transfers from one vacuum state to another is interpret as a domain wall.

Let us consider an infinite static wall lying in the (x, y)-plane located at $z = 0$. The scalar field solution $\phi(z)$ describes a kink-like wrinkle that is

localized around $z = 0$, and where the field interpolates between the two vacuum state, that are localized at the spatial infinity, $z \to -\infty, \phi \to -v_\phi$ and $z \to \infty, \phi \to v_\phi$. The equation of motion for $\phi(z)$ reads

$$\frac{\partial^2 \phi}{\partial z^2} - \frac{\partial V(\phi)}{\partial \phi} = 0. \tag{59}$$

This has the solution

$$\phi(z) = v_\phi \tanh\left[\sqrt{\lambda/2} v_\phi z\right]. \tag{60}$$

Combining the above with the canonical stress-energy tensor given in Eq. (50) and the Lagrangian in Eq. (57) allows us to write the stress-energy tensor as

$$T_{\mu\nu} = \left(\frac{\mathrm{d}\phi}{\mathrm{d}z}\right)^2 \mathrm{diag}(-1, 1, 1, 0). \tag{61}$$

From this follows for the surface density of a domain wall

$$\sigma_w = -\int T_{00} \mathrm{d}z = \frac{4}{3}\sqrt{\frac{\lambda}{2}} v_\phi^3. \tag{62}$$

The thickness of the wall is characterized by the argument of the hyperbolic tangent solution in Eq. (60)[5] through

$$\delta_w \sim \left(\sqrt{\lambda/2} v_\phi\right)^{-1} \sim \left(\sqrt{\lambda} v_\phi\right)^{-1}. \tag{63}$$

Let us next consider a more complicated model for a complex scalar field S that is related to our discussion on axion models. We assume that the field S is again of the form given in Eq. (42), and we consider the following periodic $\mathcal{Z}_N$-symmetric (when $N > 1$) Lagrangian:

$$\mathcal{L}_S = -\partial_\mu S^* \partial^\mu S - V(S) + 2\frac{m^2 v_S^2}{N^2}\left[\cos(N\theta) - 1\right], \tag{64}$$

where N is an integer. The potential $V(S)$ is again of the standard symmetry-breaking form, and we do not specify here the source of the periodic mass term. In axion models the periodic mass term arises from the periodic QCD vacuum (see Sections 4 and 5). We will consider a potential of this form when discussing the production of axions from the domain wall configurations.

[5]Keeping the factor of $\sqrt{2}$ varies within literature, e.g. Ref. [5] keeps it, but Ref. [9] neglects it.

If we assume that $m^2 v_S^2 \ll \lambda v_S^4$ the above Lagrangian has an approximate (global) U(1) symmetry, broken by the periodic mass term. At low energies where the field is trapped in the bottom of the mexican hat potential we can set $f(r) = 1$ [9]. The phase θ of the field S that is left free can be interpret as a new field obeying the following Lagrangian:

$$\mathcal{L}_\theta = -v_S^2 \partial_\mu \theta^* \partial^\mu \theta + 2\frac{m^2 v_S^2}{N^2} \left[\cos(N\theta) - 1\right]. \tag{65}$$

The potential in Eq. (65) has N-degenerate minima $\theta = 2\pi n/N$, with $n = 0, 1, \ldots, N-1$. The regions in the Universe with these N distinct vacua are separated by domain walls [15].

It might not be apparent why domain walls are formed even in the case $N = 1$. One would expect that as there is only one vacuum, there is no reason for the existence of domain walls. However, in axion models the symmetry-breaking potential $V(S)$ leads to the formation of strings that emerge from the winding of the bottom of the mexican hat potential, where θ changes by 2π around the false vacuum. The periodic symmetry-breaking term then leads to the strings being attached to N domain walls. Now the domain walls will form between regions with phases θ differing by more than 2π [16], with both sides of the wall being in the same vacuum.

There actually is an analytic solution for the equation of motion obtained from Eq. (65) in the case of a static thin wall:

$$\theta = \frac{2\pi n}{N} + \frac{4}{N}\arctan(\exp(mz)). \tag{66}$$

From this one obtains the domain wall surface energy density:

$$\sigma_w = -\int T_{00} \mathrm{d}z = 2v_S^2 \int \left(\frac{\mathrm{d}\theta}{\mathrm{d}z}\right)^2 \mathrm{d}z = 16\frac{m v_S^2}{N^2}. \tag{67}$$

An example of a periodic potential that gives rise to domain walls is the sine-Gordon model [9], whose Lagrangian is given by Eq. (64) when $N = 1$.

3.5.2 Domain wall evolution

The cosmological string evolution coheres on some level with the evolution of the domain wall systems. The domain wall configurations can collide and reconnect, possibly accompanied with the production of particles. Walls also

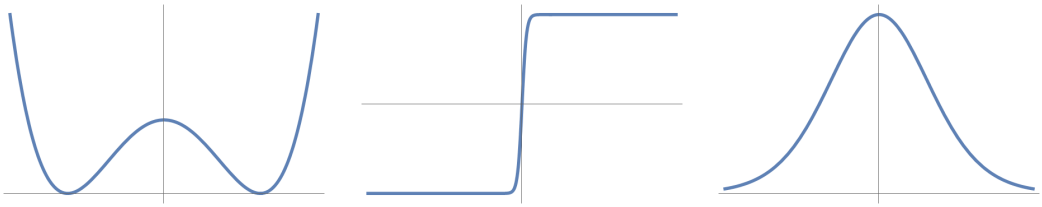

(a) (b) (c)

Figure 4: The one-dimensional Goldstone model. (a) potential in Eq. (57), (b) tanh-solution in Eq. (60) and (c) surface density in Eq. (62).

go through a damped epoch, where their velocities are slowed down by the radiation background. For $\mathcal{Z}_2$-walls one expects the evolution of domain walls to be scale-invariant and the typical size of walls to be of the horizon scale, while the evolution of $\mathcal{Z}_N$-walls might lead to different outcomes.

The domain wall configurations usually start to dominate the energy density of the Universe, which does not agree with the observations. This scenario can be avoided if there is an inflationary period that dilutes away the domain wall density. The wall domination can also be avoided in some hybrid models, where the domain walls are attached to or bounded by cosmics strings, i.e. the domain walls are part of a larger string-wall network [9].

These string-wall configurations are formed in two stages. First the strings are formed in the very early Universe in a phase transition, where for example global U(1) breaks. These strings follow the evolution described in Section 3.4.2 and approach the scale-invariant evolution. The string-bounded domain walls emerge then from a later phase transition, which can arise from a potential such as in Eq. (64). The evolution of these configurations obviously depends on the details of the model, but in certain models the string-wall network quickly fragments into smaller pieces by self-intersections, which then decay via the preferred channel to Nambu-Goldstone bosons or gravitational waves. This is usually the case with models given by Eq. (64) with $N = 1$. This is relevant for the axionic string-wall configuration studies [15, 17, 9]. However, within the axion models, usually with $N > 1$, it is possible to have long-lived configurations that are incompatible with the standard cosmological picture [15].

4 The strong CP problem and the Peccei-Quinn solution

The axion model provides an elegant solution to the so-called strong CP problem. This problem has its groundings in the so-called $\mathrm{U(1)_A}$ problem, which was solved in the 1970's when the studies revealed the complex structure of the low-energy QCD vacuum. In this chapter we describe in detail these two problems, and then move to study the Peccei-Quinn mechanism which solves the strong CP problem in terms of the axion field.

4.1 The QCD Lagrangian and the $\mathrm{U(1)_A}$ problem

The standard QCD Lagrangian that describes the strong interactions of quarks and gluons is given by

$$\mathcal{L}_{\mathrm{QCD}} = -\frac{1}{4} G^a_{\mu\nu} G^{\mu\nu}_a + \sum_r \bar{\psi}^a_r \left(\mathrm{i} \not{D}^b_a - m_r \delta^b_a \right) \psi_{rb}, \tag{68}$$

where ψ^a_r is the quark with a flavour r, colour charge a and mass m_r. The covariant derivative $\not{D}$ has the form

$$\not{D}^b_a = \gamma_\mu \left(\partial^\mu \delta^b_a + \mathrm{i} g_s \frac{1}{2} \lambda^i_{ab} G^\mu_i \right), \tag{69}$$

where G^a_μ are the gluon fields and λ^i_{ab} are the SU(3) generators. The gluon field strength tensors $G^a_{\mu\nu}$ are given by

$$G^a_{\mu\nu} \equiv \partial_\mu G^a_\nu - \partial_\nu G^a_\mu - g_s f_{abc} G^b_{\mu\nu} G^c_{\mu\nu}, \tag{70}$$

where f_{abc} are the SU(3) structure functions.

In the massless limit $m_r \to 0$ the Lagrangian (68) has a global symmetry $\mathrm{U(1)_V} \otimes \mathrm{U(1)_A}$. Here $\mathrm{U(1)_V}$ denotes the singlet vector transformation under which the chiral fields, $\psi_{R/L} \equiv (1/2)(1 \pm \gamma^5)\psi$, transform as

$$\psi_{r,R} \to \psi'_{r,R} = \mathrm{e}^{\mathrm{i}\alpha} \psi_{r,R}, \;\; \psi_{r,L} \to \psi'_{r,L} = \mathrm{e}^{\mathrm{i}\alpha} \psi_{r,L}, \tag{71}$$

and $\mathrm{U(1)_A}$ refers to the singlet axial transformation which acts differently on the chiral fields:

$$\psi_{r,R} \to \psi'_{r,R} = \mathrm{e}^{-\mathrm{i}\alpha} \psi_{r,R}, \;\; \psi_{r,L} \to \psi'_{r,L} = \mathrm{e}^{\mathrm{i}\alpha} \psi_{r,L}. \tag{72}$$

The limit of vanishing quark masses is not realized in nature, but for the lightest quarks u, d and s the symmetries $\mathrm{U}(1)_\mathrm{V}$ and $\mathrm{U}(1)_\mathrm{A}$, that are part of a larger symmetry group $\mathrm{U}(3)_\mathrm{V} \otimes \mathrm{U}(3)_\mathrm{A}$[6], are approximative symmetries as the light-quark masses are small compared to the QCD scale Λ_QCD. It turns out this *almost* agrees with what is seen experimentally. The vector symmetry $\mathrm{U}(1)_\mathrm{V}$ is invariant, and through the Noether's theorem it corresponds to the baryon number conservation. The spontaneous breaking of the subgroup $\mathrm{SU}(3)_\mathrm{V} \otimes \mathrm{SU}(3)_\mathrm{A}$ due to the formation of quark condensates to a single group $\mathrm{SU}(3)_\mathrm{V}$ is also seen as the emergence of the eight massless Nambu-Goldstone bosons according to the Goldstone's theorem. The small, but non-zero mass terms explicitly break the symmetry, and what is observed are the eight massive pseudo-Nambu-Goldstone bosons: the three pions $\pi^0, \pi^\pm$, four kaons $K^0, \bar{K}^0, K^\pm$ and the eta meson η. [18, 19]

However, what is *not* seen is any suitable ninth Nambu-Goldstone boson related to the spontaneous breaking of $\mathrm{U}(1)_\mathrm{A}$. Closest candidate is the eta prime meson η', which has the right quantum numbers but is too heavy, $m_{\eta'} \approx 960$ MeV, as one can find the following upper-bound for the $\mathrm{U}(1)_\mathrm{A}$ NGB mass [4]

$$m_A \lesssim \sqrt{3} m_\pi. \tag{73}$$

Historically, this question of the missing pseudo-NGB is dubbed as the $\mathrm{U}(1)_\mathrm{A}$ problem [18, 20, 21].

It then seems that $\mathrm{U}(1)_\mathrm{A}$ is not a genuine symmetry of QCD, albeit in the massless quark limit it seems to be present. The resolution to this problem begins from the fact that in the quantized theory the symmetry $\mathrm{U}(1)_\mathrm{A}$ is actually anomalously broken by the Adler-Bell-Jackiw (ABJ) anomaly [22]. The axial current J_5^μ corresponding to the axial symmetry gets contribution from a triangle-loop diagram, where two gluons are coupled to fields through a quark loop. It is similar anomalous-diagram that allows the neutral pions to decay into two photons, $\pi^0 \to \gamma\gamma$. Due to the chiral anomaly the divergence of the axial current is non-vanishing[7]:

$$\partial_\mu J_5^\mu = C \frac{g_s^2}{32\pi^2} G_{\mu\nu}^a \tilde{G}_a^{\mu\nu}, \tag{74}$$

where C is a numerical constant and $\tilde{G}_a^{\mu\nu} = (1/2)\epsilon^{\mu\nu\alpha\beta} G_{\alpha\beta a}$ is the so-called dual of the gauge field strength tensor. [18, 20, 22]

[6] If we consider the three lightest quarks $N_f = 3$, in a general case we would have the symmetry group $\mathrm{U}(N_f)_\mathrm{V} \otimes \mathrm{U}(N_f)_\mathrm{A}$ that can be decomposed into groups $\mathrm{SU}(N_f)_\mathrm{V/A}$ and $\mathrm{U}(1)_\mathrm{V/A}$.

[7] Note that there is also an additional term usually included that vanishes in the zero-mass limit, $2im\bar{\psi}\gamma^5\psi$.

The term $G_{\mu\nu}\tilde{G}^{\mu\nu}$ can actually be written as the divergence $\partial^\mu K_\mu$, where K_μ is the Chern-Simons current that can be expressed as [23, 24]

$$K_\mu = \frac{1}{16\pi^2}\epsilon_{\mu\nu\alpha\beta}\left(G^{a\nu}G^{a\alpha\beta} + \frac{g_s}{3}f_{abc}G^{a\nu}G^{b\alpha}G^{c\beta}\right). \tag{75}$$

When integrating over the divergence of Eq. (75) in the theory action the integral can be written as a surface-integral. One can then find boundary conditions, e.g. $G^\mu_a = 0$ at spatial infinity, that result in the surface-integral vanishing without affecting physics [23] – again restoring the presence of the $\mathrm{U(1)_A}$ symmetry. However, here is where the subtleties of the QCD vacuum come to play. The standard QCD vacuum is not gauge-invariant, and one can find gauge conditions that allow the term in Eq. (74) to be non-vanishing and to have physical consequences [20, 22].

The proper QCD vacuum can be constructed as a linear combination of the $|n\rangle$ vacua, which is usually referred to as the θ-vacuum:

$$|\theta\rangle = \sum_{n=-\infty}^{+\infty} \mathrm{e}^{-\mathrm{i}n\theta}\,|n\rangle\,, \tag{76}$$

where $\theta \in [0, 2\pi]$ and n is the winding number. As one can see, this vacuum is periodic as $|\theta + 2\pi\rangle = |\theta\rangle$. The non-vanishing configurations correspond to topologically non-trivial solutions of the classical field equations in the 4-dimensional Euclidean space called *instantons*. These solutions describe transitions between the different vacuum states. These non-trivial transitions yield a non-vanishing value for the total-derivative integral in the action [18]. If one takes into account for the possible transitions in the θ-vacuum, it is equivalent to including the so-called theta term in the theory Lagrangian:

$$\mathcal{L}_\theta = \theta q = \theta\frac{g_s^2}{32\pi^2}G^a_{\mu\nu}\tilde{G}^{\mu\nu}_a. \tag{77}$$

Here q is the so-called Pontryagin index that distinguishes between the different homotopy classes, i.e. is defined as the difference between the different vacuum states corresponding to different winding numbers (see, e.g. Refs. [18, 20, 25]).

4.2 The strong CP problem

As discussed above, due to the complex structure of the QCD vacuum one has to include the θ-term into the total QCD Lagrangian

$$\mathcal{L}_{\mathrm{QCD,tot}} = \mathcal{L}_{\mathrm{QCD}} + \mathcal{L}_\theta. \tag{78}$$

The theta term violates both parity P and charge-parity CP conservation[8] as the $G\tilde{G}$ term is CP-odd, while in the "naive" QCD Lagrangian P and CP are automatically conserved. Before discussing the effect of this term, let us study more closely how the θ parameter gets additional contribution from the weak interactions.

Let us first allow the fermion mass to be complex, i.e. $m_f = |m_f| \exp(\mathrm{i}\varphi_f)$, where φ_f is the phase of each fermion mass in the diagonal mass matrix $\mathcal{M}$. Then the fermion mass part of the Lagrangian can be written as

$$\mathcal{L}_{m,f} = -\frac{1}{2} \sum_f m_f \overline{\psi}_f \left(1 + \gamma^5\right) \psi_f - \frac{1}{2} \sum_f m_f^* \overline{\psi} \left(1 - \gamma^5\right) \psi_f \tag{79}$$

$$= -\sum_f |m_f| \, \overline{\psi}_f \mathrm{e}^{\mathrm{i}\varphi_f \gamma^5} \psi_f. \tag{80}$$

If we redefine the fermion fields ψ_f by making the U(1) transformation given in Eq. (72), i.e.

$$\psi_f \to \mathrm{e}^{\mathrm{i}(\alpha_f/2)\gamma^5} \psi_f \ , \ \overline{\psi}_f \to \overline{\psi}_f \mathrm{e}^{\mathrm{i}(\alpha_f/2)\gamma^5}, \tag{81}$$

we see that the mass Lagrangian transforms as

$$\mathcal{L}_{m,f} \to \mathcal{L}_{m,f} = -\sum_f |m_f| \, \overline{\psi}_f \mathrm{e}^{\mathrm{i}\alpha_f \gamma^5} \mathrm{e}^{\mathrm{i}\varphi_f \gamma^5} \psi_f. \tag{82}$$

Due to the axial U(1) anomaly the effect of this redefinition changes the path integration measure and one gets additional anomaly-type terms in the Lagrangian [18, 26]. The transformation (81) is then equivalent to the following shift in the QCD Lagrangian [18]

$$\theta \to \theta + \sum_f \alpha_f. \tag{83}$$

From Eq. (82) we see that the chiral transformation changes φ_f to $\varphi_f + \alpha_f$. As θ is not invariant under chiral transformation and a change of variables in the path integral cannot yield any change in physics, we have that physical observables cannot depend on the parameter θ alone [18]. However, we have

[8]Parity transformation P: inverting the spatial coordinates of a particle. Charge-conjugation transformation C: interchanging a particle with its antiparticle

that the quantity $\theta - \sum_f \varphi_f$ is invariant. Equivalently, we can say that the following quantity remains invariant under $\mathrm{U(1)_A}$

$$\mathrm{e}^{-\mathrm{i}\theta} \prod_f m_f = \mathrm{e}^{-\mathrm{i}\theta} \prod_f |m_f| \, \mathrm{e}^{\mathrm{i}\varphi_f} = \mathrm{e}^{-\mathrm{i}(\theta - \sum_f \varphi_f)} \prod_f |m_f| \, . \tag{84}$$

Let us then choose $\varphi_f = -\alpha_f$ and define the effective angle $\bar{\theta}$ as

$$\begin{aligned} \bar{\theta} &\equiv \theta + \sum_f \alpha_f = \theta - \sum_f \varphi_f = \theta - \mathrm{Arg} \left(\prod_f m_f \right) \\ &= \theta - \mathrm{Arg} \left(\det \mathcal{M} \right) . \end{aligned} \tag{85}$$

Now the total QCD Lagrangian contains a gauge-invariant, physically relevant CP violating term

$$\mathcal{L}_{\bar{\theta}} = \bar{\theta} \frac{g_s^2}{32\pi^2} G^a_{\mu\nu} \tilde{G}^{\mu\nu}_a . \tag{86}$$

Through an effective pion-nucleon coupling the CP violating term (86) gives an observable neutron electric dipole moment (NEDM). In the literature there are numerous different estimates on the $\bar{\theta}$-dependent dipole moment d_n. One of the most recent and conservative ones being [3]

$$d_n \approx 4.5 \times 10^{-15} \bar{\theta} \; e \text{ cm}. \tag{87}$$

The experimental observations set a tight upper bound $|d_n| < 2.9 \times 10^{-26} \, e$ cm [27][9], which translates into the upper bound for $\bar{\theta}$,

$$\bar{\theta} < 0.6 \times 10^{-11} . \tag{88}$$

Such a small value for $\bar{\theta}$ is of course not forbidden, but from the first principles there is no reason to expect that the two terms in Eq. (85) should almost exactly cancel each other. Solving the $\mathrm{U(1)_A}$ problem thus leads to a new fine-tuning problem, or a *naturalness* problem [21], referred to as the strong CP problem.

The proposed solutions in the literature to the strong CP problem can be roughly divided into two categories: the spontaneous (or soft) breaking of the CP symmetry and an additional chiral symmetry. The former one assumes

[9] Different methods are used to measure NEDM, the one used by Ref. [27] gives most stringent limits, but there are other methods that give similar results, see e.g. Ref. [28].

that the CP symmetry is spontaneously broken and therefore one could set $\theta = 0$ [23]. This introduces additional CP-violating phases into the fermion mass parameters, which in itself is not a problem. However, it seems that the weak interaction CP-violation agrees with the one contained in the Cabibbo-Kobayashi-Maskawa matrix [21, 3].

For the additional chiral symmetry there have been mainly two propositions in the literature: one of the lightest quarks is massless or that the Standard Model has a new global U(1) chiral symmetry[10]. We see from Eqs. (84) and (85) that in the case of a zero-mass quark the θ parameter is not physical and it can be removed with field redefinitions. However, the possibility of a zero-mass quark is not preferred by the observations or lattice-simulations [3, 31]. A more interesting solution is then the latter one, where a new global U(1) symmetry is introduced to the theory. This was first studied by Peccei and Quinn [1, 2], and their solution to the strong CP problem is referred to as the PQ-mechanism.

4.3 The Peccei-Quinn solution and the axion

The original idea of Peccei and Quinn [1, 2] was effectively to promote the coupling $\bar{\theta}$ to a dynamical parameter. The dynamical $\bar{\theta}$ theory means that the different values of $\bar{\theta}$ do not describe different theories with different coupling constants, but a single given theory, where $\bar{\theta}$ distinguishes different vacuum states with different energies [21]. In Ref. [1] it was argued that from the two possible stationary points (0 and π), which are obtained from the effective potential given by the anomalous gluon term, the true vacuum lies at $\bar{\theta} = 0$. This has later been confirmed for example in Ref. [32]. This idea was taken up by Weinberg [33] and Wilczek [34], who showed that the mechanism proposed by in Refs. [1, 2] leads to the addition of a new pseudoscalar[11] particle, the axion.

The PQ mechanism is based on the idea that the theory contains an additional global U(1) symmetry, that suffers from the chiral (or axial) anomaly described above. However, because quarks are not massless, it happens that the Standard Model does not contain such a symmetry. This additional symmetry, called the Peccei-Quinn symmetry or $\mathrm{U}(1)_{\mathrm{PQ}}$, is usually implemented

[10] Recently there have been new propositions that introduce high-colour versions of the conventional QCD, that are still conceptually close to these considerations – see Refs. [29, 30].

[11] Pseudoscalars are CP-odd, i.e. $a \to -a$ under a CP transformation.

into the theory by additional scalar fields in the Higgs-sector. We will discuss these different ways of implementing the symmetry when we study the different axion models in the next chapter.

Here we will follow the literature [21, 23] and sketch the PQ mechanism with the already added axion field. Throughout this thesis we will consider the axion field $a(x)$ as the phase degree freedom of a new complex scalar field S, that we will refer to as the PQ field. The field has the SSB-type potential discussed in Section 3.1, and we present the field S in the form

$$S(x) = \eta(x)\exp\left(\mathrm{i}\frac{a(x)}{v_S}\right), \tag{89}$$

where $v_S = \langle 0|S|0\rangle$ is the symmetry breaking scale of the global $\mathrm{U}(1)_{\mathrm{PQ}}$ symmetry. As discussed in Section 3.1, due to the SSB the axion field has a shift symmetry $a(x) \to a(x)+\alpha v_S$. In addition to the spontaneous symmetry breaking, $\mathrm{U}(1)_{\mathrm{PQ}}$ is also explicitly broken by the ABJ-anomaly and the low-energy instanton effects, meaning that the axion field acquires the anomalous coupling to gluons. The Lagrangian of the theory has then the form

$$\mathcal{L}_{\mathrm{QCD,tot}} = \mathcal{L}_{\mathrm{QCD}} + \mathcal{L}_{\bar{\theta}} + \mathcal{L}_a \tag{90}$$

$$= \mathcal{L}_{\mathrm{QCD}} + \bar{\theta}\frac{g_s^2}{32\pi^2}G^a_{\mu\nu}\tilde{G}^{\mu\nu}_a + \frac{a}{v_s}\frac{g_s^2}{32\pi^2}G^a_{\mu\nu}\tilde{G}^{\mu\nu}_a - \frac{1}{2}\partial_\mu a\partial^\mu a, \tag{91}$$

where we have for now neglected other possible interaction terms, which will be discussed in the next chapter.

One can then show that the effective potential for the axion field has a minimum at $\langle a\rangle = -v_S\bar{\theta}$ [23]

$$\langle\frac{\partial V_{\mathrm{eff}}}{\partial a}\rangle = -\frac{1}{v_S}\,\frac{g_s^2}{32\pi^2}\langle G^a_{\mu\nu}\tilde{G}^{\mu\nu}_a\rangle\Big|_{\langle a\rangle=-v_S\bar{\theta}} = 0, \tag{92}$$

where $\langle a\rangle = \langle 0|a|0\rangle$. Due to the periodicity of $\bar{\theta}$, $\langle a\rangle$ is periodic with $\langle a\rangle = 2\pi k v_S$, where k is an integer. When we substitute the physical axion field $a_{\mathrm{phys}} = a - \langle a\rangle$ [23] to the Lagrangian (91) the $\bar{\theta}$ term vanishes (in the following we will denote a_{phys} with a). We have thus seen that the axion field can solve, through the PQ mechanism, the strong CP problem.

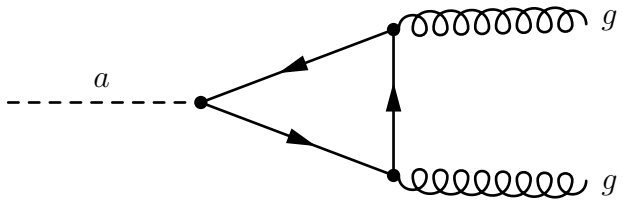

Figure 5: Triangle loop diagram corresponding to the anomalous axion-gluon-gluon coupling.

5 The axion

In this chapter we shall consider the axion in more detail. We start by reviewing the different propositions how to implement axions into the Standard Model. First we consider the "visible" axion model [1, 2, 33, 34], which predicts an axion with a mass of the electroweak scale. The model is, however, ruled out by the experimental data, and is replaced by the "invisible" axion models, which predict a very light axion that avoids the collider constraints. We also discuss the general properties and couplings of this light axion, and conclude the chapter by presenting some astrophysical bounds for the axion models and by introducing different experimental setups that try to directly detect axions. The bounds coming from the cosmological considerations are discussed in the next chapter, where we study the role of axions as a cold dark matter candidate.

5.1 Axion models

5.1.1 The visible axion model

The original axion model was formulated by Peccei and Quinn [1, 2], Weinberg [33] and Wilczek [34]. This model introduces the Peccei-Quinn symmetry through two Higgs doublets H_u and H_d, that give masses to the up- and down-quarks. The relevant parts of the Yukawa-sector of the Lagrangian are

[23]

$$\mathcal{L}_Y = \Gamma^u_{ij}\bar{q}_{Li}H_u u_{Rj} + \Gamma^d_{ij}\bar{q}_{Li}H_d d_{Rj} + \Gamma^l_{ij}\bar{L}_{Li}H_d l_{Rj} + \text{h.c.}, \tag{93}$$

where q_L and L_L are the left-handed SU(2) quark and lepton SM doublets, u_R, d_R and l_R are the corresponding right-handed quark and lepton fields. The quark sector of the Lagrangian (93) remains invariant under the chiral $\mathrm{U(1)_{PQ}}$ transformation

$$u_L \to \mathrm{e}^{\mathrm{i}\Gamma_1/2}u_L, \quad u_R \to \mathrm{e}^{-\mathrm{i}\Gamma_1/2}u_R \tag{94}$$

$$d_L \to \mathrm{e}^{\mathrm{i}\Gamma_2/2}u_L, \quad d_R \to \mathrm{e}^{-\mathrm{i}\Gamma_2/2}d_R \tag{95}$$

$$H_u \to \mathrm{e}^{\mathrm{i}\Gamma_1}H_u, \quad H_d \to \mathrm{e}^{\mathrm{i}\Gamma_2}H_d. \tag{96}$$

In this model the axion field a is not realized as a phase of a new complex scalar field as in Eq. (89), but as a common phase field of the two doublets [23]:

$$H_u \sim v_u \mathrm{e}^{\mathrm{i}a\tilde{x}/v_{\mathrm{EW}}}\left[1 \;\; 0\right]^{\mathrm{T}}, \; H_d \sim v_d \mathrm{e}^{\mathrm{i}a/\tilde{x}v_{\mathrm{EW}}}\left[0 \;\; 1\right]^{\mathrm{T}}, \tag{97}$$

where $\tilde{x} = v_d/v_u$ and $v_{\mathrm{EW}} = \sqrt{v_u^2 + v_d^2} \approx 246$ GeV. In this model the spontaneous breaking of the $\mathrm{U(1)_{PQ}}$ symmetry occurs simultaneously with the electroweak symmetry breaking when the doublets H_u and H_d acquire non-zero vacuum expectation values v_u and v_d. This results in observational signals of axions, and is in the literature therefore dubbed as the visible axion [21]. These axions interact for example with mesons, and therefore alter the branching ratios that can be measured to a high precision. The constraints coming for example from the K, J/Ψ and Υ meson decays rule out the visible axion models [21, 23]. These constraints can be avoided if the symmetry-breaking scale of $\mathrm{U(1)_{PQ}}$ is high enough, and the axions are correspondingly very light and interact very weakly. This is usually achieved by considering a complex scalar field S as in Eq. (89), which is singlet under $\mathrm{SU(2)}_L \otimes \mathrm{U(1)}_Y$. In the literature these models are referred to as the invisible axion models.

5.1.2 KSVZ

The first invisible axion model, where the symmetry breaking energy scale is high above the electroweak one, the so-called KSVZ model, was introduced by Kim [35] and Shifman, Vainshtein and Zakharov [36]. In this model one introduces a new heavy quark field Q and a new complex Higgs-like scalar singlet S field. One also introduces a discrete R symmetry, $Q_L \to -Q_L$, $Q_R \to +Q_R$, $S \to -S$, that guarantees the absence of a bare-mass term

$m_Q\bar{Q}Q$ [35]. The presence of a bare mass would spoil the realization of the PQ symmetry.

The terms in the KSVZ model relevant to us are [37]

$$\mathcal{L}_{\text{KSVZ}} = -\frac{1}{4}G^a_{\mu\nu}G^{\mu\nu}_a + \bar{\theta}\frac{g_s^2}{32\pi^2}G^a_{\mu\nu}\tilde{G}^{\mu\nu}_a + \mathrm{i}\bar{Q}\gamma^\mu\partial_\mu Q - \frac{1}{2}\partial_\mu S^*\partial^\mu S \\ - \lambda_S\left(S^*S - v_S^2\right)^2 + g_s G^a_\mu\bar{Q}\gamma^\mu\lambda_a Q - \lambda_{QS}\left(Q_L^\dagger S Q_R + \text{h.c.}\right), \quad (98)$$

where Q is a heavy quark Dirac field and $v_S = \langle 0|S|0\rangle$. This Lagrangian is invariant under the global chiral $\mathrm{U}(1)_{\text{PQ}}$ symmetry:

$$Q_L \to \mathrm{e}^{\mathrm{i}\alpha/2}Q_L,\ Q_R \to \mathrm{e}^{-\mathrm{i}\alpha/2}Q_R,\ S \to \mathrm{e}^{\mathrm{i}\alpha}S. \quad (99)$$

Just to recap, we write the complex scalar field in its polar form as in Eq. (89). At temperatures lower than v_S, it is the radial part of the field $\eta(x)$ that freezes in the vacuum expectation value, while the phase of the field remains free. As mentioned, we recognize the phase degree of freedom as the axion field $a(x)$, which is identified as the Nambu-Goldstone boson associated with the spontaneous breaking of $\mathrm{U}(1)_{\text{PQ}}$. For the axion field the PQ-transformation given in Eq. (99) corresponds to the shift $a \to a + \alpha v_S$.

After the spontaneous breaking of $\mathrm{U}(1)_{\text{PQ}}$ we can write the part of the Lagrangian in Eq. (98) that contains the axion field as

$$\mathcal{L}_{\text{KSVZ},a} = -\frac{1}{2}\partial_\mu a\partial^\mu a - v_S\lambda_{QS}\left(Q_L^\dagger \mathrm{e}^{\mathrm{i}a/v_S}Q_R + Q_R^\dagger \mathrm{e}^{-\mathrm{i}a/v_S}Q_L\right). \quad (100)$$

If we redefine the chiral heavy quark fields as

$$Q_L \to \mathrm{e}^{\mathrm{i}a/2v_s}Q_L,\ Q_R \to \mathrm{e}^{-\mathrm{i}a/2v_s}Q_R, \quad (101)$$

we see the heavy quark to obtain an effective mass, which is proportional to the symmetry breaking scale of the PQ-field. This field transformation adds both a derivative interaction term between axion and heavy quark fields and also an anomaly-type term (see the discussion in the previous chapter):

$$\mathcal{L}_{aGG} = \frac{g_s^2}{32\pi^2}\frac{a}{v_S}G^a_{\mu\nu}\tilde{G}^{\mu\nu}_a. \quad (102)$$

The disadvantage of this model might be the existence of a heavy quark with a very large effective mass, $m_Q \sim v_S\lambda_{QS}$, as $v_S \gg v_{\text{EW}} \approx 246$ GeV, not well motivated theoretically. Also, in this model the axions are entirely decoupled from the other SM particles - apart from the generic low-energy axion-gluon coupling. This may lead to the question why there is no tree-level coupling of axions to SM quarks.

5.1.3 DFSZ

Another invisible axion model is the DFSZ model, first proposed by Zhitnitsky [38] and Dine, Fischler and Srednicki [39]. Again the Standard Model is made invariant under the $\mathrm{U}(1)_{\mathrm{PQ}}$ by additional Higgs sectors. In this case the symmetry is implemented into the theory with two Higgs doublets, H_u and H_d and a Higgs-like scalar singlet S.

The most general potential for two doublets and a singlet Higgs fields can be written as [37]

$$\begin{aligned} V(H_u, H_d, S) = \lambda_u \left(H_u^\dagger H_u - v_u^2\right)^2 + \lambda_d \left(H_d^\dagger H_d - v_d^2\right)^2 + \lambda_S \left(S^* S - v_S^2\right)^2 \\ + \lambda_{uu} \left(H_u^\dagger H_u\right) \left(H_d^\dagger H_d\right) + \lambda_{ud} \left(H_u^\dagger H_d\right) \left(H_d^\dagger H_u\right) \\ + \left[\lambda_{uS} \left(H_u^\dagger H_u\right) + \lambda_{dS} \left(H_d^\dagger H_d\right)\right] S^* S + \lambda \left[\left(H_u^\dagger H_d\right) S^2 + \left(H_d^\dagger H_u\right) \left(S^*\right)^2\right], \end{aligned} \tag{103}$$

where λ_i's are dimensionless parameters. The corresponding relevant Yukawa-sector, where the light-quarks couple directly to the two Higgs doublets is given in Eq. (93).

The above Higgs-potential (103) is invariant under the transformation

$$H_u \to \mathrm{e}^{\mathrm{i}X_1} H_u, \;\; H_d \to \mathrm{e}^{\mathrm{i}X_2} H_d, \;\; S \to \mathrm{e}^{\mathrm{i}(X_1 - X_2)/2} S. \tag{104}$$

In order to maintain the invariance of the Yukawa-sector, this transformation should be accompanied by the following transformation of the right-handed quark fields

$$u_R \to \mathrm{e}^{-\mathrm{i}X_1} u_R, \;\; d_R \to \mathrm{e}^{-\mathrm{i}X_2} d_R, \;\; l_R \to \mathrm{e}^{-\mathrm{i}X_2} l_R. \tag{105}$$

The left-handed fields being inert.

Again, below the PQ phase transition we assume the radial part of the singlet S to acquire a certain vev v_S, while the phase remains free. After the electroweak phase transition at the phenomenologically required scale $v_{\mathrm{EW}} = \sqrt{v_u^2 + v_d^2} \ll v_S$, there exist additional physical neutral Higgs fields and orthogonal Nambu-Goldstone bosons as the phase degrees of freedom [40]. This mixing of the two phases is due to the last term in the Lagrangian (103). One of these massless degrees of freedom is absorbed into the gauge bosons, while the other is the axion-like field [40]. By redefining the Higgs fields and lepton fields, like in Eq. (101), one adds a derivative interaction

term between the axion and SM quarks and the needed anomalous axion couplings [37].

Advantage of this model is that one does not have to include any new exotic heavy quarks, as the SM fermions are assumed to carry the PQ-charge. However, some parameter fine-tuning is required to keep $v_S \gg v_{\mathrm{EW}}$ [41]. Additional insight may come from the fact that two-Higgs doublet models are studied in the physics beyond the Standard Model, especially in the supersymmetric extensions.

5.1.4 A general low-temperature model

While the high-energy axion model is not known, we can use an effective low-energy Lagrangian for the phenomenological studies. If we continue to interpret the axion as a phase degree freedom of the PQ-field S, we can write the low-energy axion Lagrangian during the epoch between the EW and QCD phase transitions as

$$\mathcal{L}_a = -\frac{1}{2}\partial_\mu a \partial^\mu a + \frac{g_s^2}{32\pi^2}\frac{a}{f_a} G^a_{\mu\nu}\tilde{G}^{\mu\nu}_a + \mathcal{L}_{\mathrm{int}}, \tag{106}$$

where $\mathcal{L}_{\mathrm{int}}$ is given in Eq. (115). Around and after the confinement of the quarks and gluons the instanton-induced effective potential (see Section 5.2) can be calculated yielding:

$$\mathcal{L}_a = -\frac{1}{2}\partial_\mu a \partial^\mu a - f_a^2 m_a^2 \left[1 - \cos\left(\frac{a}{f_a}\right)\right] + \mathcal{L}_{\mathrm{int}} + \mathcal{L}_{a\pi}. \tag{107}$$

Where we have added the interaction between axions and pions [5], which we shall leave unspecified for the present.

Note that compared with the earlier case we have replaced the vacuum expectation value v_S with the PQ-symmetry breaking scale parameter[12] f_a, defined as

$$f_a \equiv \frac{v_S}{\mathcal{N}}, \tag{108}$$

where $\mathcal{N}$ counts the number of PQ-charged particles species. For example, by adding another heavy quark to the standard KSVZ model with one exotic quark one also gets additional anomaly-terms as in Eq. (102). This means that in the standard KSVZ model $\mathcal{N} = 1$, while in the DFSZ model $\mathcal{N} = 6$, if there are three different quark and lepton families.

[12] Also referred to as the *PQ scale* or the *axion decay constant*.

5.2 Axion mass and potential

The effective axion potential can be calculated, in principle, from Eq. (92), but due to the complex non-perturbative nature of the low-energy QCD phenomena one cannot get an exact analytical expression [11]. In this thesis we will follow the standard way to express the axion potential:

$$V(a) = f_a^2 m_a^2(T) \left[1 - \cos\left(\frac{a}{f_a}\right)\right], \tag{109}$$

where we have replaced the zero-temperature axion mass with a temperature-dependent mass, as the instanton-effects generating the mass depend on the temperature of the plasma. The periodicity of the potential is inherited from the periodicity of the θ vacuum.

The axion mass can be computed by expanding the effective potential around its minimum:

$$m_a^2 = \langle \frac{\partial^2 V_{\text{eff}}}{\partial a^2} \rangle = -\frac{1}{f_a} \frac{g_s^2}{32\pi^2} \frac{\partial}{\partial a} \langle G^a_{\mu\nu} \tilde{G}_a^{\mu\nu} \rangle \Big|_{\langle a \rangle = -f_a \bar{\theta}}. \tag{110}$$

The mass induced by the neutral pion mixing can be calculated using current algebra methods [33, 42]. The standard estimate[13] for the zero-temperature axion mass in the standard KSVZ model is [43]

$$m_a \approx \frac{f_\pi m_\pi}{f_a} \left(\frac{\tilde{z}}{(1+\tilde{z})(1+\tilde{z}+\tilde{w})}\right)^{1/2} \approx 6 \times 10^{-6} \text{ eV} \left(\frac{10^{12} \text{ GeV}}{f_a}\right), \tag{111}$$

where f_π and m_π are the pion decay constant and pion mass, $\tilde{z} \equiv m_u/m_d \approx 0.48$ [3, 31] and $\tilde{w} \equiv m_u/m_s \approx 0.02$ [31].

The zero-temperature axion mass is applicable only well after the QCD phase transition. The axion mass that is generated by the non-perturbative instanton effects in the primordial quark-gluon plasma are temperature dependent. As mentioned, to study the temperature-dependent axion mass in the complicated QCD plasma one usually needs to rely on lattice simulations. The axion mass dependency on the instanton effects is highly non-linear, as in the high-energy limit the axion mass is usually considered to be given by non-interacting instantons, while nearer the QCD confinement their interactions need to be taken into account [11]. These complicated issues have led to different mass-extraction methods yielding slightly different results (see for example Ref. [44]).

[13] Usually referred to as the Bardeen-Tye estimate.

In this thesis we use the parametrization for the temperature-dependent axion mass obtained in Ref. [11], where the interacting instanton liquid model (IILM) is used. The dilute gas power-law approximation for the high-energy regime is

$$m_a^2(T) = 1.68 \times 10^{-7} \left(\frac{\Lambda_{\rm QCD}^4}{f_a^2}\right)\left(\frac{\Lambda_{\rm QCD}}{T}\right)^n . \tag{112}$$

where $n = 6.68$ and $\Lambda_{\rm QCD} \approx 400$ MeV [11]. In the low-energy regime, where the dilute gas estimate breaks down, the mass is given by

$$m_a^2(T) = 1.46 \times 10^{-3} \left(\frac{\Lambda_{\rm QCD}^4}{f_a^2}\right)\left(\frac{1 + 0.50T/\Lambda_{\rm QCD}}{1 + (3.53T/\Lambda_{\rm QCD})^{7.48}}\right), \tag{113}$$

giving

$$m_a^2(0) = 1.46 \times 10^{-3} \left(\frac{\Lambda_{\rm QCD}^4}{f_a^2}\right). \tag{114}$$

For $\Lambda_{\rm QCD} \sim \mathcal{O}(100)$ MeV this parametrization agrees with the standard current algebra estimation given in Eq. (111).

5.3 The domain wall number

As discussed in Section 3.5, in a cosmological setting potentials with degenerate discrete minima might result in a domain wall formation. We see that the cosine-potential given in Eq. (107) is periodic with $2\pi k f_a$, where k is an integer. For the axion models considered here, i.e. Eq. (89), the domain wall number $N_{\rm DW}$ that gives the number of domain walls attached to strings, is determined by the colour anomaly term $\mathcal{N}$, i.e. $\mathcal{N} = N_{\rm DW}$ [15, 21].

In the standard KSVZ model, where there is one new exotic heavy quark, the domain wall number is $N_{\rm DW} = 1$. This means that there is only one minimum of the axion field near the QCD phase transition, and as mentioned earlier, there is one domain wall related to each cosmic string that result from the spontaneous breaking of the global $\mathrm{U}(1)_{\rm PQ}$ symmetry. However, in the standard DFSZ model $N_{\rm DW} = 6$. As discussed earlier, the domain wall number $N_{\rm DW}$ is also related to the evolution of the string-wall network. Assuming that the Peccei-Quinn symmetry is broken after inflation, in the standard KSVZ model, $N_{\rm DW} = 1$, the formed string-wall configurations are usually taken to be short-lived. However, in the DFSZ model, $N_{\rm DW} > 1$, it is possible to have long-lived configurations – see Section 6.3

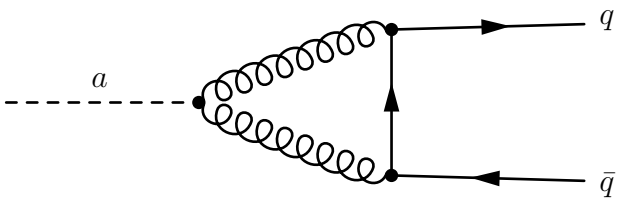

Figure 6: Axion mixing with the bound state $q\bar{q}$, which results in axions mixing with neutral pions and thus axions having a small effective mass. This mixing is present in all axion models due to the integral axion coupling to the gluons.

5.4 Axion interactions

The effective Lagrangian for the interactions between axions and the Standard Model particles is given by[14] [5]

$$\mathcal{L}_{\text{int}} = -\frac{1}{4} g_{a\gamma} a F_{\mu\nu} \tilde{F}^{\mu\nu} + \mathrm{i} \frac{g_{aN}}{2m_N} \partial_\mu a \left(\bar{N} \gamma^\mu \gamma^5 N \right) + \mathrm{i} \frac{g_{af}}{2m_f} \partial_\mu a \left(\bar{\psi}_f \gamma^\mu \gamma^5 \psi_f \right), \quad (115)$$

where N and ψ_f represent the nucleon and fermion fields, respectively, $F^{\mu\nu}$ is the electromagnetic field strength tensor and all the coupling constants $g_{a\gamma}$, g_{aN} and g_{af} are proportional to f_a^{-1}. Usually one is interested in the case where fermion f is the electron.

A generic feature of axion models is the two-photon coupling of the axion,

$$\mathcal{L}_{a\gamma} = -\frac{1}{4} g_{a\gamma} a F_{\mu\nu} \tilde{F}^{\mu\nu} = g_{a\gamma} a \vec{E} \cdot \vec{B}. \quad (116)$$

This is the coupling through which the existence of axions is experimentally studied.

The axion-photon coupling constant is given by [43, 46, 47]

$$g_{a\gamma} = \frac{\alpha}{2\pi f_a} \left(\frac{E}{\mathcal{N}} - \frac{2}{3} \frac{4 + \tilde{z} + \tilde{w}}{1 + \tilde{z} + \tilde{w}} \right), \quad (117)$$

[14] Sometimes one also includes an additional EDM-type term in the interaction Lagrangian, $-(\mathrm{i}/2) g_d a \bar{N} \sigma_{\mu\nu} \gamma^5 N F^{\mu\nu}$ [45].

where α is the fine-structure constant. The quantities E and $\mathcal{N}$ correspond to the electromagnetic and colour anomalies associated with the axion field. The term $E/\mathcal{N}$ is a model dependent quantity that stems from the loop triangle diagrams, and it is present in models where there are quarks and leptons that carry both PQ charges (X_j) and electric charges (Q_j). The parameters E and $\mathcal{N}$ are given by [43]

$$E \equiv 2\sum_j X_j Q_j^2 D_j \tag{118}$$

$$\mathcal{N} \equiv \sum_j X_j, \tag{119}$$

where D_j describes whether the fermion j in the triangle loop is a charged lepton (color singlet, $D_j = 1$) or a quark (color triplet, $D_j = 3$).

We can see how the axion-photon coupling constant differs between the KSVZ and DSFZ models. In the standard KSVZ model[15] the PQ charge is carried by the new exotic heavy quark fields that do not carry EM charge, i.e. $E = 0$ and $E/\mathcal{N} = 0$. However, in the standard DFSZ model the EM charge carrying Standard Model fermions also carry a PQ charge, and one has $E/\mathcal{N} = 8/3$.

Two-photon vertex allows axions to decay into two photons, which allows us to estimate the lifetime of axions. For KSVZ axions the order of magnitude of the decay rate in this channel is given by [43]

$$\Gamma_{a\to\gamma\gamma} = \frac{g_{a\gamma}^2 m_a^3}{64\pi} \approx 1.1 \times 10^{-24}\ \mathrm{s}^{-1} \left(\frac{m_a}{\mathrm{eV}}\right)^5. \tag{120}$$

In terms of the age of the Universe t_U, the average axion lifetime is then given by

$$\tau_{a\to\gamma\gamma} \approx 2.1 \times 10^6 t_\mathrm{U} \left(\frac{\mathrm{eV}}{m_a}\right)^5. \tag{121}$$

For masses $m_a \sim \mathcal{O}(10)$ eV or lower, axions are stable on cosmological time scales and are viable candidates for dark matter.

As we recognize the axion as the Nambu-Goldstone boson relic of the broken $\mathrm{U}(1)_\mathrm{PQ}$ symmetry, there are derivative-type interactions, that include derivatives of the axion field, present in the interaction Lagrangian (115)

[15]Note that there are also variations of the KSVZ model, where additional heavy quarks that carry both charges are added. For example, one can consider a model with $E/\mathcal{N} = 2$. [43]

that satisfy the shift $a \to a + \text{constant}$. It is possible to express the derivative interactions in the Lagrangian in a different bilinear form through field redefinitions [43]. In the literature these are often written in the lowest-order pseudoscalar-bilinear form

$$\mathcal{L}_{af} = -\mathrm{i}\frac{g_{af}}{2}\, a\bar{\psi}_f\gamma^5\psi_f \equiv -\mathrm{i}\frac{C_f m_f}{2f_a}\, a\bar{\psi}_f\gamma^5\psi_f$$
$$\mathcal{L}_{aN} = -\mathrm{i}\frac{g_{aN}}{2}\, a\bar{N}\gamma^5 N \equiv -\mathrm{i}\frac{C_N m_N}{2f_a}\, a\bar{N}\gamma^5 N,$$

where we defined the effective model-dependent PQ charges $C_x = g_{ax} f_a/m_x$, where $x = f, N$.

As axions do not couple to the SM fermions at tree-level in the KSVZ model, one has $C_f^{\mathrm{KSVZ}} = 0$. These axion models, where the axion does not have a tree-level coupling to fermions are usually referred to as the hadronic axion models. However, the tree-level coupling is present in the DFSZ model, and there the couplings to fermions are given by [43]

$$C_e^{\mathrm{DFSZ}} = C_d^{\mathrm{DFSZ}} = C_s^{\mathrm{DFSZ}} = \frac{\cos^2\beta}{N_f} \tag{122}$$

$$C_u^{\mathrm{DFSZ}} = \frac{\sin^2\beta}{N_f}, \tag{123}$$

where N_f is the number of families, usually taken to be $N_f = 3$, and $\beta = \tan^{-1}(\tilde{x})$, where $\tilde{x} = v_d/v_u$. The nucleon-axion couplings C_N are given by [43]

$$C_p = (C_u - \tilde{\eta})\,\Delta u + (C_d - \tilde{\eta}\tilde{z})\,\Delta d + (C_s - \tilde{\eta}\tilde{w})\,\Delta s \tag{124}$$
$$C_n = (C_u - \tilde{\eta})\,\Delta d + (C_d - \tilde{\eta}\tilde{z})\,\Delta u + (C_s - \tilde{\eta}\tilde{w})\,\Delta s, \tag{125}$$

where $\tilde{\eta} \equiv (1 + \tilde{z} + \tilde{w})^{-1}$. Here Δq is the fraction of the proton spin carried by a quark flavour q, obtained from the axial vector current matrix element $S^\mu \Delta q = \langle p|\bar{q}\gamma^\mu\gamma^5 q|p\rangle$, where S^μ is the proton spin.

By plugging in the rough values for $\tilde{z}$, $\tilde{w}$ and Δq [43], where $q = u, d, s$, we obtain the following estimates for the effective axion-nucleon couplings for hadronic and DFSZ axion models

$$C_p^{\mathrm{KSVZ}} \approx -0.43,\ C_n^{\mathrm{KSVZ}} \approx 0.002 \tag{126}$$
$$C_p^{\mathrm{DFSZ}} \approx -0.15 - 0.45\cos^2\beta,\ C_n^{\mathrm{DFSZ}} \approx -0.13 + 0.39\cos^2\beta, \tag{127}$$

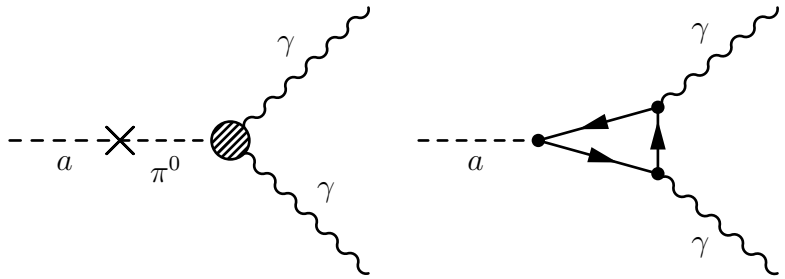

Figure 7: Axion-photon coupling. Left: photons coupling to axions via the pion mixing. Right: in models where the fermions carry both the PQ and electric charges also the ABJ-anomaly triangle loops contribute to the axion-photon coupling.

where we also used equations (122) and (123) with $N_f = 3$. We see that despite the differences between the couplings in the models, the DFSZ and KSVZ models are allowed to have comparable nucleon couplings.

One should note that there are large uncertainties involved with the quantities Δq and the above values are really rough estimates. Also, the values of the coupling constants are sensitive to the ratio m_u/m_d. This means that the frequently quoted results from Ref. [43] in the literature are slightly different that the ones obtained here, as Ref. [43] uses a larger value for the ratio[16]. This varying range for the nucleonic charges was also noted in Ref. [48], where they reported that for hadronic axions the couplings vary between $-0.51 \lesssim C_p \lesssim -0.36$ and $-0.05 \lesssim C_n \lesssim 0.1$.

5.5 Astrophysical Bounds

After thirty years of axion studies the emergence of the direct detection experiments and the cosmological high-precision measurements have allowed to probe the axion model parameter space. The contribution of the astrophysical observables is still significant and in some cases gives the most stringent axion parameter constraints. In this section we discuss how the astrophysical objects, e.g. stars, act as distant laboratories for the axion models.

[16]For example, Ref. [43] obtains $C_n^{\mathrm{KSVZ}} \approx -0.04$ with $\tilde{z} \approx 0.568$. However, the smaller value for $\tilde{z}$ seems to be preferred according to Ref. [31]

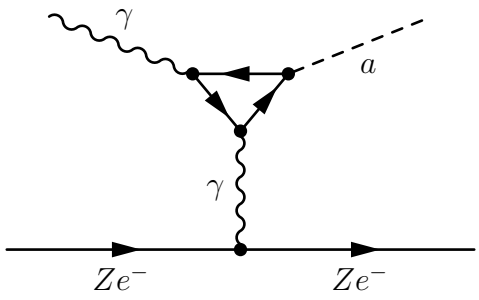

Figure 8: Feynman diagram of the Primakoff effect.

5.5.1 Axions from the Sun

If axions exist, they might be produced through different processes in the Sun's core. If the Sun were perturbed by the new pseudoscalar emission channel, it would try to restore equilibrium by contracting, simultaneously raising its temperature and nuclear energy liberation, resulting in an enhanced photon luminosity. This in turn would affect the lifespan of the Sun, allowing to constrain the axion couplings so that the addition of axions does not tarnish the Standard Solar Model.

For hadronic axions the dominant production process is the so-called Primakoff process (see Fig. 8), where photons are converted into axions by the external electromagnetic field generated by the charged particles in the plasma [5]. For the DFSZ model also the Compton-like scattering $\gamma + e \to a + e$ and the electron bremsstrahlung $e + Ze \to Ze + e + a$ contribute [49]. Requiring the total axion luminosity to be less than the known solar luminosity leads to the limit $g_{a\gamma} \lesssim 1 \times 10^{-9}$ GeV^{-1} [43] for the axion-photon coupling behind the Primakoff process. In the DFSZ model this requirement constrain the axion-electron coupling, $g_{ae} \lesssim 4.5 \times 10^{-7}$ [49].

The solar neutrino production rate of ^{8}B also constrains $g_{a\gamma}$. Ref. [50] used the neutrino flux measurements of the SNO (Sudbury Neutrino Observatory) to obtain the limit $g_{a\gamma} \lesssim 7 \times 10^{-10}$ GeV^{-1}. All in all, the limits for $g_{a\gamma}$ translate into a limit for the axion mass, roughly $m_a \lesssim \mathcal{O}(10)$ eV.

5.5.2 Globular clusters

A globular cluster is a gravitationally tightly bound collection of about 10^6 stars formed at about the same time. The globular clusters form spherical halos around galaxies. The Milky Way halo consists of about 150 globular clusters [43]. These clusters contain relatively old stars, which have already exhausted their central hydrogen supply and have moved from the main sequence (MS) to the red giant branch (RGB) and to the following horizontal branch (HB) and asymptotic giant branch (AGB) stages. As with the Sun, the addition of axions would affect the evolution of these stellar objects. It happens that the RGB and HB stars offer an excellent way to probe the axion parameter space.

As the RGB stars have used their central hydrogen supply, they usually develop a degenerate helium core with a hydrogen burning shell that fuses hydrogen into helium [43]. During this phase the helium core grows in mass and the core temperature and density increase. When the temperature and density of the star's core are high enough, i.e. when the core reaches its so-called limiting mass, the helium ignites and the helium burning commences[17]. If axions exist, they provide an additional channel to transfer energy and could stall or prevent the helium ignition. The axion cooling follows dominantly from the electron bremsstrahlung, which can then be used to constrain the axion-electron coupling, yielding an upper limit $g_{ae} \lesssim 3 \times 10^{-13}$ [43]. For the DFSZ model this corresponds to the constraint $f_a \gtrsim 0.8 \times 10^9$ GeV $\cos^2\beta$ [51].

After the helium ignition the star with both the hydrogen burning shell and helium burning core moves to the horizontal branch. The Primakoff effect that converts photons in the plasma to axions, $\gamma + Ze \to a + Ze$, is present in both RGB and HB stars. However, this conversion is negligle in RGB stars compared with the bremmsstrahlung, and it is significantly more effective in HB stars [51]. The addition of axions to the model would therefore give HB stars an additional energy loss channel and could therefore decrease their lifetime, and also decrease the number of HB stars compared with RGB stars. Measuring the number of the RGB and HB stars yields an upper bound for the photon-axion coupling constant, $g_{a\gamma} \lesssim 0.6 \times 10^{-10}$ Gev^{-1} [43].

[17] As the process of the helium ignition happens on a very short time scale, it is sometimes referred to as "helium flash".

5.5.3 Cooling of white dwarfs and neutron stars

Additional restrictions for the axion-electron coupling are obtained from the cooling of the stars that have moved from the AGB-stage to the white dwarf stage. In these compact remnants of low-mass stars the carbon and oxygen reserves never ignited, and the cooling of the dense carbon-oxygen star is dictated by the neutrino emission from the high-temperature interior and photon emission from the surface. If axions are emitted instead of neutrinos, the temperature dependence of the white dwarf energy-loss rate is modified [43]. The modified cooling of white dwarfs results in the limit $g_{ae} \lesssim 3.5{\times}10^{-13}$ [51] for the axion-electron coupling.

The main processes needed to take into account in the axion cooling of the neutron stars are the nucleon bremsstrahlung and the axion counterpart of the Cooper pair-breaking-formation (PBF), which is usually discussed in the context of neutrino pair emission via PBF [52, 53]. In the high-density and low-temperature core the neutron star may exhibit superfluidity, i.e. the nucleons form Cooper pairs. The neutrino pair (or axions) is emitted from the neutron pair breaking and formation processes, i.e. $n+n \to n+n+\nu+\bar{\nu}$. In the literature, this approach has not gathered as much as attention as the other stellar evolution probes. However, one can find similar bounds as with the other stellar sources, e.g. recently Ref. [48] found a lower bound for f_a in KVSZ-models, $f_a \gtrsim 5 \times 10^7$ GeV, and Ref. [54] obtained a similar constraint $f_a \gtrsim 7.6 \times 10^7$ GeV by using the Fermi-LAT gamma-ray data.

5.5.4 Supernova 1987A

A type-II supernova results from the violent core-collapse and explosion of a massive star, $M \gtrsim 7 - 8M_\odot$, which then leads to a neutron star. In the high nucleon density post-core collapse neutron star, the nucleon-axion bremsstrahlung, $N + N \to N + N + a$, is the dominant way of producing axions. The creation of the weakly-interacting axions would provide a more efficient cooling channel than the neutrino channel. This would affect the cooling time of the SN and the neutrino burst duration in the SN process [43].

The measurement of antineutrino flux from SN1987A by the Kamiokande II and Irvine-Michigan-Brookhaven experiments allowed one to test the axion-nucleon coupling g_{aN}. Annihilations to the axion channel would shorten the duration of the neutrino burst. However, if axions are strongly coupled to the

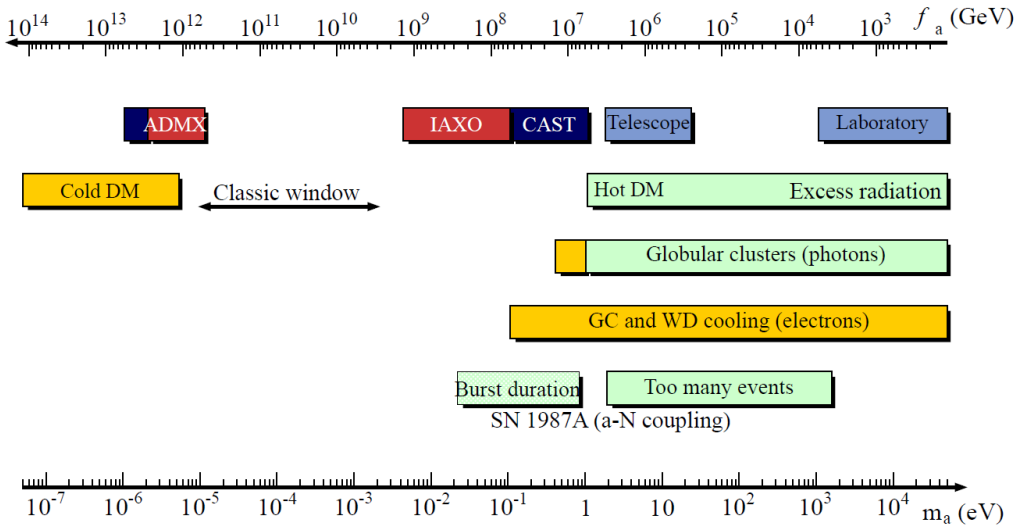

Figure 9: Astrophysical and cosmological bounds with experimental projections. Bounds with green label are less model-dependent, while orange labels indicate strong model-dependency. Figure from Ref. [55].

nucleons they will get trapped in the star's medium and form a so-called axion sphere. In this trapping regime the axions are unable to affect the neutrino signal duration. These considerations and the fact that strongly interacting axions would have produced additional events in the water Cherenkov detectors of the experiments mentioned above yield an excluded range of [51]

$$3 \times 10^{-10} \lesssim g_{aN} \lesssim 3 \times 10^{-7}. \tag{128}$$

5.6 Direct detection of axions

As the original PQWW-axions were ruled out by the experimental data, the interest shifted towards the new high-scale axions models. For a brief period it was thought that the "invisible" axions predicted by these models are so light and weakly-coupled that they could avoid any direct observation techniques. However, it was soon shown by Ref. [56] that the detection of the galactic and solar axions was indeed possible by exploiting the axion-photon coupling, which allows the conversion of axions to monochromatic photons in a microwave cavity encompassed by a strong external magnetic field.

The present experimental axion search strategies can be divided into three

categories depending on the source of axions: the haloscope experiments look for cold dark matter axions in the galactic halo, the helioscope experiments search for the solar axions, and the laboratory experiments try to produce and detect axions. Basically the detection strategies of all of these experiments are based on the coherent mixing of axions and photons in strong magnetic fields. There are also experiments planned that exploit the nuclear magnetic resonance techniques to detect dark matter axions.

5.6.1 Axion haloscope

The haloscope experiments are based on the idea of Ref. [56] that the axions with masses in the μeV range that permeat the galactic halo could be detected in the microwave cavity experiments. The detection techniques of these non-relativistic axions, gravitationally bound to the Milky Way, were first used and developed in the experiments at the Brookhaven National Laboratory, University of Florida and CARRACK experiment in Kyoto [57]. Today the most sensitive experimental setup is offered by the Axion Dark Matter eXperiment (ADMX), with two different experimental platforms, ADMX (1995-) and ADMX-HF (commissioned) [57].

For the experiments to detect axions through the resonant conversion, the cavity frequency has to be tuned exactly to the energy of the galactic axions, i.e. axion mass [56]. This means that the size of the cavity and therefore the magnetic field has to be adjustable in order to scan a range of different axion masses. During its two operational phases ADMX has scanned and excluded KSVZ dark matter axion masses between the range $1.96 - 3.69$ μeV [58, 59]. However, one should note that these results assume that axions are the dominant CDM component in the galactic halo.

The microwave cavity based experiments are not sensitive to the lower axion frequencies, and they may hence miss ultralight axions and axion-like particles [57]. The search for these high-scale axions is highly motivated, as the string-theory motivated theories that contain axions and ALPs prefer much higher energy scale such as $f_a \sim 10^{15} - 10^{16}$ GeV, which would result in a nanoelectronvolt range axion mass [57][18]. Additional motivation for these high-scale axions may come from the possible observation of transparency of the Universe to very high-energy photons - for example see Ref. [62].

[18]For these values the standard axions tend to overclose the Universe, but there are suggested mechanisms that allow the existence of these high-scale axions [60, 61].

For this reason there have been proposals for new search concepts for the detection of lighter dark matter axions. One of these is the Cosmic Axion Spin Precession Experiment (CASPEr), which aims to detect spin precession induced by axions using nuclear magnetic resonance (NMR) techniques. The two experiments, CASPER-Wind and CASPER-Electric, are able to detect the effects induced by the direct coupling of axions to the spin of the nucleus and electric dipole moment interaction term (see Eq. (115) and the corresponding footnote) and measure the precession of the nuclear spin in the sample material [57]. Final CASPEr experiment should have sensitivity to detect axions with a mass $m_a \sim 10^{-9} - 10^{-12}$ eV [57]. Another recently proposed experimental design for the dark matter axion detection, ABRACADABRA[19], uses broadband (or resonant) detection of an oscillating magnetic flux [63]. The sensitivity of this experiment will be in the range of masses from 10^{-13} eV to 10^{-6} eV [63].

5.6.2 Axion helioscope

The principle idea of the helioscope detection technique is to use the generic axion-photon coupling and convert solar axions with energies up to keV regime to photons in an electromagnetic field [56]. Axions are produced in the solar interior mainly by the Primakoff process, but for non-hadronic axions, which have a tree-level coupling with the electrons other processes such as the bremsstrahlung, Compton scattering and axion recombination need to be taken into account [64].

Helioscope experiments are usually sensitive to the axion masses of $10^{-3} - 1$ eV, and they are able to scan a wider range of the axion parameter space than the haloscope experiments as the observed signal is independent of the axion mass, contrary to the haloscope case [57]. The first generation experimental setup was build at the Brookhaven National Laboratory, with the University of Tokyo following with a second generation experiment, the SUMICO axion helioscope [57]. Solar axions have also been searched with the Bragg scattering technique used by many dedicated WIMP experiments, such as the SOLAX [65], COSME [66], DAMA [67], CDMS [68] and EDELWEISS [69]. However, the limits obtained by these experiments are less stringent than the ones obtained from the astrophysical analyses.

The most stringent constraints from the helioscope experiments come from

[19] A Broadband/Resonant Approach to Cosmic Axion Detection with an Amplifying B-field Ring Apparatus.

the third generation CAST (CERN Axion Solar Telescope) [57, 70]. It has been able to compete with the limits from astrophysical data, and the scanned parameter range covers models with $f_a \sim 10^7 - 10^8$ GeV. For example, CAST has reported to exclude ranges $g_{a\gamma} < 8.8 \times 10^{-11}$ GeV^{-1} for $m_a < 0.02$ eV [70], $g_{a\gamma} < 2.3 \times 10^{-10}$ GeV^{-1} for 0.39 eV $\lesssim m_a \lesssim$ 0.64 eV [71] and $g_{a\gamma} < 3.3 \times 10^{-10}$ GeV^{-1} for 0.64 eV $\lesssim m_a \lesssim$ 1.17 eV [72].

A proposed next-generation helioscope detector is the CERN-based IAXO experiment (International AXion Observatory) [73]. The expected goal of IAXO is to lower the axion-photon coupling sensitivity to the level of $g_{a\gamma} \sim 10^{-12}$ GeV^{-1} for $m_a \sim 10^{-3}$ eV axions [73]. This increase in sensitivity allows IAXO in addition to standard QCD axions also search for lighter ALPs.

5.6.3 Laboratory experiments

The principle idea of the laboratory axion experiments is to investigate how the axion-photon conversion in a magnetic field affects a photon beam. This is achieved by directing the photon beam into a transverse magnetic field, where a fraction of the photons should convert into axions. The task is then to reconvert axions back to observable photons. For this part there are two methods used in the experiments. First one is the so-called Light-Shining-through-Wall (LSW) experimental setup, where photons are regenerated from the converted axions by inserting an optical barrier in the front of the axion-photon beam that blocks the beam photons but allow the weakly-interacting axions to pass through. Behind the barrier a second transverse magnetic field is used to regenerate detectable photons from the propagating axions.

The LSW setups have been realized in the ALPS-I at DESY and the OSQAR[20] and CROWS[21] at CERN. The next-generation LSW experiments the ALPS-II and JURA should be able to surpass the limits obtained for ALPs from the astrophysical data [57]. However, the searches of the standard QCD axion may lead to less stringent limits on the parameters [57].

Another way to study the effects of the axion-photon coupling is to look at the polarization of the photon beam in a magnetic field. If the photon-axion-photon conversion is present in the beam, the once-converted photons

[20]Optical Search of QED vacuum magnetic birefringence, Axion and photon Regeneration.

[21]CERN Resonant WISP Search.

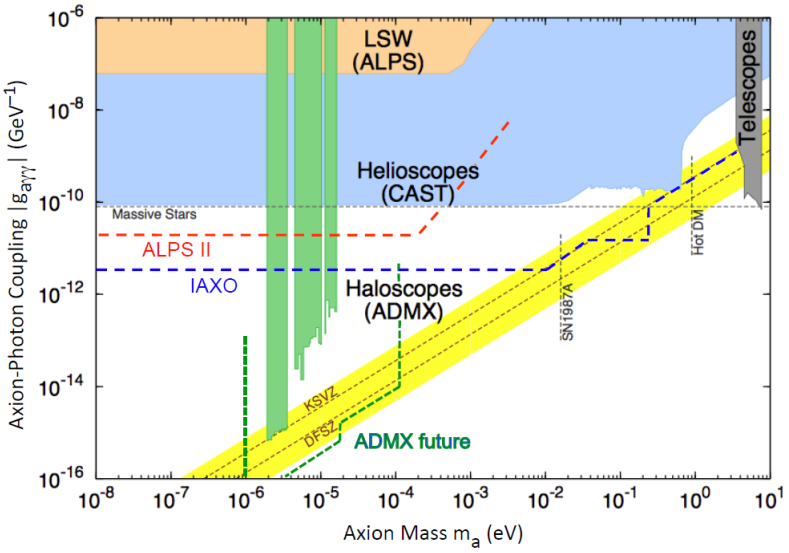

Figure 10: Existing and projected limits on the photon-axion coupling as a function of axion mass. Figure from Ref. [57].

should have **E** and **B** components deviating from those of the non-converted photons in the polarized beam. This is the idea of the PVLAS experiment [74].

6 Axion dark matter

Due to the high-scale symmetry breaking axions have many properties required from dark matter: they are massive, non-baryonic, stable on cosmological time scales and extremely weakly-interacting. However, we know that axions have to be extremely light, which is worrying as we would like the axion dark matter population to be cold, i.e. particles which relax to non-relativistic velocities quickly in the early Universe – see Section 2.4. This actually happens in the case of thermally produced axions generated from the interactions in the primordial plasma. The small axion population produced constitutes hot dark matter. However, the story of axion CDM does not end here.

Through the coherent oscillation of the axion field and the decay of topological defects the Universe can have a significant cold axion population. In the former mechanism (Section 6.2), the evolution of the axion field in the early Universe allows the emergence of an axion population that behaves like cold dark matter, albeit the particles themselves are extremely light. After the PQ phase transition the axion field evolves like a massless scalar field in the expanding Universe. However, close to the QCD phase transition it generates an effective potential due to the anomalous interactions discussed earlier. One can then follow the evolution of the so-called zero-momentum mode axions, that are solutions to the equations of motion in the expanding Universe. The effective potential then results in the coherent oscillation of the zero-modes. This oscillation of the field behaves effectively like non-relativistic matter, and is then suitable as cold dark matter. In the literature this coherent oscillation of the zero-modes is sometimes referred to as the *misalignment mechanism*.

The non-thermal production mechanisms are sensitive to the critical temperature when the $\mathrm{U}(1)_{\mathrm{PQ}}$ symmetry breaks spontaneously. If inflation occurs after the PQ symmetry breaking, the randomly chosen initial value of the axion field within the causal horizon is homogenized over all the different causal patches. In this scenario, we can treat the axion field as having one initial value and assume that the defects produced in the PQ phase transition are diluted away. A problem is that this initial value is not known. Luckily, in estimating the energy density of the axions in this scenario we can couple this initial value to the inflationary model constraints – see Section 6.5. As we assume that inflation smoothens the field space out of any momentum dependence, the evolution of the axion field is determined by the so-called

zero-momentum modes of the field.

If the PQ symmetry breaks after inflation, the axion field chooses an uncorrelated random initial value in every causal region. In the zero-mode computation we can average over all the possible initial values and get an estimate for the zero-mode axion contribution to the overall energy density. In this case there can also be additional non-zero momentum modes of the field, that can contribute to the energy density. This scenario also leads to the formation of cosmic strings and string-wall systems, which provide an additional channel to produce axions. These axions should also be considered as a CDM constituent, as the energy spectrum of the radiated axions is midly relativistic.

6.1 Thermal production

6.1.1 Freeze-out scenario

The non-thermally produced axions are thought to have a greater role than thermally produced axions as the dark matter constituent, but it is possible to have an additional populations of axions as thermal relics from the primordial plasma. This production of the thermal axions follows the standard freeze-out scenario so we will sketch the steps of this somewhat routine calculation.

The number density of the thermal axions n_a obeys the Boltzmann equation, which connects the expansion of the Universe to the microphysics of particle interactions [5]

$$\frac{\mathrm{d}n_a}{\mathrm{d}t} + 3Hn_a = -\sum_i \langle v\sigma_i \rangle \left(n_a n_i - n_a^{\mathrm{eq}} n_i^{\mathrm{eq}} \right), \tag{129}$$

where n_a^{eq} is the number density of the axions in thermal equilibrium, $\langle v\sigma_i \rangle$ is the flux-averaged cross-section for the scattering of the axions with the i-species particle n_i in the thermal bath.

The axion self-interactions are heavily suppressed and we neglect them in the calculation and set $i \neq a$. In our treatment we also assume that the axions interact only with particles in thermal equilibrium and set $n_i = n_i^{\mathrm{eq}}$. We can

then write the Boltzmann equation in the following form

$$\frac{\mathrm{d}n_a}{\mathrm{d}t} + 3Hn_a = -\sum_i \langle v\sigma_i \rangle \, n_i \left(n_a - n_a^{\mathrm{eq}}\right) \tag{130}$$

$$\equiv \Gamma \left(n_a^{\mathrm{eq}} - n_a\right), \tag{131}$$

where we have defined

$$\Gamma \equiv \sum_i \Gamma_i \equiv \sum_i \langle v\sigma_i \rangle \, n_i, \tag{132}$$

the total interaction rate between the axions and all the particle species present in the bath. Both Γ and H depend on the plasma temperature.

From Eq. (132) we see that if the expansion rate H is much larger than the total interaction rate Γ, one can approximatively neglect the right hand side and obtain the so-called dilution solution, where the change of the particle number density is given by the ratio of the scale factor $R(t)$ at different times,

$$n_a(t_2) = n_a(t_1) \left(\frac{R(t_1)}{R(t_2)}\right)^3, \tag{133}$$

where $t_2 > t_1$.

If the interactions between axions and other particles in the bath at given temperature or time are larger than the expansion rate of the Universe, i.e. $\Gamma > H$, the axion number density follows the thermal equilibrium one. However, as the temperature of the Universe drops down there is an epoch, where $\Gamma < H$. During this epoch, axion loses contact with the thermal bath of other particle species and its interactions are said to freeze-out. This process is called the particle decoupling, and the temperature T_{D} at this occurs is usually defined through $\Gamma(T_{\mathrm{D}}) = H(T_{\mathrm{D}})$[22].

After decoupling the evolution of the particle number density is described by the dilution solution (133) and the number density in a co-moving volume remains (effectively) constant. If we can then compute the decoupling temperature T_{D} of the axions, we also obtain their present number density. However, as the time-dependent quantity Γ depends on the interactions between the axions and the particles in the bath, in order to solve Eq. (132)

[22]Note that we do not distinguish between freeze-out temperature and decoupling temperature. However, in a more general case, i.e. when studying more massive WIMPs, this difference usually needs to be taken into account. Decoupling temperature is the temperature when the particle drops out-of-equilibrium, while the freeze-out temperature describes the temperature after which the final yield of particles is constant.

we need to study the different interactions that the axions can have with the available particle content during different epochs of the early Universe, as discussed below. In a general case this way of computing the relic number density should be considered as an approximation and the rigorous treatment would require numerical work. In the case of light axions that will decouple at very early times compared with the standard WIMPs, this approximation actually yields a reasonably accurate result.

Note that here we have only discussed the particle production from thermal axions interacting with other particles. It is of course also possible to produce axions when they are already decoupled from the bath, i.e. via scatterings and decays of the particles in thermal equilibrium that couple to the axions.

6.1.2 Different interactions epochs of axions

The axion interactions in the early Universe can be roughly divided into three different epochs, where the watershed is given by the QCD phase transition: $T \gtrsim \Lambda_{\mathrm{QCD}}$, $\Lambda_{\mathrm{QCD}} \gtrsim T \gtrsim m_\pi$, $m_\pi \gtrsim T$, where m_π is the neutral pion mass. During the last epoch, where the temperature of the Universe has dropped below the pion mass, the axion interactions, such as the Primakoff process and the Compton-like process, are the most model-dependent. Fortunately, the astrophysical observations provide stringent limits for these interactions[23], showing that these processes are not significant in the thermal axion production [76].

In the range $\Lambda_{\mathrm{QCD}} \gtrsim T \gtrsim m_\pi$, where the confinement of quarks and gluons to hadrons has taken place, the main processes involving axions are the scatterings of axions on pions and nucleons, $a + \pi \Leftrightarrow \pi + \pi$ and $a + N \Leftrightarrow N + \pi$ [76]. In order the axions to decouple during this phase, the parameter f_a should be in the range f_a would be $f_a \sim 10^4 - 10^7$ GeV and consequently the contribution to the overall energy density could be significant [37]. Nevertheless, this window for the thermal axions is effectively ruled out by the CMB and LSS measurements [76, 77, 78]. The most recent constraints comes from the temperature and polarization measurements of the Planck satellite experiment, which sets a lower bound $f_a > 1.13 \times 10^7$ GeV at 95 % C.L. [78].

The lower bound for the decay constant f_a implies that the thermal ax-

[23]Historically, the first thermal axion production calculations were done in Ref. [75], where they considered the heavily model-dependent Primakoff process $q + \gamma \Leftrightarrow q + a$ and photoproduction of axions $Q + \gamma \Leftrightarrow Q + a$, where Q is a new heavy quark.

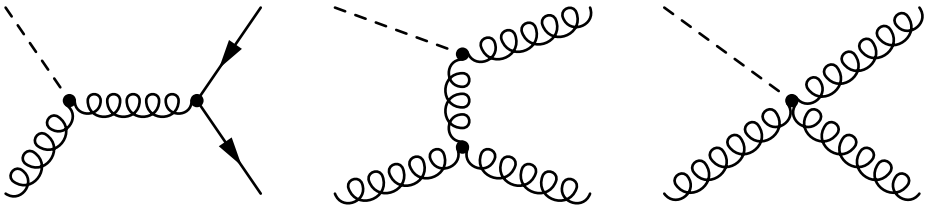

Figure 11: Feynman diagrams of processes in the primordial quark-gluon plasma involving axions.

ion production should have a decoupling temperature $T \gtrsim \Lambda_{\rm QCD}$, which translates to $f_a \sim 10^8 - 10^{12}$ GeV. The upper bound is to avoid axions overclosing the Universe. During this epoch, $T \gtrsim \Lambda_{\rm QCD}$, the most significant contribution is given by the interactions of the axions in the primordial quark-gluon plasma [79, 80]. Luckily, these processes (see Figure 11) involve the almost model-independent axion-gluon interaction, which alleviates the model-dependencies of the calculations.

6.1.3 Production from the quark-gluon plasma

In this section we compute the yield of thermal axions produced from the quark-gluon plasma. In the period of interest, i.e. before the confinement, we neglect the possible Primakoff and photoproduction processes. We shall assume that there actually is a window of time, in which the axions are in thermal equilibrium with the other particles [79].

The three essential axion processes taking place in the hot quark-gluon plasma are

$$\begin{gathered} a + g \Leftrightarrow q + \bar{q} \\ a + q(/\bar{q}) \Leftrightarrow g + q(/\bar{q}) \\ a + g \Leftrightarrow g + g, \end{gathered}$$

depicted in Fig. 11. In total there are seven different diagrams, from which the different channel and crossing diagrams can be obtained from the ones in Fig. 11.

Let us define

$$Y \equiv \frac{n_a}{s}, \tag{134}$$

where n_a is the axion number density and s is the entropy density, given in

Eqs. (132) and (26), respectively. We then have

$$\dot{Y} = \frac{1}{s}\left(\dot{n}_a - n_a\frac{\dot{s}}{s}\right) = \frac{1}{s}\left(\dot{n}_a + 3Hn_a\right), \tag{135}$$

where we have used Eq. (29). Eq. (132) can then be written as

$$\dot{Y} = \Gamma\left(Y^{\rm eq} - Y\right). \tag{136}$$

In the ultrarelativistic limit we can express the equilibrium value $Y^{\rm eq}$ as

$$Y^{\rm eq} = \frac{n_a^{\rm eq}}{s} \simeq \frac{1}{s}\frac{\zeta(3)}{\pi^2}T^3 = \frac{45\zeta(3)}{2\pi^4}\frac{1}{g_{*\rm s}\left(T\right)}. \tag{137}$$

We assume that during the axion production the entropy degrees of freedom does not change, i.e. $g_{*\rm s}(T) = g_{*\rm s}$, implying that the equilibrium $Y^{\rm eq}$ is approximately constant.

Let us introduce a new variable $x \equiv f_a/T$. In terms of it Eq. (136) has the form

$$x\frac{\rm d}{{\rm d}x}\left(\frac{Y}{Y^{\rm eq}}\right) = \frac{\Gamma}{H}\left(1 - \frac{Y}{Y^{\rm eq}}\right). \tag{138}$$

To compute the thermal yield we need to know the interaction rate $\Gamma(T)$ of the axions in the quark-gluon plasma. According to Ref. [79],

$$\Gamma(T) \approx 7.1\times 10^{-6}\frac{T^3}{f_a^2}. \tag{139}$$

Let us define

$$k \equiv x\frac{\Gamma}{H} \approx 7.1\times 10^{-6}\left(\frac{45}{4\pi^3}\right)^{1/2}\frac{m_{\rm Pl}}{g_*(T)f_a}, \tag{140}$$

and $\beta \equiv Y/Y^{\rm eq}$. Then, Eq. (138) can be written as

$$x^2\frac{{\rm d}\beta}{{\rm d}x} = k\left(1-\beta\right), \tag{141}$$

whose solution is

$$\beta\left(x\right) = 1 - C{\rm e}^{k/x}, \tag{142}$$

where C is a constant.

The relic yield given by Eq. (142) depends on the thermal history of the Universe. We assume that the PQ symmetry is broken after inflation only

if the condition $T_{\rm RH} > f_a$ is satisfied, where $T_{\rm RH}$ is the inflationary reheat temperature. We end up with six different alternatives where the order of the reheating temperature $T_{\rm RH}$, the Peccei-Quinn scale f_a and the decoupling temperature $T_{\rm D}$: (i) $T_{\rm RH} > f_a > T_{\rm D}$, (ii) $T_{\rm RH} > T_{\rm D} > f_a$, (iii) $T_{\rm D} > T_{\rm RH} > f_a$, (iv) $T_{\rm D} > f_a > T_{\rm RH}$, (v) $f_a > T_{\rm D} > T_{\rm RH}$ and (vi) $f_a > T_{\rm RH} > T_{\rm D}$.

However, this is a simplification, as it is possible that the maximum temperature after inflation is much higher than the reheating temperature [81], thus allowing PQ symmetry breaking even if $T_{\rm RH} < f_a$. This does not take into account the possibility that the PQ symmetry is broken before inflation, then restored during inflation, with axion field fluctuations growing larger than f_a, and broken again at the end of inflation [82].

To find the decoupling temperature $T_{\rm D}$ we use $\Gamma \approx H$,

$$\Gamma(T_{\rm D}) \simeq 7.1 \times 10^{-6} \frac{T_{\rm D}^3}{f_a^2} \approx \sqrt{\frac{4\pi^3}{45 g_*(T_{\rm D})}} \frac{T_{\rm D}^2}{m_{\rm Pl}} = H(T_{\rm D}), \tag{143}$$

which yields

$$T_{\rm D} \simeq 1.4 \times 10^5 \sqrt{\frac{4\pi^3}{45 g_*(T_{\rm D})}} \frac{f_a^2}{m_{\rm Pl}} \simeq 2 \times 10^{11}\ {\rm GeV} \left(\frac{f_a}{10^{12}\ {\rm GeV}} \right)^2 . \tag{144}$$

In the above we have approximated that $g_* \approx 100$. This assumes that above the electroweak scale the new degrees of freedom do not significantly contribute to the value of g_*, and thus its value is close to the Standard Model value $g_* = 106.75$.

Let us now briefly discuss the results obtained from the two scenarios where axions may enter thermal equilibrium, (i) $T_{\rm RH} > f_a > T_{\rm D}$ and (vi) $f_a > T_{\rm RH} > T_{\rm D}$. Other scenarios lead to non-equilibrium configurations. The following treatment can be easily carried to these non-equilibrium cases [82], and it is also possible to take a different approach yielding to similar results (see e.g. Ref. [80]).

If $T_{\rm RH} > f_a > T_{\rm D}$, axions are created at $T \sim f_a$. We then have the initial condition $\beta\,(x) = 0$ for $x = 1$, and Eq. (142) can be written as

$$\beta = 1 - {\rm e}^{k(1/x - 1)}. \tag{145}$$

At $x = k$ the axions decouple from the thermal bath and we have

$$\beta(x = k) = \frac{Y(T_{\rm D})}{Y^{\rm eq}} = 1 - {\rm e}^{1-k}. \tag{146}$$

After the decoupling, β is roughly constant with the decoupling value $\beta(x = k)$. Following Ref. [79], we are interested in the situation where the axions follow the thermal spectrum. Requiring that deviation from the spectrum is at most 5 % yields the constraint

$$\frac{Y(T_{\rm D})}{Y^{\rm eq}} > 0.95 \ \rightarrow k > 4. \tag{147}$$

This condition guarantees that a thermal population of axions can be created in the early Universe [79]. Combining this with Eq. (144) gives an upper bound for the symmetry breaking scale f_a

$$f_a < 1.25 \times 10^{12} \text{ GeV}. \tag{148}$$

In the case of (vi) the PQ symmetry is broken before inflation, which is assumed to dilute the axion number density. This scenario results in a upper bound for f_a that depends on the reheating temperature:

$$f_a < 1.15 \times 10^6 \ T_{\rm RH}^{1/2} \text{ GeV}^{1/2}. \tag{149}$$

The present day relic number density of thermal axions $n_{a,\rm th}$ for the cases (i) and (vi) is approximately given by

$$n_{a,\rm th} \approx Y(T_{\rm D}) s(t_0) \approx Y^{\rm eq}(T_{\rm D}) s(t_0) \approx \frac{829}{g_{*\rm s}(T_{\rm D})} \text{ cm}^{-3}, \tag{150}$$

where we used $s(t_0) = 2985 \text{ cm}^{-3}$.

The present contribution of thermal axions, which are considered to be part of HDM, to the mass density is [5]

$$\Omega_{a,\rm th} h^2 = \frac{m_a n_{a,\rm th}}{\rho_{c,0}/h^2} \approx 4.7 \times 10^{-9} \left(\frac{100}{g_{*\rm s}(T_{\rm D})} \right) \left(\frac{10^{12} \text{ GeV}}{f_a} \right). \tag{151}$$

We see that, if the value of $g_{*\rm s}$ at the time of decoupling is $\mathcal{O}(100)$, the typical PQ symmetry breaking scale, i.e. $f_a \sim 10^8 - 10^{12}$ GeV, lead to a thermal axion density $\Omega_{a,\rm th} h^2 \sim 5 \times 10^{-5} - 5 \times 10^{-9}$. It is clear that for these parameter values, while comparing with the observed CDM density (31), thermal axions are not a significant contributor to the overall energy density.

6.2 Coherent oscillation of the axion field

6.2.1 Axion field evolution

After the breaking of the PQ symmetry the Universe contains an extra scalar field, the axion field. In a FLRW universe the equation of motion of this the axion field is given by

$$\left[\frac{\partial^2}{\partial t^2} + 3H\frac{\partial}{\partial t} - \frac{1}{R^2(t)}\nabla^2_{\vec{x}}\right] a(x) + \frac{\mathrm{d}V}{\mathrm{d}a} = 0, \tag{152}$$

where the subscript $\vec{x}$ of the Laplacian refers to operating with respect to co-moving coordinates, $x = (t, \vec{x})$. In principle, there could be a term $\Gamma\dot{a}(t)$ that describes the decay of the axion field, included in the above [5]. However, as we mentioned earlier in Section 5.4, the axions are stable on cosmological time scales and therefore the decay (damping) term is negligible.

Assuming that the axion field values are smaller than the symmetry breaking scale f_a, we can approximate the potential given in Eq. (109) to be quadratic

$$V(a(x)) = f_a^2 m_a^2(T)\left(1 - \cos\left(\frac{a(x)}{f_a}\right)\right) \approx \frac{1}{2}m_a^2(T)a^2(x), \tag{153}$$

where the parametrization of the temperature-dependent axion mass $m_a(T)$ is given in Eq. (112). The equation of motion for the axion field is therefore

$$\left[\frac{\partial^2}{\partial t^2} + 3H\frac{\partial}{\partial t} - \frac{1}{R^2(t)}\nabla^2_{\vec{x}} + m_a^2(T)\right] a(x) = 0. \tag{154}$$

During the radiation domination era the scale factor scales as $R(t) \propto t^{1/2}$ and the Hubble parameter is therefore $H = 1/2t$. Using Eq. (23) we can see that the first three terms in Eq. (154) scale as t^{-2}, while the axion mass term is proportional to $t^{n/2} \sim t^{3.34}$. It is therefore reasonable to assume that there is an era, during which the mass term can be neglected. This period ends at a critical time t_1 when the axion mass turns on. We will define t_1 to be the time, when the time-dependent axion mass is proportional to t^{-1} [24],

$$m_a(t_1)t_1 = 1. \tag{155}$$

[24] In literature one can usually see two kinds of definitions for the critical time. First is the one used here, and second is $m_a(t_1) = 3H(t_1)$. However, as $H = 1/2t$ these definitions are more or less the same.

We expect that this is not that far above of the temperature of the QCD phase transition, as it is the low-energy QCD effects that generate the axion mass.

By using Eqs. (23), (112) and (155) we can find the following expressions for the critical temperature T_1 and critical time t_1

$$T_1 = 1.058 \text{ GeV} \left(\frac{70}{g_*(T_1)}\right)^{1/(4+n)} \left(\frac{10^{12} \text{ GeV}}{f_a}\right)^{2/(4+n)} \left(\frac{\Lambda_{\text{QCD}}}{400 \text{ MeV}}\right) \quad (156)$$

$$t_1 = 2.584 \times 10^{-7} \text{ s} \left(\frac{70}{g_*(T_1)}\right)^{n/(8+2n)} \left(\frac{f_a}{10^{12} \text{ GeV}}\right)^{4/(4+n)} \left(\frac{400 \text{ MeV}}{\Lambda_{\text{QCD}}}\right)^2. \quad (157)$$

It is assumed that the critical temperature T_1 to be well above the region where one considers the zero-temperature value of the axion mass [44, 82]. For the usually quoted values $f_a \sim 10^{10} - 10^{12}$ GeV, $\Lambda_{\text{QCD}} \sim \mathcal{O}(100)$ MeV and $g_*(T_1) \approx 70 - 80$ the critical temperature is $T_1 \sim 1$ GeV. With the above values the axion mass at time t_1 is around $m_a(t_1) \sim 1.5 \times 10^{-8} - 3 \times 10^{-9}$ eV.

6.2.2 Inflation after the PQ phase transition

If the inflation occurs after the Peccei-Quinn phase transition, the axion field can be thought to be a spatially homogeneous field with one initial value, i.e. $a(t, \vec{x}) = a(t)$. Dropping the gradient term and considering the radiation dominated era the Eq. (152) then reduces to

$$\left[\frac{\mathrm{d}^2}{\mathrm{d}t^2} + \frac{3}{2t}\frac{\mathrm{d}}{\mathrm{d}t} + m_a^2(t)\right] a(t) = 0. \quad (158)$$

In the epoch $t \ll t_1$ the axion mass can be neglected and the equation simplifies to

$$\left[\frac{\mathrm{d}^2}{\mathrm{d}t^2} + \frac{3}{2t}\frac{\mathrm{d}}{\mathrm{d}t}\right] a(t) = 0, \quad (159)$$

which has a solution

$$a(t) = c_0 + c_{-1/2} t^{-1/2}, \quad (160)$$

where c_0 and $c_{-1/2}$ are constants. This solution implies that when $t \ll t_1$, the expansion of the Universe makes the axion field to evolve to a constant value.

When the critical time t_1 is approached, the axion mass term becomes non-negligible. Defining $\Psi(t) \equiv t^{3/4}a(t)$, Eq. (158) can be written in the following form

$$\left[\frac{\mathrm{d}^2}{\mathrm{d}t^2} + \omega^2(t)\right]\Psi(t) = 0, \tag{161}$$

where

$$\omega^2(t) \equiv \frac{3}{16t^2} + m_a^2(t). \tag{162}$$

We can use WKB(J)-approximation to solve this. For the sake of clarity, let us briefly mention the few steps required for this solution. For a field trapped between t_1 and t the effective solution is given by

$$\Psi(t) \approx \frac{C}{\sqrt{\omega(t)}}\cos\left(\int_{t_1}^{t}\omega(t')\mathrm{d}t'\right), \tag{163}$$

where C is a constant. In the standard quantum mechanical framework the WKB-approximation assumes that the particle's de Broglie wavelength is slowly varying with respect to its position. In our scenario this translates into the requirement that

$$\left|\frac{\mathrm{d}}{\mathrm{d}t}\left(\frac{1}{\omega(t)}\right)\right| \ll 1. \tag{164}$$

This can be also expressed in the form

$$\frac{\mathrm{d}}{\mathrm{d}t}\log(\omega(t)) = \frac{1}{\omega(t)}\frac{\mathrm{d}\omega(t)}{\mathrm{d}t} \ll \omega(t), \tag{165}$$

called the adiabatic condition.

It is quite clear from the expression (162) that well after t_1 the mass term dominates and the axion field oscillates with a frequency proportional to its mass, $w(t) \approx m_a(t)$. The adiabatic condition (165) then implies that the change of the mass is small compared with the value of the mass. One can check using numerical results that in the region $t \gg t_1$ the above condition is satisfied. However, around $t \sim t_1$ it is not valid and obviously numerical studies are required for a more thorough treatment.

In terms of the axion field $a(t)$ the approximative solution for Eq. (161) in the regime $t \gg t_1$, where $\omega(t) \approx m_a(t)$, is

$$a(t) \approx a(t_1)\left[\frac{m_a(t_1)}{m_a(t)}\left(\frac{R(t_1)}{R(t)}\right)^3\right]^{1/2}\cos\left(\int_{t_1}^{t}\omega(t')\mathrm{d}t'\right) \equiv A(t)\alpha_{\mathrm{osc}}(t), \tag{166}$$

where we defined the amplitude of the oscillation as $A(t)$ and the oscillating cosine term as $\alpha_{\rm osc}(t)$.

Let us next study the energy density of the zero-momentum mode axion field $\rho_{a,0}$. According to Eq. (166),

$$\rho_{a,0} = \frac{1}{2}\dot{a}^2(t) + V(a) \approx \frac{1}{2}\dot{a}^2(t) + \frac{1}{2}m_a^2(t)a^2(t) \approx \frac{1}{2}A^2(t)m_a^2(t), \tag{167}$$

where we have neglected the sub-leading terms proportional to the derivatives of $A(t)$ as in the regime $t \gg t_1$ we have $m_a(t) \gg H$.

As we want the axion to act as a CDM component, we expect it to behave like non-relativistic matter. We can check this by considering the time-averaged form of the pressure $p_{a,0} = (1/2)\dot{a}^2(t) - V(a)$. Substituting Eq. (166) to this equation and taking time-average we get

$$\langle p_{a,0}\rangle = \langle \frac{1}{2}\dot{A}^2(t)\alpha_{\rm osc}^2\rangle \approx \frac{1}{4}\dot{A}^2(t). \tag{168}$$

The equation of state parameter $\omega_{\rm eos,a}$ can then be solved from the equation of state, $p_a = w_{{\rm eos},a}\rho_a$, and is now given by

$$\omega_{\rm eos,a} = \frac{\langle p_{a,0}\rangle}{\langle \rho_{a,0}\rangle} \approx \frac{1}{4}\left(\frac{\dot{A}(t)}{m_a(t)A(t)}\right)^2 \approx 0. \tag{169}$$

As discussed earlier in Section 2.1, the vanishing equation of state parameter implies that the zero-momentum mode axion field behaves like non-relativistic matter, which is the wanted scaling behaviour for cold dark matter.

6.2.3 Inflation before the PQ phase transition

As the PQ phase transition occurs after inflation, there is no mechanism that would spatially homogenize the scalar field over large distances. Therefore there are different k-modes present in the field. This means there might be additional contribution to the energy density coming from the non-zero modes of the axion field, as we cannot straight away neglect the gradient terms present in the equation of motion

$$\left[\frac{\partial^2}{\partial t^2} + 3H\frac{\partial}{\partial t} - \frac{1}{R^2(t)}\nabla_{\vec{x}}^2 + m_a^2(t)\right] a(t,\vec{x}) = 0. \tag{170}$$

In the period $t \ll t_1$, when the axion mass can be neglected, this becomes

$$\left[\frac{\partial^2}{\partial t^2} + 3H\frac{\partial}{\partial t} - \frac{1}{R^2(t)}\nabla^2_{\vec{x}}\right] a(t,\vec{x}) = 0. \tag{171}$$

The solution of this equation is found by expanding $a(t,\vec{x})$ in the Fourier k-space

$$a(t,\vec{x}) = \frac{1}{(2\pi)^{3/2}} \int \mathrm{d}^3k \; a(t,\vec{k}) \; \mathrm{e}^{\mathrm{i}\vec{k}\cdot\vec{x}}, \tag{172}$$

where $\vec{k}$ is the co-moving wavevector. The equation of motion for a single independently evolving k-mode is

$$\left[\frac{\partial^2}{\partial t^2} + 3H\frac{\partial}{\partial t} + \frac{k^2}{R^2(t)}\right] a(t,\vec{k}) = 0. \tag{173}$$

For the modes outside the horizon, for which $H \gg k/R(t)$, the third term can be neglected, yielding the solution

$$a(t,\vec{k}) = c_0(\vec{k}) + c_{-1/2}(\vec{k})t^{-1/2}. \tag{174}$$

This is the same behaviour that was observed in the previous zero-momentum mode calculation. In this period, i.e. when $t \ll t_1$, the modes that are outside of the horizon are frozen to a constant value. Obviously, as the axion mass turns on at $t \sim t_1$, the field starts to oscillate, similarly as the zero-momentum modes discussed in Section 6.2.2.

For the modes inside the horizon, for which $H \ll k/R(t)$, the third term in Eq. (173) cannot be neglected. Defining $\tilde{\Psi}(t,\vec{k}) \equiv R^{3/2}(t)a(t,\vec{k})$, Eq. (173) can be written in the form

$$\left[\frac{\partial^2}{\partial t^2} + \omega^2(t)\right] \tilde{\Psi}(t,\vec{k}) = 0, \tag{175}$$

where $\omega^2(t)$ is defined as

$$\omega^2(t) \equiv \frac{k^2}{R^2(t)} + \frac{3}{16t^2} = \frac{k^2}{R^2(t)} + \frac{3}{4}H^2. \tag{176}$$

As these modes are well within the horizon, we can approximate $\omega(t) \approx k/R(t)$. Substituting this into Eq. (164) yields $\omega(t) \gg H(t)$, allowing us to use WKB-approximation yielding the following solution:

$$a(t) \approx a(t_1)\left[\frac{\omega(t_1)}{\omega(t)}\left(\frac{t_1}{t}\right)^{3/2}\right]^{1/2} \cos\left(\int_{t_1}^{t} \omega(t')\mathrm{d}t'\right) \tag{177}$$

The number of axions in each mode produced in this regime is conserved if one assumes the adiabaticity condition to hold [83], and one can follow the evolution of these modes and estimate their overall contribution to the energy density – see Ref. [83] for further discussion. However, the so-called gradient energy in Eq. (170) related to the k-modes is negligible compared with the potential energy near the time of the QCD phase transition, as the gradient energy is roughly of the order of $(f_a H)^2$, while the mass potential is proportional to $(m_a f_a)^2$ [84]. In the literature one then usually neglects the contribution of these modes in the discussion of cold dark matter axions, and the treatment reduces again to cover only the zero-momentum modes.

6.3 Production from topological defects

6.3.1 Formation of axionic strings and domain walls

Axionic strings[25] are formed from the spontaneous symmetry breaking of the familiar global $\mathrm{U}(1)_{\mathrm{PQ}}$ symmetry. The Lagrangian of the complex Peccei-Quinn field S is given by

$$\mathcal{L} = -\frac{1}{2}\partial_\mu S^* \partial^\mu S - V(S,T), \tag{178}$$

where the effective high-temperature potential $V(S,T)$ is given by

$$V(S,T) = \frac{1}{4}\lambda\left(|S|^2 - v_S^2\right)^2 + \frac{1}{6}\lambda T^2 |S|^2. \tag{179}$$

As discussed earlier, for $T \gg \sqrt{3}v_S \equiv T_c$ the equilibrium value of the scalar field is at the false vacuum $|\langle S\rangle| = 0$. When the temperature drops below the critical temperature T_c, the PQ phase transition occurs and the field starts to roll towards its new equilibrium value. After some time, the PQ field acquires vacuum expectation value $|\langle S\rangle| = v_S$ and the $\mathrm{U}(1)_{\mathrm{PQ}}$ symmetry is spontaneously broken, with the field phase recognized as the axion field.

As described in Section 3, axionic cosmic strings are formed during the PQ phase transition, when the phase of the PQ field, the axion, lies in the degenerate circle of minima in the mexican hat potential described by Eq. (179). As the symmetry breaks in different regions of space, there is a non-trivial winding around the false vacuum, which corresponds to the formation of a

[25] In this section we will mainly follow Ref. [85] and references therein.

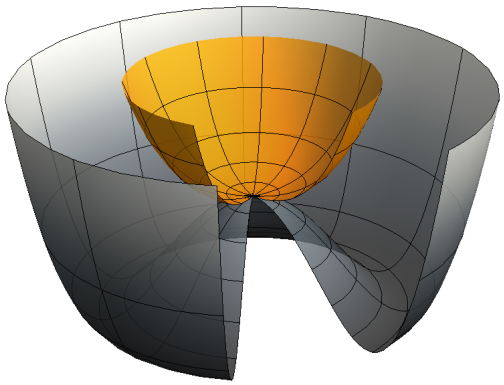

Figure 12: Potential of the PQ-scalar before (orange) and after (grey) the spontaneous symmetry breaking.

cosmic string. These strings then decay to axions, which is the their preferred decay channel. Let us do a small modification to the string linear energy density and add the scaling term ξ_s in Eq. (54) to Eq. (53) [85]

$$\mu_s = \pi v_S^2 \log\left(\frac{t}{\delta_s\sqrt{\xi_s}}\right). \tag{180}$$

Note that there is a factor of two differences between this and the expression given in Eq. (53). This is due to the normalization convention used in Eq. (178), where the extra factor of $1/2$ in front of the kinetic term finds its way to the energy density.

Near the QCD phase transition the axion potential is generated and is given in Eq. (109) with $f_a = v_S/N_{\mathrm{DW}}$. The axion potential is then of the same form as the periodic potential in Eq. (65). Referring to the earlier discussion in Section 3.5, these kind of periodic potentials give rise to string-wall configurations, where the domain walls are attached to and bounded by the cosmic strings formed in the earlier phase transition. In the case of the axion, this means that the axionic domain walls emerge around the QCD phase transition, when the axion field chooses one minimum of its periodic potential, i.e. discrete set of minima. These walls are then connected to the axionic strings formed in the PQ phase transition.

6.3.2 Production from the strings

As discussed in Section 3.4, there are uncertainties involved in the study of the evolution of global strings, and the studies rely heavily on field-theoretic lattice simulations. As expected, this has led to different treatments in the literature, but it seems that most of the studies do agree with the magnitude of the string-radiated axion contribution to the axion energy density. In this section we choose to mainly follow the treatment used in Ref. [85]. Different estimates on the axionic string production are given for example in Refs. [11, 83, 86].

The equations governing the evolution of the energy densities of the long strings ρ_s and axions produced from these strings $\rho_{a,s}$ can be modelled as [83, 85]

$$\frac{\mathrm{d}\rho_s}{\mathrm{d}t} = -2H\rho_s - \frac{\mathrm{d}\rho_{s\to a}}{\mathrm{d}t}, \tag{181}$$

and

$$\frac{\mathrm{d}\rho_{a,s}}{\mathrm{d}t} = -4H\rho_{a,s} + \frac{\mathrm{d}\rho_{s\to a}}{\mathrm{d}t}. \tag{182}$$

Hence the term $\mathrm{d}\rho_{s\to a}/\mathrm{d}t$ describes the conversion of the string energy to axions. This term effectively contains the discussed loop production ($\Gamma_{\mathrm{loop}}\rho_s$) and NGB emission ($\Gamma_{\mathrm{NG}}\rho_s$) terms that are present in Eq. (55). We have also assumed that the strings are slowly moving, i.e. $c^2 \gg \langle v^2 \rangle$.

By substituting Eq. (54) into Eq. (181) we can find

$$\frac{\mathrm{d}\rho_{s\to a}}{\mathrm{d}t} = \pi v_S^2 \frac{\xi_s}{t^3}\left[\log\left(\frac{t}{\delta_s\sqrt{\xi}}\right) - 1\right]. \tag{183}$$

Let us define the comoving energy of the radiated axions as [82]

$$E_{a,s}(t) \equiv R^4(t)\rho_{a,s}(t), \tag{184}$$

in terms of which Eq. (182) takes the form

$$\frac{\mathrm{d}E_{a,s}}{\mathrm{d}t} = R^4(t)\left(\frac{\mathrm{d}\rho_{s\to a}}{\mathrm{d}t}\right). \tag{185}$$

Then the differential number the axions radiated is

$$\mathrm{d}N_{a,s}(t) = R^3(t)\,\mathrm{d}n_{a,s}(t) = R^3(t)\frac{\mathrm{d}\rho_{a,s}}{\omega_{a,s}(t)} = \frac{\mathrm{d}E_{a,s}}{R(t)\;\omega_{a,s}(t)}, \tag{186}$$

where $\omega_{a,s}(t)$ is the mean energy of axions radiated at the time t. The amount of the NGB axions that the strings radiate between the time of the spontaneous symmetry breaking t_c and the time when the axion mass turns on at t_1 is obtained from the integral

$$\begin{aligned} N_{a,s} &= \int_{t_c}^{t_1} \mathrm{d}t \ \frac{1}{R(t)\ \omega_{a,s}(t)} \left(\frac{\mathrm{d}E_{a,s}}{\mathrm{d}t}\right) \\ &= \int_{t_c}^{t_1} \mathrm{d}t \ \left(\frac{R^3(t)}{\omega_{a,s}(t)}\right) \pi v_S^2 \frac{\xi_s}{t^3} \left[\log\left(\frac{t}{\delta_s\sqrt{\xi_s}}\right) - 1\right]. \end{aligned} \tag{187}$$

In the literature there has been discussion about the shape of the energy spectrum of the radiated axions. Some studies assume that the energy spectrum is peaked around the horizon, and therefore the typical mean energy is comparable to the curvature size of the string, $w_{a,s} \sim t^{-1}$ [13, 87, 88, 89, 90]. In Refs. [91, 92, 93] it was argued that the global strings lose their energy more quickly, in just few oscillations, and the energy spectrum of radiated axions is consequently "hard", $w_{a,s} \sim k^{-1}$. In this case all scales between string core width scale and largest horizon scale give similar contribution to the spectrum. This actually suppresses the number of produced axions and leads to a smaller total axion abundance.

Numerical studies seem the prefer the former view, where the axion spectrum is peaked [12, 14, 94]. We will follow here Ref. [85] and assume that

$$\omega_{a,s}(t) = \epsilon_s \frac{2\pi}{t}, \tag{188}$$

where ϵ_s is a numerical factor to be determined in lattice simulations.

The number of produced axions via radiation from strings is then given by

$$\begin{aligned} N_{a,s} &= \frac{v_S^2 \xi_s}{\epsilon_s} \left[\frac{R^3(t)}{t}\left(\log\left(\frac{t}{\delta_s\sqrt{\xi_s}}\right) - 3\right)\right]\Bigg|_{t=t_c}^{t_1} \\ &\approx \frac{v_S^2 \xi_s}{\epsilon_s} \frac{R^3(t_1)}{t_1} \left[\log\left(\frac{t_1}{\delta_s\sqrt{\xi_s}}\right) - 3\right], \end{aligned} \tag{189}$$

where we have ignored the small contribution of axions created at the critical time t_c. The present energy density of the axions radiated between t_c and t_1 is then given by

$$\begin{aligned} \rho_{a,s}(t_0) &= m_a(0) n_{a,s}(t_0) = m_a(0) R^{-3}(t_0) N_{a,s} \\ &\approx m_a(0) \frac{v_S^2}{t_1} \frac{\xi_s}{\epsilon_s} \left(\frac{R(t_1)}{R(t)}\right)^3 \left[\log\left(\frac{t_1}{\delta_s\sqrt{\xi_s}}\right) - 3\right]. \end{aligned} \tag{190}$$

Since bulk of the contribution to the energy density comes from the axions that have a mean energy $\omega_{a,s} \sim t_1^{-1}$, these axions become non-relativistic fairly quick due to the momentum redshift and the acquired mass. We thus assume that axions produced in the string decays contribute to the cold dark matter.

6.3.3 Production from the string-wall configurations

The formation of the domain walls and their role in the axion physics was first addressed in Ref. [15]. The formed string-wall configurations may be either short- or long-lived, with the long-lived systems being usually incompatible with the standard cosmological picture. As mentioned earlier, the structure and evolution of string-wall systems depend on the domain wall number $N_{\rm DW}$. It happens that if the configuration is specified by $N_{\rm DW} = 1$, where there is one string attached to each wall, the string-wall network is unstable and vanishes rapidly due to the fragmentation and decay into axions [17]. However, stable long-lived systems are created in scenarios where $N_{\rm DW} > 1$, which introduces the so-called axionic domain wall problem [15, 21].

The contribution of the collapsing domain wall systems to the overall axion abundance has not received as much as attention as the axionic strings in the literature. Earlier studies have been performed for example in Refs. [95, 96, 97, 98, 99, 100], and in section we will follow Ref. [85].

Due to the low-energy mixing between pions and axions, the domain wall surface mass density given in Eq. (67) needs to be modified, as the neutral pion field affects the domain wall structure [101]. In a general model the surface density of an axionic domain wall is given by [101]

$$\begin{aligned}\sigma_w &\simeq 2\sqrt{2}\left(\frac{v_S}{N_{\rm DW}}\right) f_\pi m_\pi \int_0^\pi {\rm d}x \left[1 - \left(\cos^2(x) + \left(\frac{1-\tilde{z}}{1+\tilde{z}}\right)^2 \sin^2(x)\right)^{1/2}\right]^{1/2} \\ &\approx 4.195\left(\frac{v_S}{N_{\rm DW}}\right) f_\pi m_\pi \approx 8.96 m_a f_a^2, \end{aligned} \tag{191}$$

where on the second line the Bardeen-Tye estimation (111) is used. As we are interested in the epoch where the zero-temperature axion mass is not valid, we will replace the above zero-temperature mass with the temperature-dependent axion mass:

$$\sigma_w \to \sigma_w(T) \simeq 8.96 m_a(T) f_a^2. \tag{192}$$

After the domain wall formation at around t_1 there is a short epoch where the string tension governs the evolution of the whole string-wall configuration [85, 99]. However, the domain wall surface tension quickly becomes the dominating component of the system [99]. Following Ref. [99], we define the time t_2 as the time when the string linear energy density (μ_s) is equal to the domain wall surface energy density (σ_w) times the curvature radius. Assuming that the curvature radius is comparable to the horizon scale at t_2, this translates into the condition [99]

$$\sigma_w(t_2) = \frac{\mu_s(t_2)}{t_2}. \tag{193}$$

We can express the corresponding temperature T_2 to the time t_2 as

$$T_2 \approx 1.296 \text{ GeV } N_{\text{DW}}^{-4/(n+4)} \left(\frac{65}{g_*(T_2)}\right)^{1/(n+4)} \left(\frac{10^{12} \text{ GeV}}{f_a}\right)^{2/(n+4)} \times \left(\frac{\Lambda_{\text{QCD}}}{400 \text{ MeV}}\right) \left[\log\left(\frac{t_2}{\delta_s\sqrt{\xi_s}}\right)\right]^{-2/(n+4)}. \tag{194}$$

As mentioned earlier, the production of axions from the string-wall configurations depends on the evolution of system. This evolutionary history is notably different for the cases $N_{\text{DW}} = 1$ and $N_{\text{DW}} > 1$, and here we will only consider the case with $N_{\text{DW}} = 1$. The latter case leads to the formation of long-lived string-wall systems, where the string-wall network enters the discussed scaling regime and can then dominate the energy density. These configurations can be made unstable with potential modifications, but this might introduce additional fine-tuning to the theory. For the treatment of string-wall configurations in the case $N_{\text{DW}} > 1$ see Refs. [82, 85, 95].

Let us assume that the domain wall energy density at t_1 to be of the form [99]

$$\rho_w(t_1) = \mathcal{A}\left(\frac{\sigma_w(t_1)}{t_1}\right), \tag{195}$$

where $\mathcal{A}$ is the scaling area parameter, similar to the length scaling parameter ξ_s in Eq. (54). We assume that for a short period after t_1 the energy density of the whole-string wall system ρ_{sw} is given by the sum of energy densities of strings and domain walls:

$$\rho_{sw}(t) \simeq \xi_s \frac{\mu_s(t)}{t^2} + \mathcal{A}\frac{\sigma_w(t)}{t}. \tag{196}$$

Numerical studies show these configurations collapse quickly after the walls start to dominate the energy density [85, 99]. This happens around $t_d \sim t_2$, as this is the time when the tension between walls and strings is equal [85]. The total energy density of the string-wall configuration at the time of collapse can then be estimated to be

$$\rho_{sw}(t_d) = \xi_s \frac{\mu_s(t_2)}{t_2^2} + \mathcal{A}\frac{\sigma_w(t_2)}{t_2}. \tag{197}$$

Assuming that the dominating decay channel is to axions we can estimate the the number density of produced axions

$$n_{a,sw}(t) = \frac{N_{a,sw}}{R^3(t)} = \frac{1}{w_{a,sw}} \left(\frac{R(t_d)}{R(t)}\right)^3 \left[\xi_s \frac{\mu_s(t_2)}{t_2^2} + \mathcal{A}\frac{\sigma_w(t_2)}{t_2}\right], \tag{198}$$

where $w_{a,sw}$ is the mean energy of the emitted axions.

As in the case of the global axionic strings, there is no overall agreement in the literature concerning the shape of the axion energy spectrum. In Ref. [95] it is argued that also in this case the spectrum is "hard", $\mathrm{d}E/\mathrm{d}k \sim 1/k$. This argument relies on the reasoning that the domain walls bounded by strings transfer their energy into the strings, which then radiate axions. However, this requires that the energy spectrum of the axions radiated by strings follow the "hard" spectrum (see Section 6.3.2).

Let us parametrize the average momentum carried by the emitted axions at t_d as [99]

$$\epsilon_{sw} \equiv \frac{1}{m_a(t_d)} \frac{k(t_d)}{R(t_d)}. \tag{199}$$

The mean energy is then written as

$$w_{a,sw} = \sqrt{m_a^2(T_d) + (k(t_d)/R(t_d))^2} = m_a(T_d)\sqrt{1+\epsilon_{sw}^2}. \tag{200}$$

Assuming $t_d \simeq t_2$, the energy density of axions produced from the collapse of the string-wall network today would be

$$\begin{aligned}\rho_{a,sw}(t_0) &\simeq m_a(0) n_{a,sw}(t_0) \\ &= \frac{\xi_s + \mathcal{A}}{\sqrt{1+\epsilon_{sw}^2}} \left(\frac{m_a(0)}{m_a(T_2)}\right) \left(\frac{R(t_2)}{R(t_0)}\right)^3 \frac{\pi v_S^2}{t_2^2} \log\left(\frac{t_2}{\delta_s \sqrt{\xi_s}}\right).\end{aligned} \tag{201}$$

As mentioned, the values of the quantities ξ_s, $\mathcal{A}$ and ϵ_{sw} are to be determined from the numerical simulations. As in the case of axionic strings, we assume that the axions created from the string-wall system become non-relativistic fairly quickly, and thus contribute to the cold dark matter.

6.4 Axion cold dark matter abundance

6.4.1 Zero-momentum modes of the axion field

Let us move to estimate the contribution of the zero-modes to the overall axion dark matter abundance, limiting the discussion to the zero-momentum mode axions. In Eq. (167) we saw that the the energy density of the zero-momentum mode axions is

$$\rho_{a,0} \approx \frac{1}{2}A^2(t)m_a^2(t) = \frac{1}{2}a^2(t_1)m_a(t)m_a(t_1)\left(\frac{R(t_1)}{R(t)}\right)^3. \tag{202}$$

As one can see, the energy density is not conserved in a comoving volume, $\rho_{a,0}R^3(t)$. However, the axion number density

$$n_{a,0} = \frac{\rho_{a,0}}{m_a(t)} = \frac{1}{2}a^2(t_1)m_a(t_1)\left(\frac{R(t_1)}{R(t)}\right)^3 \tag{203}$$

is conserved. By defining the initial misalignment angle of the axion field as $\bar{\theta}_{\rm ini} \equiv a(t_1)/f_a$, the present axion number density is given by

$$n_{a,0}(t_0) = \frac{1}{2}m_a(t_1)\bar{\theta}_{\rm ini}^2 f_a^2\left(\frac{R(t_1)}{R(t)}\right)^3. \tag{204}$$

The contribution of the zero-mode axions to the total energy density is then

$$\Omega_{a,0}h^2 \approx 0.061\times\bar{\theta}_{\rm ini}^2\left(\frac{g_*(T_1)}{70}\right)^{-(n+2)/(8+2n)}\left(\frac{f_a}{10^{12}\ {\rm GeV}}\right)^{(6+n)/(4+n)}\left(\frac{\Lambda_{\rm QCD}}{400\ {\rm MeV}}\right). \tag{205}$$

These results suffer from uncertainties, which stem mainly from the anharmonic axion potential and the adiabaticity condition that was assumed in the calculation. The anharmonic effects originate in the quadratic approximation of the axion potential. This linearization of the sine-function in the equation of motion for the axion field results in a smaller energy density than in the case of the non-quadratic sine-potential due to the fact that for larger values of the argument a/f_a the sine-function is flatter than the used potential, resulting in the axion field oscillations starting later [102].

The standard way to incorporate the anharmonic effects to the approximative calculation was devised in Refs. [102, 103][26]. The idea is to include a function

[26]Similar calculations of the anharmonic evolution of the axion field have also been performed for example in Refs. [44, 104, 105, 106].

$f(\bar{\theta}_{\rm ini})$ that parametrizes the anharmonicities, i.e. $\bar{\theta}_{\rm ini} \to f(\bar{\theta}_{\rm ini})\bar{\theta}_{\rm ini}$. For small values of $\bar{\theta}_{\rm ini}$ the function converges to one, $f(\bar{\theta}_{\rm ini}) \to 1$, and diverges for larger values.

In the scenario where the PQ symmetry is broken after inflation, the Universe is comprised of a vast number of distinct causal patches with an independent value for the angle $\bar{\theta}_{\rm ini}$. It might then be reasonable to replace $f(\bar{\theta}_{\rm ini})\bar{\theta}_{\rm ini}^2$ with the root-mean-square value $\langle \bar{\theta}_{\rm ini}^2 \rangle_{\rm RMS}$, which assumes a uniform distribution of the possible values for the misalignment angle:

$$\langle \bar{\theta}_{\rm ini}^2 \rangle_{\rm RMS} = \frac{1}{\pi} \int_0^\pi f(\bar{\theta}_{\rm ini}) \bar{\theta}_{\rm ini}^2 {\rm d}\bar{\theta}_{\rm ini}. \tag{206}$$

If there are no anharmonic effects, i.e. the linearization of sine-function is acceptable, the anharmonicity function is just an identity and the rms-value is

$$\langle \bar{\theta}_{\rm ini}^2 \rangle_{\rm RMS} = \frac{1}{3}\pi^2. \tag{207}$$

However, if we take into account the anharmonic effects, the averaged value for the misalignment angle receives a correction factor, which was estimated in Ref. [102] to be $\alpha_{\rm anh} \equiv \langle f(\bar{\theta}_{\rm ini})\bar{\theta}_{\rm ini}^2 \rangle / \langle \bar{\theta}_{\rm ini}^2 \rangle = 1.9 - 2.4$. We will use the value $\alpha_{\rm anh} = 2.2$, i.e. instead of Eq. (207) we assume

$$f(\bar{\theta}_{\rm ini})\bar{\theta}_{\rm ini}^2 = 2.2 \times \frac{\pi^2}{3}. \tag{208}$$

Another improvement to the analysis is to numerically study the regime around the critical time t_1. In our calculation we just assumed fulfillment of the adiabatic condition during the instantaneous axion mass turn-on at t_1. Ref. [106] showed that when the expansion of the Universe around t_1 is taken into account, the energy density is corrected by the factor $\alpha_{\rm adi} \approx 1.85$.

Taking the correction factors mentioned above into account, we end up with the following estimate for the contribution of the zero-momentum mode axions to the cold dark matter in the case when the Peccei-Quinn phase transition happens after the inflation:

$$\Omega_{a,0}h^2 \approx 0.74 \left(\frac{g_*(T_1)}{70}\right)^{-(n+2)/(8+2n)} \left(\frac{f_a}{10^{12}\ {\rm GeV}}\right)^{(6+n)/(4+n)} \left(\frac{\Lambda_{\rm QCD}}{400\ {\rm MeV}}\right). \tag{209}$$

If inflation occurs after the PQ phase transition, the entire observable Universe has the same value of the misalignment angle $\bar{\theta}_{\rm ini}$. In this case we

cannot average over different regions and do not have an estimate for the value of $\bar{\theta}_{\rm ini}$. However, we can couple $\bar{\theta}_{\rm ini}$ through the perturbations of the axion field to the inflationary models as will be explained later on.

6.4.2 Axionic strings and string-walls configurations

From Eq. (190) we can estimate the energy density of the string-radiated axions today:

$$\Omega_{a,s}h^2 \approx 0.122 N_{\rm DW}^2 \frac{\xi_s}{\epsilon_s}\left(\frac{g_*(T_1)}{70}\right)^{-(n+2)/(8+2n)}\left(\frac{f_a}{10^{12}\ {\rm GeV}}\right)^{(6+n)/(4+n)} \times \left(\frac{\Lambda_{\rm QCD}}{400\ {\rm MeV}}\right)\left[\log\left(\frac{t_1}{\delta_s\sqrt{\xi}}\right)-3\right], \quad (210)$$

where $\eta = f_a N_{\rm DW}$. To avoid the creation of long-lived string-wall configurations, we limited our discussion to the case with $N_{\rm DW} = 1$. This effectively reduces our estimates to cover only the standard KSVZ model, if we want to include the contribution of axions coming from the decay of string-wall configurations. Substituting the previous values and the other numerical factors obtained by Ref. [85], $g_*(T_1) \approx 80$, $\log(t_1/\delta_s\sqrt{\xi_s}) \approx 61$, $\xi_s = 1.0 \pm 0.5$ and $\epsilon_s = 4.02 \pm 0.70$, we obtain

$$\Omega_{a,s}h^2 \approx 1.667 \times \left(\frac{f_a}{10^{12}\ {\rm GeV}}\right)^{(6+n)/(4+n)} \times \left(\frac{\Lambda_{\rm QCD}}{400\ {\rm MeV}}\right). \quad (211)$$

In our estimation we have neglected the error margins and used the central values of the numerical quantities. Taking into account the different error sources, the result may deviate up to 30–40 % from the one reported here (see e.g. Ref. [85]).

The contribution of the axions from the string-wall network collapse to the present axion dark matter energy density can be computed from Eq. (201):

$$\Omega_{a,sw}h^2 \approx 0.924 \frac{\xi_s + \mathcal{A}}{\sqrt{1+\epsilon_{sw}^2}}\left(\frac{g_*(T_2)}{65}\right)^{-(n+2)/(8+2n)}\left(\frac{f_a}{10^{12}\ {\rm GeV}}\right)^{(n+6)/(n+4)} \times \left(\frac{\Lambda_{\rm QCD}}{400\ {\rm MeV}}\right)\left[\log\left(\frac{t_2}{\delta_s\sqrt{\xi_s}}\right)\right]^{2/(4+n)}. \quad (212)$$

As mentioned, this estimation covers only models where $N_{\rm DW} = 1$. The computation of axion production from the long-lived string-wall configurations

in models where $N_{\rm DW} > 1$, such as the DFSZ model, is given, e.g. in Ref. [85].

Substituting the values obtained by Ref. [85], $\mathcal{A} = 0.50 \pm 0.25$, $\epsilon_{sw} = 1.96 \pm 0.23$, $\log(t_1/\delta_s\sqrt{\xi_s}) \approx 62$ and $g_*(T_2) \approx 75$, into Eq. (212), we get

$$\Omega_{a,sw}h^2 \approx 1.287 \times \left(\frac{f_a}{10^{12}\ \text{GeV}}\right)^{(6+n)/(4+n)} \times \left(\frac{\Lambda_{\rm QCD}}{400\ \text{MeV}}\right). \tag{213}$$

Where we again used the central values of the numerical quantities. We see that the contribution of the string-wall configurations to the axion dark matter can be comparable with that of the string-radiated axions. However, the axion production from the string-wall network is still often omitted in the literature, with the focus being on the zero-momentum mode and string-radiated axions.

6.5 Axion isocurvature fluctuations

If the PQ symmetry is broken before inflation, axions can produce isocurvature fluctuations due to quantum effects. This can be used to constrain the parameters of axion models. In this section we will discuss[27] how to couple the axion parameters to the parameters of the inflationary model through the initial misalignment angle.

For now we neglect the anharmonic effects, i.e. set $f(\bar{\theta}_{\rm ini}) = 1$, and replace the value of the initial misalignment angle to include variance:

$$\langle\bar{\theta}_{\rm ini}^2\rangle \to \langle\bar{\theta}^2\rangle = \bar{\theta}_{\rm ini}^2 + \sigma_\theta^2, \tag{214}$$

where σ_θ is the amplitude of the fluctuations in the misalignment angle $\bar{\theta}$, or in the axion field.

During inflationary stage, the spectrum of the quantum fluctuations of the massless, weakly-coupled scalar axion field is described by [5]

$$\langle|\delta a(t,\vec{k})|^2\rangle = \int \frac{\mathrm{d}^3\vec{x}}{(2\pi)^3}\langle\delta a(t,\vec{x})\delta a(t,\vec{x'})\rangle \mathrm{e}^{-\mathrm{i}\vec{k}\cdot(\vec{x}-\vec{x'})} = \left(\frac{H_{\rm I}}{2\pi}\right)^2 \frac{2\pi^2}{k^3}, \tag{215}$$

[27] We will follow mainly Refs. [11, 84, 107, 108, 109].

where $H_{\rm I}$ is the Hubble parameter during inflation. The amplitude of the misalignment angle fluctuation in real space is then given by[28] [11]

$$\sigma_\theta = \delta\left(\frac{a(x)}{f_a}\right) = \frac{H_{\rm I}}{2\pi f_a}. \tag{216}$$

As discussed earlier, the isocurvature perturbations are characterized by the fixed total energy density, $\delta\rho = 0$, in the very early Universe. In order to maintain the fixed energy density, the fluctuations in the axion energy density need to be compensated by the fluctuations in other fields [109]. The different constituents in the isocurvature fluctuations in the total energy density then arrange such that [5, 109]

$$\delta\rho_{\rm iso} = 0 = \delta\rho_a + \sum_{i\neq a}\delta\rho_i + \delta\rho_r, \tag{217}$$

where $\delta\rho_a$, $\delta\rho_i$ and $\delta\rho_r$ are the perturbations of the energy densities of axions, other massive species and radiation, respectively. As $\rho_r \propto T^4$, we can express the radiation energy perturbation also as $\delta\rho_r = 4\rho_r(\delta T/T)$. Assuming that all species have become massive (non-relativistic), we have $\delta\rho_a = m_a\delta n_a$ and $\delta\rho_i = m_i\delta n_i$, where n_a and n_i are the number densities of axions and other massive species, respectively.

It is customary to define the following entropy quantity when studying isocurvature perturbations [5]:

$$S_i \equiv \frac{\delta(n_i/s)}{(n_i/s)} = \frac{\delta n_i}{n_i} - \frac{\delta s_i}{s} = \frac{\delta n_i}{n_i} - 3\frac{\delta T}{T}, \tag{218}$$

where in the last stage we used Eq. (26). This is zero for adiabatic species and non-zero for isocurvature species. Assuming that all other fields than axions have adiabatic perturbations, i.e. $\delta\rho_i/\rho_i = (3/4)\delta\rho_r/\rho_r$, allows us to organize Eq. (217) as

$$\left(S_a + 3\frac{\delta T}{T}\right)\rho_a + 3\frac{\delta T}{T}\sum_{i\neq a}\rho_i + 4\frac{\delta T}{T}\rho_r = 0. \tag{219}$$

If we define the non-relativistic energy density $\rho_M \equiv \rho_a + \sum_{i\neq a}\rho_i$ we then have

$$\frac{\delta T/T}{S_a} = -\frac{1}{4}\frac{\rho_a/\rho_r}{1 + (3/4)(\rho_M/\rho_r)}. \tag{220}$$

[28]Note that in the literature there are sometimes different $\mathcal{O}(1)$ factors in front of Eq. (216), e.g. [109] has a factor of two.

In the early Universe the energy density is dominated by radiation, i.e. $\rho_r \gg \rho_a, \rho_M$. Thus $(\delta T/T)/S_a \ll 1$ and we can approximate[29]

$$S_a = \frac{\delta n_a}{n_a} - 3\frac{\delta T}{T} \approx \frac{\delta n_a}{n_a}. \tag{221}$$

Next we relate S_a to the observed perturbation spectrum.

Let us assume that the cold dark matter sector consists of axions and other "ordinary" CDM species, i.e. the total CDM energy density is given by $\Omega_c = \Omega_{a,0} + \Omega_x$. We assume that only axions contribute to the isocurvature mode. In this case the total cold dark matter entropy perturbation $\mathcal{I}_{\rm k,CDM}$ can be written in terms of the axion entropy quantity S_a [84]:

$$\mathcal{I}_{\rm k,CDM} \equiv \frac{\delta\rho_c}{\rho_c} = \frac{\delta(\rho_a + \rho_x)}{\rho_a + \rho_x} = \frac{\Omega_{a,0}}{\Omega_c}\frac{\delta\rho_a}{\rho_a} = \frac{\Omega_{a,0}}{\Omega_c}S_a. \tag{222}$$

The CDM isocurvature spectrum is then given by [84]

$$\langle|\mathcal{I}_{\rm k,CDM}|^2\rangle = \left(\frac{\Omega_{a,0}}{\Omega_c}\right)^2 \langle|S_a|^2\rangle. \tag{223}$$

We can express Eq. (221) in terms of the misalignment angle $\bar{\theta}$ [11, 108, 109]

$$S_a \approx \frac{\delta n_a}{n_a} = \frac{\bar{\theta}^2 - \langle\bar{\theta}^2\rangle}{\langle\bar{\theta}^2\rangle}. \tag{224}$$

Then, assuming a Gaussian distribution and that mean value $\langle\bar{\theta}\rangle = \bar{\theta}_{\rm ini}$, we can calculate the entropy perturbation spectrum:

$$\langle|S_a(\vec{k})|^2\rangle = \int \mathrm{d}\bar{\theta} \left|\frac{\bar{\theta}^2 - \langle\bar{\theta}^2\rangle}{\langle\bar{\theta}^2\rangle}\right|^2 \frac{1}{\sqrt{2\pi}\sigma_\theta} \mathrm{e}^{-(\bar{\theta}-\langle\bar{\theta}\rangle)^2/(2\sigma_\theta^2)} \tag{225}$$

$$= \frac{2\sigma_\theta^2(\sigma_\theta^2 + 2\bar{\theta}_{\rm ini}^2)}{(\bar{\theta}_{\rm ini}^2 + \sigma_\theta^2)^2}. \tag{226}$$

The relative magnitude of the isocurvature perturbations is usually parametrized as [110]

$$\beta_{\rm iso} = \frac{\langle|\mathcal{I}_{\rm k,CDM}|^2\rangle}{\langle|\mathcal{I}_{\rm k,CDM}|^2\rangle + \langle|\mathcal{R}_{\rm k}|^2\rangle}, \tag{227}$$

[29] Note that due to this approximation, isocurvature perturbations are sometimes referred to as isotermal fluctuations [5].

where $\langle|\mathcal{R}_{\rm k}|^2\rangle$ describes the adiabatic perturbation spectrum. In the above we have already taken into account, that only the dark sector may produce isocurvature perturbations. The recent Planck measurements [8, 110] set an upper bound for the relative isocurvature magnitude at the pivot scale $k = 0.002$ Mpc^{-1} as $\beta_{\rm iso} < 0.035$, meaning that most of the seen perturbations are in the form of adiabatic fluctuations. Taking into account that the magnitude of the isocurvature perturbations is almost negligible compared to the adiabatic ones, and substituting Eqs. (223) and (226) into Eq. (227) yields

$$\beta_{\rm iso} \approx \left(\frac{\Omega_{a,0}}{\Omega_c}\right)^2 \frac{1}{\langle|\mathcal{R}_{\rm k}|^2\rangle} \frac{2\sigma_\theta^2(\sigma_\theta^2 + 2\bar{\theta}_{\rm ini}^2)}{(\bar{\theta}_{\rm ini}^2 + \sigma_\theta^2)^2}. \tag{228}$$

If $\bar{\theta}_{\rm ini}^2 \gg \sigma_\theta^2$ we find that

$$\beta_{\rm iso} \approx \left(\frac{\Omega_{a,0}}{\Omega_c}\right)^2 \frac{4}{\langle|\mathcal{R}_{\rm k}|^2\rangle} \frac{\sigma_\theta^2}{\bar{\theta}_{\rm ini}^2}. \tag{229}$$

On the other hand, if $\sigma_\theta^2 \gg \bar{\theta}_{\rm ini}^2$ we have

$$\beta_{\rm iso} \approx \left(\frac{\Omega_{a,0}}{\Omega_c}\right)^2 \frac{2}{\langle|\mathcal{R}_{\rm k}|^2\rangle}. \tag{230}$$

From the observed value for the amplitude of the adiabatic fluctuations $\langle|\mathcal{R}_{\rm k}|^2\rangle \approx 2.4 \times 10^{-9}$ [8, 110], we can see that the case $\sigma_\theta^2 \gg \bar{\theta}_{\rm ini}^2$ is in tension with the observations.

Assuming that $\bar{\theta}_{\rm ini}^2 \gg \sigma_\theta^2$ we obtain the following bound from Eqs. (216) and (229):

$$\left(\frac{H_{\rm I}}{\bar{\theta}_{\rm ini} f_a}\right)^2 < 2.9 \times 10^{-5} \frac{\Omega_c}{\Omega_{a,0}}. \tag{231}$$

If the zero-mode axions are the dominant component of CDM the Eq. (231) implies a tight bound for the combination of the model parameters. However, if $\Omega_c \gg \Omega_{a,0}$ the bound is not that restrictive. Let us next assume $\Omega_c \approx \Omega_{a,0}$. It is then possible to estimate the bounds for either the misalignment angle $\bar{\theta}_{\rm ini}$ or the axion decay constant f_a from the expression (205) (including the factor $\alpha_{\rm adi}$). With $g_*(T_1) \approx 80$ and $\Lambda_{\rm QCD} \approx 400$ MeV [11, 85] we obtain

$$f_a > 1.31 \times 10^{11} H_{\rm I} \left(\frac{H_{\rm I}}{10^{12}\ {\rm GeV}}\right)^{(n+6)/(n+2)} \tag{232}$$

$$\bar{\theta}_{\rm ini} < 2.44 \times 10^{-7} \left(\frac{10^{12}\ {\rm GeV}}{H_{\rm I}}\right)^{(n+6)/(n+2)}. \tag{233}$$

6.6 Discussion

If the PQ symmetry breaks after the inflation, the total energy density of axions is the sum of the zero-momentum mode and topological defect axions,

$$\Omega_{a,\mathrm{tot}}h^2 = \Omega_{a,0}h^2 + \Omega_{a,s}h^2 + \Omega_{a,sw}h^2. \tag{234}$$

From the condition $\Omega_{a,\mathrm{tot}} \lesssim \Omega_c$, it follows

$$f_a \lesssim 5.6 \times 10^{10}\ \mathrm{GeV} \tag{235}$$

where we used $\Lambda_{\mathrm{QCD}} \approx 400$ MeV [11, 85]. Eq. (235) can also be expressed as a lower bound for the axion mass:

$$m_a \gtrsim 1.1 \times 10^{-4}\ \mathrm{eV}. \tag{236}$$

We can see that the contribution of the defects can be of the same order magnitude as the contribution of the zero-momentum modes. There are still large uncertainties in the computation of axion production from the strings and string-wall configurations, so one cannot really determine which one is the most dominant production mechanism. Often in the older axion literature one can see that only the zero-momentum contribution is given. If one neglects the defect contribution, the bounds on the parameters are alleviated, as in our case we would get $f_a \lesssim 2.2 \times 10^{11}$ GeV and $m_a \gtrsim 2.7 \times 10^{-5}$ eV. In Section 5.5 we mentioned that the astrophysical observations give the lower bound $f_a \gtrsim 10^8$ GeV, meaning that the so-called "classical" axion parameter window, where the axion mass is considered to be $m_a \sim 10^{-3} - 10^{-6}$ eV, is now quite narrow.

If the PQ symmetry is broken before inflation, the contribution of the topological defects on the axion production can be neglected. However, in this case we face the problem of the value of the initial misalignment angle. We have seen that we can use the isocurvature fluctuations to couple the axion model parameters to inflationary models and obtain constraints for the symmetry-breaking scale or the misalignment angle. These bounds depend on whether the zero-momentum axions are a dominant or sub-dominant CDM component. In the former case the bounds given in Eq. (232) imply that high-scale inflationary models, $H_{\mathrm{I}} > 10^8$ GeV, are disfavoured as they would yield a very-high symmetry breaking scale f_a which in turn would lead to the axions overclosing the Universe. The constraints can be avoided by fine-tuning the misalignment angle $\bar{\theta}_{\mathrm{ini}} \ll 1$, but this would effectively

reinstate the original θ parameter fine-tuning problem. The case of a high-value f_a and very small $\bar{\theta}_{\text{ini}}$ is sometimes referred to as the anthropic axion window. There are proposed mechanisms in the literature, such as an additional short inflationary period [61], which would allow the axion and axion-like particle models to achieve a GUT-scale symmetry-breaking scale, i.e. $f_a \sim 10^{15} - 10^{16}$ GeV, without fine-tuning the value of $\bar{\theta}_{\text{ini}}$.

7 Bose-Einstein condensate of axions

It is an interesting question if it is possible to distinguish between dark matter axions and other candidates, such as WIMPs, in astrophysical and cosmological dark matter observations. In the absence of direct detection of dark matter particles, the nature of the dark matter could be probed with the possible distinguishable observables, which could for example be seen in the LSS observations. As we will discuss in this section, one possible difference between axions and WIMPs is the proposed idea of axionic Bose-Einstein condensate (BEC) and long-range correlations that can affect the non-linear galaxy evolution [111].

It has been proposed that the cold dark matter population is made up of a Bose-Einstein condensate [112, 113, 114]. This could alleviate some CDM problems, such as cusp-core halo problem [115]. According to Ref. [111] the zero-momentum mode axions are a promising candidate for BEC dark matter. They are non-relativistic, and produced in high occupancy, and as we have seen, their number density is approximately conserved. It was proposed in Refs. [111, 116] that the axions form a condensate by reaching thermal equilibrium via gravitational self-interactions.

So far we have assumed that the classical field equations hold for axions, i.e. we treat axion as a classical field. This has generated slight confusion in the literature, as differing jargon and computational techniques are used, and the distinction between the coherently oscillating classical field and the axion Bose-Einstein condensate is not clear. Ref. [117] tackles this issue by proposing that the classical axion field generated by the misalignment mechanism *is* a Bose-Einstein condensate, at least to the appropriate level that is needed to describe the dynamics of the axion system. This also makes the interpretation of Ref. [116] that the gravitational interaction thermalizes the system moot, as in the interpretation of Ref. [117] it is just the gravitational interaction between the axions in the already formed condensate.

Whatever the interpretation or calculational technique, in the literature there seems to be agreement with the observation of Ref. [116] that the stress-energy tensors for the axions and WIMPS are different in the case of a condensate formation. This can be seen from the Euler-like equation for a classical scalar field

$$\partial_t \vec{v} + (\vec{v} \cdot \nabla)\vec{v} = -\nabla\psi - \nabla Q_{\rm QP} - \rho^{-1}\nabla Q_{\rm SI}, \tag{237}$$

where ψ is the Newtonian potential, $Q_{\rm QP}$ is referred to as "quantum pressure"

of the field, that is related to the Heisenberg principle and the tendency of a field wavepacket to spread [118], and $Q_{\rm SI}$ arises from the self-interaction of the field [117]. The quartic axion self-interaction term is obtained by expanding the cosine-potential to a higher order:

$$V(a) \approx \frac{1}{2} m_a^2 a^2 + \frac{\lambda}{4!} a^4, \tag{238}$$

where $\lambda = -m_a^2/f_a^2 < 0$.

In the case of non-relativistic non-interacting particles, i.e. dust or CDM, the Euler equation (237) does not contain the latter two terms in Eq. (237) [111, 117]. It is not clear how the extra terms of the classical axion field affect the structure growth and whether they are observable at any scale. It seems that in the period of the linear structure growth these additional pressure and viscosity effects do not contribute, and the classical axion field behaves like the standard CDM from the structure growth point of view [117]. However, it is possible that during the epoch of the non-linear growth, the standard cold dark matter particles and classical field can have different affect on the growth of galaxies due to gravitational interactions and self-interactions [119, 120, 121, 122]. In Refs. [111, 116, 123] it was argued that the long-range correlation length between the BEC axions in a rotating galaxy results in a creation of unique ring-like caustics via mergence of small vortices into a single large vortex.

Recently the argued dramatic growth of the axion correlation length and the affect that it has on the galaxy evolution has been questioned [124]. In Ref. [124] it is argued that while the Bose-Einstein condensate does form, the attractive interactions of the axions - the gravitation and quartic self-interaction - do not lead to long-range correlation length between the BEC axions. It is also proposed that axions form a different type of BEC, where the axions group into smaller clumps, which could be of a solitonic nature or Bose stars depending on their interactions [124].

There is an additional problem of how to include the axions originating from the topological defects. Virtually all the studies consider situations, where the Peccei-Quinn symmetry breaks after inflation, so in addition to the zero-mode axions there should be other axion populations as well. However, these populations do not have condensate characteristics that the zero-mode axions have [117]. The modified dynamics of the BEC resulting from interactions between the BEC axions (or classical axion field) and string axions have been recently studied in Refs. [125, 117]. It then seems that the question of the axion Bose-Einstein condensate and its observable effects is still an open one.

8 Conclusion

In this thesis we have studied the properties and cosmological consequences of the axion, the scalar particle that appears in the $\mathrm{U}(1)_{\mathrm{PQ}}$ extension of the Standard Model. We have seen that the axion studies are theoretically motivated, as the axion provides an elegant solution to the naturalness problem that is referred to as the strong CP problem. We described in detail the historical background of the strong CP problem and solution provided by the so-called Peccei-Quinn mechanism.

After the discussion on the strong CP problem, we moved to describe the properties and details of axion models. Despite the discussed model-dependencies of the axion models, such as the KSVZ and DFSZ models, the parameter space related to these extensions of the Standard Model is relatively minimal. As discussed, the parameter space has been probed and constrained by the astrophysical observations, but recently there has been great progress in the development and realization of direct detection experiments, such as CAST and IAXO, which are able to detect QCD axions and axion-like particles. In addition to the observations of astrophysical objects, the observation of large-scale structure dynamics deviating from the standard cold dark matter picture could also be interpreted as hints of axions through the discussed Bose-Einstein condensation of axions.

We have shown that the axion is an excellent cold dark matter candidate. If the $\mathrm{U}(1)_{\mathrm{PQ}}$ symmetry is broken after inflation, the axion cold dark matter density gets contribution from both the zero-momentum modes of the axion field and the decay of topological defects. As we have seen, in the case of the KSVZ model, the contribution of the zero-momentum modes, string-radiated axions and the axions coming from the decay of string-wall configurations can be of the same order. However, the computation includes significant uncertainties originating from the numerical simulations. In the axion models where $N_{\mathrm{DW}} > 1$, such as the DFSZ model, there is the additional problem of long-lived string-wall configurations, which we did not discuss in great detail. However, if inflation occurs after the PQ phase transition, one needs to consider only the computationally straightforward zero-momentum modes of the axion field. In this case we are left with the question of the value of the initial misalignment angle $\bar{\theta}_{\mathrm{ini}}$, but as we have shown, the isocurvature fluctuations of the axion field can be used to couple the axion model parameters to the parameters of the inflationary models. In addition to the CDM axions, we have also shown how to obtain a population of hot dark matter axions.

References

[1] R. D. Peccei and H. R. Quinn: *CP Conservation in the Presence of Pseudoparticles*. Physical Review Letters, 38(25), 1977. doi:10.1103/PhysRevLett.38.1440.

[2] R. D. Peccei and H. R. Quinn: *Constraints imposed by CP conservation in the presence of pseudoparticles*. Physical Review D, 16(6), 1977. doi:http://dx.doi.org/10.1103/PhysRevD.16.1791.

[3] J. Kim and G. Carosi: *Axions and the Strong CP Problem*. Reviews of Modern Physics, 82:557–602, 2010. doi:10.1103/RevModPhys.82.557.

[4] S. Weinberg: *The U(1) problem*. Physical Review D, 11(12), 1975. doi:10.1103/PhysRevD.11.3583.

[5] E. W. Kolb and M. S. Turner: *The Early Universe*. Westview Press, 1994. ISBN-13: 978-0201626742.

[6] A. D. Linde: *Particle physics and inflationary cosmology*. Contemporary Conect in Physics, 5:1–362, 1990. arXiv:hep-th/0503203.

[7] D. Baumann: *Inflation*. In *Physics of the large and the small, TASI 09, proceedings of the Theoretical Advanced Study Institute in Elementary Particle Physics, Boulder, Colorado, USA, 1-26 June 2009*, pages 523–686, 2011. arXiv:hep-th/0907.5424.

[8] Planck Collaboration: P. A. R. Ade et al.: *Planck 2015 results. XIII. Cosmological parameters*, 2015. arXiv:1502.01589.

[9] A. Vilenkin and E. P. S. Shellard: *Cosmic Strings and Other Topological Defects*. Cambridge University Press, 1995. ISBN-13: 978-0521391535.

[10] A. Vilenkin: *Gravitational field of vacuum domain walls and strings*. Physical Review D, 23(4), 1981. doi:10.1103/PhysRevD.23.852.

[11] O. Wantz and E. P. S. Shellard: *Axion Cosmology Revisited*. Physical Review D, 82(12), 2010. doi:10.1103/PhysRevD.82.123508.

[12] T. Hiramatsu et al.: *Improved estimation of radiated axions from cosmological axionic strings*. Physical Review D, 83(12), 2011. doi:10.1103/PhysRevD.83.123531.

[13] R. A. Battye and E. P. S. Shellard: *Recent Perspectives on Axion Cosmology*, 1997. arXiv:astro-ph/9706014.

[14] M. Yamaguchi and J. Yokoyama: *Quantitative evolution of global strings from the Lagrangian viewpoint.* Physical Review D, 67(10), 2013. doi:10.1103/PhysRevD.67.103514.

[15] P. Sikivie: *Axions, Domain Walls, and the Early Universe.* Physical Review Letters, 48(17), 1982. doi:10.1103/PhysRevLett.48.1156.

[16] E. P. S. Shellard: *Axionic Domain Walls And Cosmology.* In Demaret, J. (editor): *Origin And Early History Of The Universe. Proceedings, 26th International Astrophysical Colloquium, Liege*, 1986.

[17] S. M. Barr, K. Choi, and J. E. Kim: *Some aspects of axion cosmology in unified and superstring models.* Nuclear Physics B, 283:591 – 604, 1987. doi:10.1016/0550-3213(87)90288-4.

[18] S. Weinberg: *The Quantum Theory of Fields: Volume II. Modern Applications.* Cambridge University Press, 2005. ISBN-13: 978-0521670548.

[19] M. Ammon and J. Erdmenger: *Gauge/Gravity Duality: Foundations and applications.* Cambridge University Press, 2015. ISBN-13: 978-1107010345.

[20] G. 't Hooft: *How instantons solve the U(1) problem.* Physics Reports, 142(6), 1986. doi:10.1016/0370-1573(86)90117-1.

[21] J. E. Kim: *Light pseudoscalars, particle physics and cosmology.* Physics Reports, 150(1-2), 1987. doi:10.1016/0370-1573(87)90017-2.

[22] G. 't Hooft: *Symmetry Breaking through Bell-Jackiw Anomalies.* Physical Review Letters, 37(1), 1976. doi:10.1103/PhysRevLett.37.8.

[23] R. D. Peccei: *The Strong CP Problem and Axions.* Lecture Notes in Physics, 741:3–17, 2006. arXiv:hep-ph/0607268.

[24] G. Gabadadze and M. Shifman: *QCD vacuum and axions: what's happening?* International Journal of Modern Physics A, 17(26), 2002. doi:10.1142/S0217751X02011357.

[25] R. Rajaraman: *Solitons and Instantons.* Elsevier Science Publishers (North-Holland), 1989. ISBN-13: 978-0444870476.

[26] M. Srednicki: *Quantum Field Theory.* Cambridge University Press, 2007. ISBN-13: 978-0521864497.

[27] C. A. Baker et al.: *Improved Experimental Limit on the Electric Dipole Moment of the Neutron.* Physical Review Letters, 97(13), 2006. doi:10.1103/PhysRevLett.97.131801.

[28] A. P. Serebrov et al.: *New measurements of neutron electric dipole moment.* JETP Letters, 99(1), 2014. doi:10.1134/S0021364014010111.

[29] F. Wilczek and G. Moore: *Superheavy Light Quarks and the Strong P, T Problem*, 2016. arXiv:hep-ph/1601.02937.

[30] A. Kobakhidze: *Solving the Strong CP Problem with High-Colour Quarks and Composite Axion*, 2016. arXiv:hep-ph/1602.06363.

[31] Particle Data Group Collaboration: K. A. Olive et al.: *Review of Particle Physics.* Chinese Physics, C38:090001, 2014. doi:10.1088/1674-1137/38/9/090001.

[32] C. Vafa and E. Witten: *Parity Conservation in Quantum Chromodynamics.* Physical Review Letters, 53(6), 1984. doi:10.1103/PhysRevLett.53.535.

[33] S. Weinberg: *A New Light Boson?* Physical Review Letters, 40(4), 1978. doi:10.1103/PhysRevLett.40.223.

[34] F. Wilczek: *Problem of Strong P and T Invariance in the Presence of Instantons.* Physical Review Letters, 40(5), 1978. doi:10.1103/PhysRevLett.40.279.

[35] J. E. Kim: *Weak-Interaction Singlet and Strong CP Invariance.* Physical Review Letters, 43(2), 1979. doi:10.1103/PhysRevLett.43.103.

[36] M. A. Shifman, A. I. Vainshtein, and V. I. Zakharov: *Can confinement ensure natural CP invariance of strong interactions?* Nuclear Physics B, 166(3), 1980. doi:10.1016/0550-3213(80)90209-6.

[37] D. Cadamuro: *Cosmological limits on axions and axion-like particles.* Ph.D. thesis, Ludwig Maximilian University of Munich, 2012.

[38] A.R. Zhitnitsky: *On Possible Suppression of the Axion Hadron Interactions. (In Russian).* Soviet Journal of Nuclear Physics, 30(260), 1980.

[39] M. Dine, W. Fischler, and M. Srednicki: *A Simple Solution to the Strong CP Problem with a Harmless Axion.* Physics Letters B, 104(3), 1981. doi:10.1016/0370-2693(81)90590-6.

[40] A. G. Dias et al.: *The Quest for an Intermediate-Scale Accidental Axion and Further ALPs*. Journal of High Energy Physics, 2014(6), 2014. doi:10.1007/JHEP06(2014)037.

[41] R. D. Peccei: *Particle physics footprints of the invisible axion*. Physica Scripta, 1991(T36), 1991. doi:10.1088/0031-8949/1991/T36/022.

[42] W. A. Bardeen and S.-H. H. Tye: *Current algebra applied to properties of the light Higgs boson*. Physics Letters B, 74(3), 1978. doi:10.1016/0370-2693(78)90560-9.

[43] G. G. Raffelt: *Stars as Laboratories for Fundamental Physics*. University of Chicago Press, 1996. ISBN-13: 978-0226702728.

[44] L. Visinelli: *Axions in cold dark matter and inflation models*. Ph.D. thesis, University of Utah, 2011.

[45] P. W. Graham and S. Rajendran: *New observables for direct detection of axion dark matter*. Physical Review D, 88(3), 2013. doi:10.1103/PhysRevD.88.035023.

[46] D. B. Kaplan: *Opening the axion window*. Nuclear Physics B, 260(1):215 – 226, 1985. doi:10.1016/0550-3213(85)90319-0.

[47] M. Srednicki: *Axion couplings to matter: (I). CP-conserving parts*. Nuclear Physics B, 260(3-4):689 – 700, 1985. doi:10.1016/0550-3213(85)90054-9.

[48] A. Sedrakian: *Axion Cooling of Neutron Stars*, 2015. arXiv:astro-ph/1512.07828.

[49] P. Murphy: *Bounds on axion parameters from supernova emission*. Ph.D. thesis, Durham University, 1991.

[50] P. Gondolo and G. Raffelt: *Solar neutrino limit on axions and keV-mass bosons*. Physical Review D, 79(10), 2009. doi:10.1103/PhysRevD.79.107301.

[51] G. G. Raffelt: *Astrophysical Axion Bounds*. Lecture Notes in Physics, 741:51–71, 2006. arXiv:hep-ph/0611350.

[52] H. Umada et al.: *Axion Mass Limits from Cooling Neutron Stars*. In al., N. Shibazaki et (editor): *Proceedings of the Symposium (17-20 November 1997, Tokyo) "Neutron Stars and Pulsars"*, 1998.

[53] J. Keller and A. Sedrakian: *Axions from cooling compact stars: pair-breaking processes.* Nuclear Physics A, 897:62 – 69, 2013. doi:10.1016/j.nuclphysa.2012.11.004.

[54] B. Berenji, J. Gaskins, and M. Meyer: *Constraints on Axions and Axionlike Particles from Fermi Large Area Telescope Observations of Neutron Stars.* Physical Review D, to appear, 2016. arXiv:astro-ph/1602.00091.

[55] J. A. Garcia: *Solar Axion search with Micromegas detectors in the CAST Experiment with He-3 as buffer gas.* Ph.D. thesis, University of Zaragoza, 2015. arXiv:astro-ph/1506.02601.

[56] P. Sikivie: *Experimental Tests of the "Invisible" Axion.* Physical Review Letters, 51(16), 1983. doi:10.1103/PhysRevLett.51.1415.

[57] P. W. Graham et al.: *Experimental Searches for the Axion and Axion-like Particles.* Annual Review of Nuclear and Particle Science, 65:485–514, 2015. arXiv:hep-ex/1602.00039.

[58] S. J. Asztalos et al.: *An Improved RF Cavity Search for Halo Axions.* Physical Review D, 69(1), 2004. doi:10.1103/PhysRevD.69.011101.

[59] S. J. Asztalos et al.: *SQUID-Based Microwave Cavity Search for Dark-Matter Axions.* Physical Review Letters, 104(4), 2010. doi:10.1103/PhysRevLett.104.041301.

[60] J. Kearney, N. Orlofsky, and A. Pierce: *High-Scale Axions without Isocurvature from Inflationary Dynamics*, 2016. arXiv:hep-ph/1601.03049.

[61] H. Davoudiasl, D. Hooper, and S. D. McDermott: *Inflatable Dark Matter.* Physical Review Letters, 116(3), 2016. doi:10.1103/PhysRevLett.116.031303.

[62] M. Meyer, D. Horns, and M. Raue: *First lower limits on the photon-axion-like particle coupling from very high energy gamma-ray observation.* Physical Review D, 87(3), 2013. doi:10.1103/PhysRevD.87.035027.

[63] Y. Kahn, B. R. Safdi, and J. Thaler: *A Broadband Approach to Axion Dark Matter Detection*, 2016. arXiv:hep-ph/1602.01086.

[64] J. K. Vogel: *Searching for Solar Axions in the eV-MassRegion with the CCD Detector at CAST.* Ph.D. thesis, University of Freiburg, 2009.

[65] SOLAX Collaboration: F. T. Avignone et al.: *Experimental Search for Solar Axions via Coherent Primakoff Conversion in a Germanium Spectrometer.* Physical Review Letters, 81(23), 1998. doi:10.1103/PhysRevLett.81.5068.

[66] COSME Collaboration: A. Morales et al.: *Particle dark matter and solar axion searches with a small germanium detector at the Canfranc Underground Laboratory.* Astroparticle Physics, 16(3), 2002. doi:10.1016/S0927-6505(01)00117-7.

[67] R. Bernabei et al.: *Search for solar axions by Primakoff effect in NaI crystals.* Physics Letter B, 515(1-2), 2001. doi:10.1016/S0370-2693(01)00840-1.

[68] CDMS Collaboration: Z. Ahmed et al.: *Search for Axions with the CDMS Experiment.* Physical Review Letters, 103(14), 2009. doi:10.1103/PhysRevLett.103.141802.

[69] E. Armengaud et al.: *Axion searches with the EDELWEISS-II experiment.* Journal of Cosmology and Astroparticle Physics, 2013(11), 2013. doi:10.1088/1475-7516/2013/11/067.

[70] CAST Collaboration: K. Zioutas et al.: *First Results from the CERN Axion Solar Telescope.* Physical Review Letters, 94(12), 2005. doi:10.1103/PhysRevLett.94.121301.

[71] CAST Collaboration: M. Arik et al.: *Search for Sub-eV Mass Solar Axions by the CERN Axion Solar Telescope with He-3 Buffer Gas.* Physical Review Letters, 107(26), 2011. doi:10.1103/PhysRevLett.107.261302.

[72] CAST Collaboration: M. Arik et al.: *Search for Solar Axions by the CERN Axion Solar Telescope with He-3 Buffer Gas: Closing the Hot Dark Matter Gap.* Physical Review Letters, 112(9), 2014. doi:10.1103/PhysRevLett.112.091302.

[73] J. K. Vogel et al.: *The Next Generation of Axion Helioscopes: The International Axion Observatory (IAXO).* In W. Haxton and F. Avignone (editors): *13th International Conference on Topics in Astroparticle and Underground Physics*, 2015.

[74] G. Cantatore: *"Recent Results from the PVLAS Experiment on the Magnetized Vacuum.* In Kuster, M. (editor): *Axions: Theory, Cosmology, and Experimental Searches*, pages 157–197. Springer-Verlag, 2008. doi:10.1007/978-3-540-73518-2.

[75] M. S. Turner: *Early-Universe Thermal Production of Not-So-Invisible Axions*. Physical Review Letters, 59(21), 1987. doi:10.1103/PhysRevLett.59.2489. Erratum (1988), doi:10.1103/PhysRevLett.60.1101.3.

[76] S. Hannestad, A. Mirizzi, and G. Raffelt: *A new cosmological mass limit on thermal relic axions*. Journal of Cosmology and Astroparticle Physics, 2005(7), 2005. doi:10.1088/1475-7516/2005/07/002.

[77] S. Hannestad, A. Mirizzi, G. Raffelt, and Y. Wong: *Neutrino and axion hot dark matter bounds after WMAP-7*. Journal of Cosmology and Astroparticle Physics, 2010(8), 2010. doi:10.1088/1475-7516/2010/08/001.

[78] E. Di Valentino et al.: *Cosmological axion and neutrino mass constraints from Planck 2015 temperature and polarization data*. Physics Letters B, 752(10), 2016. doi:10.1016/j.physletb.2015.11.025.

[79] E. Masso, F. Rota, and G. Zsembinski: *On Axion Thermalization in the Early Universe*. Physical Review D, 66(2), 2002. arXiv:hep-ph/0203221.

[80] P. Graf and F. D. Steffen: *Thermal axion production in the primordial quark-gluon plasma*. Physical Review D, 83(7), 2011. arXiv:hep-ph/1008.4528.

[81] G. F. Giudice, E. W. Kolb, and A. Riotto: *Largest temperature of the radiation era and its cosmological implications*. Physical Review D, 64(2), 2001. doi:10.1103/PhysRevD.64.023508.

[82] K. Saikawa: *Production and evolution of axion dark matter in the early universe*. Ph.D. thesis, University of Tokyo, 2013.

[83] P. Sikivie: *Axion Cosmology*. In Kuster, M. (editor): *Axions: Theory, Cosmology, and Experimental Searches*, pages 19–50. Springer-Verlag, 2008. doi:10.1007/978-3-540-73518-2.

[84] M. Beltran, J. Garcia-Bellido, and J. Lesgourgues: *Isocurvature bounds on axions revisited*. Physical Review D, 75(10), 2010. doi:10.1103/PhysRevD.75.103507.

[85] M. Kawasaki, K. Saikawa, and T. Sekiguchi: *Axion dark matter from topological defects*. Physical Review D, 91(6), 2015. doi:10.1103/PhysRevD.91.065014.

[86] L. Fleury and G. D. Moore: *Axion dark matter: strings and their cores*. Journal of Cosmology and Astroparticle Physics, 2016(1), 2016. doi:10.1088/1475-7516/2016/01/004.

[87] R. L. Davis: *Cosmic axions from cosmic strings*. Physics Letters B, 180(3), 1986. doi:10.1016/0370-2693(86)90300-X.

[88] R. L. Davis and E. P. S. Shellard: *Do axions need inflation?* Nuclear Physics B, 324(1), 1989. doi:10.1016/0550-3213(89)90187-9.

[89] A. Dabholkar and J. M. Quashnock: *Pinning down the axion*. Nuclear Physics B, 333(3), 1990. doi:10.1016/0550-3213(90)90140-9.

[90] R. A. Battye and E. P. S. Shellard: *Axion String Constraints*. Physical Review Letters, 73(22), 1994. doi:10.1103/PhysRevLett.73.2954.

[91] D. Harari and P. Sikivie: *On the evolution of global strings in the early universe*. Physics Letters B, 195(3), 1987. doi:10.1016/0370-2693(87)90032-3.

[92] C. Hagmann and P. Sikivie: *Computer simulations of the motion and decay of global strings*. Physics Letters B, 363(1), 1991. doi:10.1016/0550-3213(91)90243-Q.

[93] C. Hagmann, S. Chang, and P. Sikivie: *Axion radiation from strings*. Physical Review D, 63(12), 2001. doi:10.1103/PhysRevD.63.125018.

[94] M. Yamaguchi, M. Kawasaki, and J. Yokoyama: *Evolution of Axionic Strings and Spectrum of Axions Radiated from Them*. Physical Review Letters, 82(23), 1999. doi:10.1103/PhysRevLett.82.4578.

[95] S. Chang, C. Hagmann, and P. Sikivie: *Studies of the motion and decay of axion walls bounded by strings*. Physical Review D, 59(2), 1998. doi:10.1103/PhysRevD.59.023505.

[96] D. H. Lyth: *"Estimates of the cosmological axion density*. Physics Letters B, 275(3-4), 1992. doi:10.1016/0370-2693(92)91590-6.

[97] M. Nagasawa and M. Kawasaki: *Collapse of axionic domain wall and axion emission*. Physical Review D, 50(8), 1994. doi:10.1103/PhysRevD.50.4821.

[98] M. Nagasawa and M. Kawasaki: *Cold dark matter generation by axionic domain wall collapses*. Nuclear Physics B, 43(1-3), 1995. doi:10.1016/0920-5632(95)00457-K.

[99] T. Hiramatsu et al.: *Production of dark matter axions from collapse of string-wall systems.* Physical Review D, 85(10), 2012. doi:10.1103/PhysRevD.85.105020; Erratum: doi:10.1103/PhysRevD.86.089902.

[100] T. Hiramatsu et al.: *Axion cosmology with long-lived domain walls.* Journal of Cosmology and Astroparticle Physics, 2013(01), 2013. doi:10.1088/1475-7516/2013/01/001/.

[101] M. C. Huang and P. Sikivie: *Structure of axionic domain walls.* Physical Review D, 32(6), 1985. doi:10.1103/PhysRevD.32.1560.

[102] M. S. Turner: *Cosmic and local mass density of "invisible" axions.* Physical Review D, 33(4), 1986. doi:10.1103/PhysRevD.33.889.

[103] D. H. Lyth: *Axions and inflation: Vacuum fluctuations.* Physical Review D, 45(10), 1992. doi:10.1103/PhysRevD.45.3394.

[104] K. Strobl and T. J. Weiler: *Anharmonic evolution of the cosmic axion density spectrum.* Physical Review D, 50(12), 1994. doi:10.1103/PhysRevD.50.7690.

[105] K. J. Bae, J-H. Huh, and J. E. Kim: *Update of axion CDM energy density.* Journal of Cosmology and Astroparticle Physics, 9(5), 2009. arXiv:hep-ph/0806.0497.

[106] J-H. Huh: *Updated of axion CDM energy density.* In P. Ko and D. K. Hong (editors): *Supersymmetry and the Unification of Fundamental Interactions.*, volume 1078 of *AIP Conference Proceedings*, 2008.

[107] L. Visinelli and P. Gondolo: *Dark Matter Axions Revisited.* Physical Review D, 80(3), 2009. doi:10.1103/PhysRevD.80.035024.

[108] J. Hamann et al.: *Isocurvature forecast in the anthropic axion window.* Journal of Cosmology and Astroparticle Physics, 2009(6), 2009. arXiv:0904.0647.

[109] M. P. Hertzberg, M. Tegmark, and F. Wilczek: *Axion Cosmology and the Energy Scale of Inflation.* Physical Review D, 78(8), 2008. doi:10.1103/PhysRevD.78.083507.

[110] Planck Collaboration: P. A. R. Ade et al.: *Planck 2015 results. XX. Constraints on inflation*, 2015. arXiv:1502.02114.

[111] P. Sikivie and Q. Yang: *Bose-Einstein Condensation of Dark Matter Axions*. Physical Review Letters, 103(11), 2009. doi:10.1103/PhysRevLett.103.111301.

[112] S.-J. Sin: *Late-time phase transition and the galactic halo as a Bose liquid*. Physical Review D, 50(6), 1994. doi:10.1103/PhysRevD.50.3650.

[113] W. Hu, R. Barkana, and A. Gruzinov: *Fuzzy Cold Dark Matter: The Wave Properties of Ultralight Particles*. Physical Review Letters, 85(6), 2000. doi:10.1103/PhysRevLett.85.1158.

[114] F. Ferrer and J. A. Grifols: *Bose-Einstein condensation, dark matter and acoustic peaks*. Journal of Cosmology and Astroparticle Physics, 2004(12), 2004. doi:10.1088/1475-7516/2004/12/012/.

[115] J.-W. Lee and S. Lim: *Minimum mass of galaxies from BEC or scalar field dark matter*. Journal of Cosmology and Astroparticle Physics, 2010(01), 2010. doi:10.1088/1475-7516/2010/01/007.

[116] O. Erken, P. Sikivie, H. Tam, and Q. Yang: *Cosmic axion thermalization*. Physical Review D, 85(6), 2012. doi:10.1103/PhysRevD.85.063520.

[117] S. Davidson: *Axions: Bose Einstein condensate or classical field?* Astroparticle Physics, 65:101–107, 2015. doi:10.1016/j.astropartphys.2014.12.007.

[118] N. Banik, A. Christopherson, P. Sikivie, and E. M. Todarello: *The Rethermalizing Bose-Einstein Condensate of Dark Matter Axions*, 2015. arXiv:astro-ph/1509.02081.

[119] P. J. E. Peebles: *Fluid Dark Matter*. The Astrophysical Journal Letters, 534(2), 2000. doi:10.1086/312677.

[120] P. J. E. Peebles: *Dynamics of a dark matter field with a quartic self-interaction potential*. Physical Review D, 62(2), 2000. doi:10.1103/PhysRevD.62.023502.

[121] T. Rindler-Daller and P. R. Shapiro: *Finding New Signature Effects on Galactic Dynamics to Constrain Bose-Einstein-Condensed Cold Dark Matter*. In C. M. Gonzalez et al. (editor): *Accelerated Cosmic Expansion: Proceedings of the Fourth International Meeting on Gravitation and Cosmology*, volume 39 of *Astrophysics and Space Science Proceedings*, 2014.

[122] T. Rindler-Daller and P. R. Shapiro: *Angular momentum and vortex formation in Bose-Einstein-condensed cold dark matter haloes.* Monthly Notices of the Royal Astronomical Society, 422(1), 2012. doi:10.1111/j.1365-2966.2012.20588.x.

[123] N. Banik and P. Sikivie: *Axions and the galactic angular momentum distribution.* Physical Review D, 88(12), 2013. doi:10.1103/PhysRevD.88.123517.

[124] A. H. Guth, M. P. Hertzberg, and C. Prescod-Weinstein: *Do dark matter axions form a condensate with long-range correlation?* Physical Review D, 92(10), 2015. doi:10.1103/PhysRevD.92.103513.

[125] J. Berges and J. Jaeckel: *Far from equilibrium dynamics of Bose-Einstein condensation for Axion Dark Matter.* Physical Review D, 91(2), 2015. doi:10.1103/PhysRevD.91.025020.